

FINAL REPORT

Assessment of Aerosol Transport  
into the Mojave Desert

Leonard O. Myrup

and

Robert G. Flocchini

Land, Air and Water Resources  
University of California, Davis

A Report to the California Air Resources  
Board for Research Contract  
A1-153-32

February, 1986

The statements and conclusions in this report are those of Contractor and not necessarily those of the State Air Resources Board. The mention of commercial products, their source of their use in connection with material reported herein is not to be considered as either an actual or implied endoresment of their products.

QC  
880.4  
T7  
M97  
1986

The project was concerned with an assessment of the transport of atmospheric aerosols into the Western Mojave in southern California. The data used in this assessment was derived from a field study conducted in the western Mojave Desert during the summer of 1983. Three locations were utilized in the experiment: (1) Five miles east of Tehachapi Pass to assess transport from the San Joaquin Valley (2) Palmdale, to assess transport from the general direction of the Los Angeles basin and (3) Cajon Pass, to assess transport from the San Bernadino-Riverside area. Measurements were made for approximately two weeks at each location for the following time periods: (1) Tehachapi, July 17-30 (2) Palmdale, July 31-August 12 and (3) Cajon Pass, August 13-26, 1983. At each location the following measurements were made (1) particulates utilizing both a five stage Lundgren rotating drum impactor and a two stage high sensitivity stacked filter unit (2) hourly averages of temperature, humidity, windspeed, and direction at heights of 2m and 10m above the ground (3) pibal measurements at four-hourly intervals (4) Continuous acoustic sounding and (5) occasional tethersondes.

Modified principal component analysis was utilized for the specific purpose of assessing the transport of particulates into the Mojave Desert from the Los Angeles basin and the San Joaquin Valley.

Specific findings included in the report are as follows:

1. Since the measurements at the three sites were not made simultaneously, their values in interpreting differences in transport patterns depends on how representative conditions were during the observation periods. These differences were evaluated by performing a statistical analysis of aerometric data from Edwards Air Force Base.

These analyses indicate that average wind direction was essentially constant and average nephelometer readings were uniform between the three observation periods. However, the wind speed was significantly lower and the humidity was significantly higher during the "Cajon" period.

2. Flux calculation at the three sites for K, S, Si, Pb, Fe and Ca indicate that during periods of substantial flux, the transport is primarily from the <sup>w</sup>est at Tehachapi; from the southwest at Palmdale; and from the south at Cajon.

3. Silicon, Potassium, Calcium and Iron are crustal elements, and the general level of these elements are directly related to wind speed. The source of these elements appears to be locally generated windblown dust in the Mojave Desert.

4. On the other hand, the major sources of lead and sulfur appears to lie outside of the Western Mojave Desert in the Los Angeles Basin and the San Joaquin Valley.

5. At Cajon Pass and Palmdale relative humidity, sulfur and lead vary together, suggesting a common source of these factors.

6. At Palmdale, there is clear evidence of a broad flow of sulfur-laden air associated with stable, nocturnal transport.

## Contents

	<u>Page</u>
1. Introduction	3
2. Climatology and Meteorology of the Western Mojave Desert	4
3. Methodologies Employed	6
4. Principal Component Analysis	8
5. Mojave Transport Experiment	11
6. Results	14
7. Conclusions	27

## 1. INTRODUCTION

In this report we are concerned with assessment of transport of atmospheric aerosols into the western Mojave Desert in southern California. Measurements allowing direct assessment of wind transport of aerosols in this region have been made only recently. Transport into the Mojave Desert from the San Fernando and southern San Joaquin Valleys has been studied by Reible, et al., 1982 using tracer experiments. These experiments showed that material released in the San Fernando Valley impacted the southern region of the Mojave Desert while a tracer released at Oildale in the southern San Joaquin Valley reached the northern portion of the desert. Reible found the tracer material to be diluted only by a factor of two to three. The resultant desert concentrations were considered to be surprisingly high considering the long travel time over rough terrain. It is believed that visibility in the Mojave Desert has degraded in recent years [Trijonis, 1979]. Visibility is unusually significant in this area. Safe landing of the Space Shuttle is dependent on good visibility as are various operations of the U.S. Air Force and Navy. In addition, the western Mojave is a major recreational area for the high population areas of Southern California. Good visibility is an important recreational amenity for such areas. For these reasons, it is important to study the physical processes giving rise to reduced visibility. One of these is wind transport of particulate matter or aerosol into the Mojave Desert from nearby urban and industrialized areas.

The kind of questions which we seek to answer are the following. What is the relative importance of transport from the Los Angeles basin in comparison to that from the southern portion of the San Joaquin Valley? Is there a identifiable difference in the composition of the aerosol in these

two airstreams? What is the relative importance of locally generated aerosol and can this be distinguished from that transported from other air basins? What meteorological processes act to control or modulate the atmospheric concentration of particulates in this region? In this section we show how the techniques set out earlier [Flocchini and Myrup, 1985] can be used to clarify some of these questions.

## 2. CLIMATOLOGY AND METEOROLOGY OF THE WESTERN MOJAVE DESERT

The western Mojave Desert is an extension of the arid Basin and Range Province, characterized by rocky mountain ranges separated by alluvium-filled basins. This region is essentially a subtropical desert which experiences in the winter months fairly frequent incursions of middle-latitude weather, in the form of frontal systems. In the summer, somewhat less frequent incursions of tropical weather, in the form of bursts of moist monsoon air and locally intense rainfall, occur throughout the Desert.

This paper is concerned with wind transport in the summer. We will, therefore, concentrate here on the relevant facts of the wind climatology primarily in that season. Away from the mountains, this portion of the Mojave Desert is dominated by westerly flow at all times of the year and all hours of the day [Hayes, et al., 1984]. The average winds are strongest during the late spring and early summer months. During middle-latitude synoptic events, which can occur at any time of the year, strong southerlies and northerlies may appear. During the spring, summer and fall there is a pronounced tendency for the strongest winds to occur in the late afternoon and early evening, i.e., after inversion conditions have

set in. Figure 1 shows data from Hayes, et al., for Edwards Air Force Base in the center of the western Mojave Desert.

Near the mountains, two effects are observed. Strong channeling occurs in the mountain passes and in the basins where adjacent mountains are strongly alligned, as they usually are in Nevada. In California, the mountain-channeling effect can be seen in the China Lake data where the wind is predominantly southwesterly, reflecting the orientation of the Sierra Nevada and Argus ranges.

In addition, the mountains generate local mountain - valley wind systems which often dominate airflow near the mountain slopes. The evening mountain or drainage winds may be particularly important to the understanding to our data. Fig. 1, (Hayes, 1984), illustrates the diurnal variability in the wind vector at Edwards Air Force which is particularly noteworthy in the summer months. The same general features are seen at other desert stations although the direction of the mean wind may be diverted by mountain and canyon channeling.

In summary, the wind regime in the western Mojave Desert is dominated by strong westerly winds at all times of the year. This picture can be changed by synoptic events, which can generate strong southerlies and northerlies and by mountain channeling effects. Near the mountains relatively weak upslope winds may develop over solar-heated slopes during the day. At night, stably stratified nocturnal drainage winds flowing out of the San Gabriel, Tehachapi and Sierra Nevada Mountain may be substantially augmented by late sea breeze and valley systems generated in the Los Angeles Basin and in the San Joaquin Valley.

### 3. METHODOLOGIES EMPLOYED

The problem we are interested in is representation of the detailed relationship between elemental aerosol concentration, wind direction and associated meteorological parameters. The problem is complex and well suited for the method of principal components analysis. In this section we shall use some modifications of this technique which we believe clarify the problem.

A number of investigators have used the method of empirical orthogonal function analysis (also known as factor analysis by principal components) to examine spatial patterns of measured meteorological parameters or to determine source contributions or spatial patterns of air pollutants. Kidson (1975) carried out a principal component analysis on the monthly means of surface pressure, temperature, and rainfall defined as grids extending over both hemispheres and the tropical belt. Walsh (1978) represented the high latitude fields of sea level pressure, surface temperature, and 700 mb height and temperature in terms of empirical orthogonal functions in order to evaluate the daily persistence of arctic pressure anomalies. Walsh and Mostek (1980) utilized monthly meteorological data for the years 1900-77 in an eigenvector analysis of the anomaly patterns of surface temperature, precipitation, and sea level pressure over the United States. Walsh and Richman (1981) evaluated the seasonal dependence of the associations between large scale temperature anomalies over the United States and the North Pacific ocean. Wallace and Gutzler (1981) examined the large-scale associations in the winter time planetary circulations by statistical techniques including empirical orthogonal function analysis. Horel (1981) extended the work of Wallace and Gutzler by rotating the eigenvectors. Richman (1981) performed a detailed analysis of obliquely rotated principal components as a map typing



technique. Cohen (1983) classified 500 mb height anomaly patterns for North America using principal component analysis with oblique rotation. Hardy and Walton (1978) generalized the method of principal component analysis to allow the treatment of vector fields. They applied the analysis to a 12-month record of mean hourly wind velocities from 10 measurement locations in a mesoscale region.

Principal component analysis has also been applied to air pollution measurements. Blifford and Meeker (1967) constructed a factor analysis model of large scale pollution. Gaarenstroom (1977) constructed eigenvectors of particulate matter composition for daily samples collected throughout 1974 in and near Tuscon, Arizona. The first two eigenvectors which accounted for 60% of the variance were attributed to soils and sulfate. Gatz (1978) performed an empirical orthogonal factor analysis of eleven elemental concentrations measured in particulate matter during three summer seasons in St. Louis. Upon rotation four physically identifiable eigenvectors were obtained: soil and flyash, sulfur with metals, auto exhaust, and metals without sulfur. Alpert and Hopke (1980, 1981) performed a target transformation factor analysis to identify sources of air pollution in Boston and St. Louis. Flocchini et al. (1981) constructed eigenvectors of elemental composition at each of the forty sites in the Western Fine Particle network. The two major source contributions of this analysis, which explained an average of 50% of the variance, were identified as windblown dust and sulfur. Pitchford et al. (1981) performed a principal component analysis at selected sites in the Western Fine Particle Network using elemental data and visibility measurements. Ashbaugh (1984) performed a spatial principal component analysis of sulfur concentrations utilizing the forty sites of the Western Fine Particle

network. (Flocchini et al., 1980). After rotation of the initial eigenvectors, two large geographic regions were identified which accounted for 33% of the variance of the data. Three other smaller regions were identified which also had significant variance. The first eigenvector included most of Utah, Colorado, Arizona, and New Mexico. The second eigenvector included sites in the northern great plains. The remaining eigenvectors were attributed to locally important conditions.

#### 4. PRINCIPAL COMPONENTS ANALYSIS

It was felt that to aid the interpretation of these data a procedure for incorporating wind velocity was essential. This report describes several possible methods and attempts to assess relative strengths and weaknesses of the techniques. The authors have utilized principal component analysis as an interpretive tool and the results should be viewed in this light.

The primary advantage of principal component analysis is its ability to reduce a large number of variables to a smaller number of uncorrelated factors which explain a large part of the variance of the original set. Several methods of initial factor extraction have been developed. These are discussed in standard texts such as Harman (1976). In the factor analysis model, each of the  $n$  variables is replaced by a linear combination of  $m$  ( $m < n$ ) common factors plus a unique factor. The unique factor contains the residual variance not explained by the common factors. In the principal component model the  $n$  variables are replaced by  $n$  principal components or eigenvectors. A unique factor is not necessary since all the variance is explained by the  $n$  principal components. The principal component model, then, amounts to a rotation of coordinate axes in

n-dimensional variable space to a new reference frame (Harman, 1976). The first principal component extracted accounts for the maximum possible variance in the data set. Each succeeding principal component accounts for the maximum remaining variance. Although the number of principal components can equal the number of original variables, in general only the first few principal components are required to explain a large fraction of the variance.

The first set of principal components extracted is not unique; it can be linearly transformed, or rotated to obtain an equivalent description of the data. The principal components themselves are, after all, simply a rotation of the original data set. After rotation, however, each factor in turn will not explain the maximum remaining variance in the data. Only the original principal component extraction has this property. The decision of whether or not to rotate the principal components rests with the investigator. Harman suggested that the preferred types of factor solutions are based on two general principles of (1) statistical simplicity and (2) scientific meaningfulness. Statistical simplicity is achieved by constraining the analysis to the initial extraction. If the investigator desires to explain the maximum amount of variance with the fewest possible factors, the eigenvectors should not be rotated. However, the price paid for this constraint may be reduced scientific meaningfulness. Without rotation, interpretation of the first one or two eigenvectors is not generally a problem, but higher numbered components may be difficult to interpret. Furthermore, as Horel (1981) pointed out, the initial principal component solution (and certain rotated solutions, as well) is dependent on the domain of the analysis. Without rotation, higher numbered components may be present in the analysis under one domain, but not under another. The

varimax method is one of the most widely used orthogonal rotations, in part because it is often independent of the domain of the analysis. The effect of rotation is to align the axes of the principle components along the direction of the clusters of variables. Thus, the eigenvalues tend to be either high or low, with very few intermediate values. The rotated eigenvectors are generally easier to explain physically than are the unrotated eigenvectors. Two general types of rotation can be employed. An orthogonal rotation constrains the alternative eigenvectors to be uncorrelated, as in the initial analysis. An oblique rotation allows partial correlation between the eigenvectors. If the investigator expects that the underlying physical mechanisms within the system are correlated, then an oblique solution may be desirable. In general, however, an orthogonal rotation is desired.

Briefly, two major techniques, derived from principal components analysis, are used to study associations between variables in this study. First, an analysis is made of the entire data set in which wind direction is represented by eight binary variables which take on the value one when the wind is from a particular octant. Thus, eight new variables are added to the data set. This technique will be referred to as the 8-sector binary analysis. The chief advantage of this approach is that the principal components analysis can be made in "one pass" with no directional ambiguity. The disadvantage is that the technique is relatively blunt since, for our data set, it was necessary to specify a wind acceptance window of at least one octant in order to achieve coherent results.

The second technique employed is more complex. Here, wind direction is specified by means of a direction "pointer", which selects the direction for analysis. For each direction selected, a complete principal components

analysis is made. The specific value of the direction variable associated with each data point is determined by the shape of the acceptance window relative to the actual wind direction for the particular data point. If the wind direction falls within the acceptance window, then the value of the directional variable falls between zero and one, depending on the shape of acceptance window. For these reasons, we refer to this approach as the "shaped acceptance window" technique. In this study, the acceptance window was specified by  $\cos^5 \theta$ , where  $\theta$  is the angle between the pointer and the wind direction. The shaped acceptance window technique has the advantage of providing a much more detailed analysis of aerosol loadings with respect to wind direction than does the 8-sector binary technique. On the other hand the shaped acceptance window technique is computationally and analytically laborious since a separate principal components analysis is made for each rotation of the wind direction pointer. In this study, the wind direction pointer (analysis direction) was rotated at 3 degree direction intervals so that 120 principal component analyses were made per data set.

## 5. THE MOJAVE TRANSPORT EXPERIMENT

The data used in this paper was derived from a field study conducted in the western Mojave Desert during the summer of 1983. The overall objective of the experiment was to develop techniques to assess transport of particulate pollution into the Mojave Desert from the Los Angeles Basin and San Joaquin Valley. Three locations were utilized in the experiment: (1) Five miles east of Tehachapi Pass to assess transport from the San Joaquin Valley. (2) Palmdale, to assess transport from the general direction of The Los Angeles Basin. (3) Cajon Pass, to assess transport

from the San Bernadino - Riverside area. The three locations are shown on Fig. 2 which displays a map of the Western Mojave Desert. Measurements were made for approximately two weeks at each location for the following time periods: (1) Tehachapi, July 17-30 (2) Palmdale, July 31-August 12 (3) Cajon Pass, August 13-26, 1983.

At each location the following measurements were made. (1) Particulates, using two sampling systems. (2) hourly averages of temperature, humidity, windspeed and direction at heights of 2m and 10m above the ground. (3) pibal measurements at four-hourly intervals. (4) Continuous acoustic soundings (5) Occasional tether sondes.

Aerosol sampling was accomplished by means of a five stage Lundgren greased drum impactor with a six hour sampling time (Lundgren, 1967) and a two stage high sensitivity stacked filter unit (Flocchini, et al., 1981). The aerosol samples were analyzed for mass and elemental composition by the UCD Particle Induced X-ray Emission (PIXE) system (Cahill, et al., 1976).

In our analysis, we have laid greatest stress on the surface data. Since upper air data regarding particulate concentrations were not obtained, transport could not be assessed above the surface layer. In addition, the acoustic soundings in this mountainous terrain were too incoherent to provide useful information on boundary layer structure.

The result of this effort was 40 days of data, approximately 13 days at each site, taken over a 6-week period. At each site, we have paid most attention to a 168 point time series consisting of fine and coarse elemental particulate concentration, wind speed, direction and humidity at 10m and the bulk Richardson number,  $R_b$ , defined by

$$R_b = \frac{g}{T} \frac{\Delta T}{\bar{U}^2} z \quad (1)$$

where  $\Delta T$  is the temperature difference between 1 and 10 meters,  $\bar{U}$  is the wind speed at the 10m level and  $z$  is the height of the wind measurement.

Since the measurements at these three sites were not made simultaneously, their value in interpreting differences in transport patterns at the locations depends on how representative conditions were, during the observations periods, of normal summertime meteorology in the Mojave Desert. We have chosen the following approach to this problem. During the total six-week observation period, conventional meteorological data as well as nepholometer measurements were available from Edwards Air Force Base, centrally located in the study region as shown on Fig. 2.

The question we asked was how similar was the meteorology and visibility at Edwards Air Force Base for each two-week period to the overall six-week behavior? For each hour, six-week average conditions were determined. For each two-week period corresponding to the site observation periods, deviations from the six-week hourly means were computed. From this information, various statistics were obtained. Table 2 shows some results from this analysis, including two-week means for each observation period, the mean deviation and the standard deviations for all hourly values for each variable. It can be seen that wind direction, the most important variable for the kind of transport study we are attempting, is essentially constant over the three observation period, varying from a direction of 249.9 deg. for the "Tehachapi period" to 258.9 deg. for the "Cajon period", with a standard deviation of 12.55 deg. The nepholometer data showed even more uniformity between the three observation periods with the three means agreeing to within 1.05 miles of visibility range. The most serious discrepancy between the three periods is for wind speed and humidity during the period of the Cajon measurement. The wind speed was

significantly lower for this period and the humidity was significantly higher than the other periods. It is possible that this difference may affect the interpretation of the analysis to follow below.

The net result of the field experiment was the generation of three data sets for the three contrasting locations specified above, each consisting of approximately 168 data points, containing elemental aerosol concentration and wind direction, windspeed, temperature, and humidity, all at 2 and 10m. Since meteorological conditions were reasonably constant during the total six-week period, we feel the data set is a good one for both the purpose of exploring the utility of the modified principal components analysis for transport studies and also for the specific purpose of assessing transport of particulate into the Mojave Desert from the Los Angeles Basin and San Joaquin Valley.

## 6. RESULTS

In this section we will present the results of our analysis of the data set discussed above using the 8-sector binary and shaped acceptance window techniques. These will lead to certain conclusions which can be drawn regarding transport of aerosol into this region from distance sources.

In order to illustrate the nature of the data a set of time series of elemental fluxes is presented for each site. (Figure 3-8) the elements presented are fine K, S, Si, Pb, Fe, and Ca. The arrows represent the wind direction during the two hour period. The vertical ordinate represents local flux or transport rate associated with the horizontal wind. This quantity is computed as the product of the indicated aerosol concentration at the surface and the wind at a height of 10 meters. These diagrams



provide a convenient visual representation of the general features of these data. Several generalizations are immediately apparent on inspection of figures 3-8. At Tehachapi, during those periods of strong flux, the transport is primarily from the west, the direction of the Tehachapi Pass leading to the San Joaquin Valley. Occasional transport incursions from the south and southwest also occur. At Palmdale, the prevailing local transport is from the southwest whereas at Cajon, the prevailing transport direction is southerly. At all sites, the periods of low flux correspond to periods of northerly winds. Also, the most of the fluxes at Palmdale appear to be larger at Palmdale than at the other two sites. Both sulfur and lead transport appear prominently at all three sites whereas Potassium is most noticeable at Tehachapi. Finally, comparison of the various local elemental fluxes at a particular site suggests that there is a degree of association or correlation between some of these curves, as would be expected if there were common sources for the various elements or common modulating influences acting on distance sources. These descriptive remarks illustrate only the most general characteristics of these data. More specific information can be obtained through various statistical analyses presented in the following pages. The data has also been analyzed to evaluate the diurnal nature of the parameters. The day is divided into 12 2 hour time periods.

All available data for a specific time period was analyzed to yield a mean and standard deviation, Tables, 3,4,5 include the means, standard deviations, and mean standard deviations of the major parameters measured. Table 6 presents overall means of all variables for the three observation periods. The meteorological data shows that the Tehachapi site was the warmest, driest and most westerly. In general, the Palmdale site had the

highest values of particulate concentration. There were two exceptions to this conclusion. Sulfur tended to be high at all three sites but highest at Palmdale and Cajon. Similarly, lead was relatively high both at Palmdale and Cajon. Potassium a signature for agricultural burning was markedly higher at Tehachapi. The flux portion of Table 6 largely reflects the concentrations and winds. The result is that the stronger winds at Tehachapi make the fluxes at that location relatively larger. In fact, the elemental particulate fluxes are generally larger at Tehachapi than at Cajon.

The diurnal behavior of the meteorological parameters and the elemental compositions at the three sites is shown in figures 9 through 29. All the meteorological data shows a strong diurnal signal. Wind speed and temperature are high during the day and relative humidity low during the day with opposite conditions at night. The relative humidity at night is markedly higher at the Palmdale and Cajon sites than at Tehachapi. This is an indication of transport of relatively moist air from the Los Angeles Basin at these two sites. Vector wind direction at all three sites is generally southwesterly but with a great deal of variability as indicated by the large standard deviations. The one exception is the appearance of winds from the southwest at Tehachapi in the late morning.

Figures 16 through 22 show the hourly averages for course mass, Si, S, K, Ca, Fe and Pb for the three observation periods and locations. A few generalizations are immediately obvious. Palmdale generally shows the highest concentrations of "crustal" aerosols, i.e., Si, Ca, Fe and course mass. From this information alone, it cannot be determined whether this material is locally generated or has been transported into the Palmdale regions from distant sources. On the other hand, S appears at comparable

levels at all sites with somewhat higher concentrations at Palmdale and Cajon. K is markedly higher at Tehachapi compared to the other sites. This is believed to reflect the influence of agricultural burning in the Central Valley. Pb is highest at Palmdale and Cajon, where the highest concentration were reached around midnight. Such a late maximum may be associated with transport from a distant source such as the Los Angeles Basin or Kern County.

Figures 23 through 29 show the local transport or flux for the same elements as above. This is calculated as the simple product of average windspeed and concentration for the indicated hour. For the most part, these graphs look much like those for concentration. For the crustal elements, the late afternoon maximum is emphasized since both wind speed and the concentration of these elements have late afternoon maxima. The correlation between concentration and wind speed for the crustal elements may indicate a local source, i.e., fine particles raised from the desert soils by strong late afternoon winds. A summary of all collected information is presented in Appendix I.

Since there are a large number of elemental concentrations and meteorological parameters, it is difficult to make progress through a purely qualitative examination. Our purposes in the following section are to investigate the general utility of the approaches discussed above to data analysis and also to gain increased understanding of the visibility and air pollution problem in the western Mojave Desert. We will first illustrate our techniques with data from the Tehachapi site and then present a comparison of the remaining sites.

Figure 30 shows the result of a 8-sector binary analysis of the data for the Tehachapi site. Shown, in bar-graph form, are the factor scores

for the first six factors, deleting those factor scores with absolute magnitude less than 0.3. The quantity "VP" indicates the relative amount of variance explained by the factor. The first factor, explaining 24% of the variance, consists of mainly crustal elements with only marginal association with meteorological parameters. In this case, the analysis indicates a weak association with winds from the sixth quadrant, i.e., flow from west-southwest direction. It should be noted, however that this association falls just above our 0.3 cutoff and is probably of marginal significance. A factor like this one was found in almost all analysis we have made of Mojave data. In each case, a grouping of mostly crustal elements are found with no or weak association with wind direction or meteorology.

The second factor, explaining 12% of the variance shows a strong reciprocal relationship between temperature and relative humidity. This reflects the fact that these two variables are markedly out of phase, presumably due to the normal diurnal variation of these variables. This factor is always present in our analysis. Elemental concentrations whose variation is strongly diurnal, sometimes load on this factor. In the case of the Tehachapi site, only temperature and humidity appear in the diurnal factor.

The third factor, explaining 10% of the variance, is another purely meteorological one. A strong positive association is indicated between vector windspeed and flow from the 7th octant (WNW), showing that the strongest winds tended to come from that direction at this site. This is roughly in the direction of the Tehachapi Pass and appears to illustrate the strong channeling effect of mountain passes.

The fourth factor, explaining 9% of the variance, shows a strong positive association between flow from the 8th octant (NNW), lead concentration and the Richardson number. This is interpreted as indicating, for the period of this data, a flow of lead aerosol from the north-northwest direction. The strong association with positive Richardson number indicates that this flow of lead aerosol occurs at night since large positive values of Richardson number occurs only at night. At this site the north-northwesterly direction is indicated and will be examined. Although transport inference cannot be made from these point measurements, this result does suggest a different process for this northerly lead aerosol in comparison with those contained in the first three factors.

The loadings on factor 5 are small and the pattern does not appear to be particularly significant. On the other hand, Factor 6, 6% of the variance, shows an unambiguous association between coarse mass concentration and flow from the 2nd octant (ENE). We interpret this result as indicating that there was a source of dust nearby in the east-northeast direction.

Turning now to the shaped acceptance window analysis, we note at the start that with this technique there are problems in absorbing and displaying information. In the analysis to be shown here, we rotated the acceptance angle by 3-degree increments. Hence, 120 separate principal components analyses were made for each site. Straightforward techniques, such as plotting the percent of the variance explained by a particular factor as a function of acceptance angle, fail because the nature of the factors constantly changes as the acceptance angle is varied. After investigating several techniques for displaying results of the shaped acceptance angle approach, for the specific purpose of evaluating local

wind transport, we have adopted the following methodology for presenting the general nature of associations revealed.

For each acceptance angle, we have simply counted the number of positive associations between the wind direction variable and another variable, say calcium concentration. Factors with no wind direction loading do not contribute to the total. This is done for all factor scores greater than 0.3 for the first six factors. This simple procedure is repeated for all acceptance angles. Fig. 31 shows one kind of display that can be derived from the procedure. Here only occurrence of at least one association between the indicated variable and the wind direction variable is shown, without regard to how many associations might have been noted at a particular acceptance angle. The result of this approach is a diagram which shows the directions for which there is an association with a particular variable and those sectors for which there is no association with wind direction. Note that there is no wind speed information used here and that the strength of the association has been filtered out by the on-off technique for counting associations. Consequently, this diagram does not indicate transport magnitude, but instead shows only those directions where it does and does not occur.

Figure 31 is derived from measurements taken at the Tehachapi site, and shows the relationship between selected variables and wind direction, as defined above. Certain patterns can be immediately related to the 8-sector binary analysis, as discussed above. For instance, potassium, calcium, iron and, to a lesser extent, silicon and sulfur show a common pattern of association with winds from the southwest. This pattern corresponds to the first factor in the 8-sector binary analysis. In Fig.

31, lead indicates an association with north-northwest winds, as also indicated by the fourth factor of the previous analysis.

Other interesting interpretations and observations can be made this diagram. The concentration of positive Richardson number associations into the north-northwest and a narrow sector to the south means that the stable nocturnal airflow is restricted to these directions at the Tehachapi site. The almost exact correspondence, over the northern quadrants, between the association patterns for lead and positive Richardson number suggests that lead transport is associated with positive Richardson numbers in this data set. The association with stable air suggested that stable conditions are required to overcome dispersion generated by the mountains. The well defined association pattern for temperature shows that warm air arrives at this site from the south-southeast. It's noteworthy that no elemental concentration seems to be associated with this warm, daytime flow of air. Finally, the association pattern for windspeed identifies west-northwest as a preferred sector for strong winds, as did the 8-sector binary analysis. In addition, due south and northeast are shown to be sectors where strong winds also occurred in this data set.

It's striking how much information can be gained from two-way associational analysis without reference to the multi-variable associations contained in the various factors which provided the bases for this analysis. In order to provide a simple objective analysis of three-way associations between the wind direction variable and two other variables, we have identified four pairs of variables of some special interest. These are (1) calcium and potassium, to represent the "crustal elements" factor identified in the 8-sector binary analysis, although we note that potassium may also reflect the influence of agricultural or forest fires, (2)

relative humidity and temperature at 10m to represent the "diurnal factor", (3) lead and the Richardson number to stand as indicators of nocturnal transport of lead and (4) lead and sulfur to represent urban pollutants associated with transport from distant sources.

Figure 32 shows a result of this 3-way associational analysis for the Tehachapi site. Represented are acceptance angles for which both of the indicated variables appeared as factor scores greater than 0.3 in the same factor. The first triplet shows that the crustal association drifts from the southwest at the Tehachapi site. The second three-way grouping is the diurnal factor which delineates those wind directions for which the reciprocal temperature/humidity relationship is found. The directions shown, north, west and south, may reflect the impact of diurnal wind regimes associated with the major topographical features in those three directions. The third grouping shows a pronounced tendency for lead to be associated with positive Richardson number when the wind is from the north-northwest. This is the same factor as discussed above as apparently indicating local nocturnal transport of lead from a northerly direction. Finally, the last grouping suggests that associations between lead and sulfur are relatively rare but when they do occur it is when the wind is from the west-southwest and are probably associated with the crustal factor.

In the following section we present a similar analysis for the Palmdale and Cajon sites. Time series illustrative of the data gathered at these sites are shown in figures 33 through 38. The general level of some of the variables at Palmdale appears to be higher than at El Cajon. It will be recalled from the analysis of the Edwards Air Force data, presented in Table 2, that the Palmdale period had stronger mean winds than did the



Cajon period (6.5 mph to 3.23 mph). In order to investigate the effect of this difference on the means of the various aerosol measurements, Table 6 was prepared.

There are several interesting interpretations of this table. It can be seen that the actual on-site wind measurements do not reflect the factor or two difference measured at Edwards during this same period. We presume that since the Edwards site is located near the center of the region with a much more open exposure, this measurement represents a regional wind speed. In contrast, the Palmdale and especially the Cajon wind measurements represent local conditions. In Table 6 it can be seen that Coarse Mass, Silicon, Potassium, Calcium and Iron (all fine) are much larger, approximately by a factor of two, at the Palmdale compared to the El Cajon site. At the same time, Lead and Sulfur are essentially the same at the two sites. We believe the explanation lies in the difference between sources of aerosol within the Mojave Desert and those without. Silicon, Potassium, Calcium and Iron are members of the crustal factor which we have previously identified as a regional phenomenon, whose source is sand and soil of the Mojave Desert. For these elements the general level of the crustal group appears to be directly related to the regional wind speed as approximated by the Edwards measurement. On the other hand the major sources of lead and sulfur lies outside of the Western Mojave Desert in the Los Angeles Basin and the San Joaquin Valley. No association with local or regional wind speed would be expected for these elements as is shown in the table.

Figures 33 and 34 show the results of the 8-sector binary analysis of the Palmdale and Cajon data sets, respectively. By comparison with Figure 30, it can be seen that there are pronounced similarities between the three

sites for the first two factors. At Tehachapi, the first factor indicated a strong association with the crustal elements, iron, silicon, potassium, calcium and coarse mass plus a sulfur association and a weak indication of flow from the west-southwest. At the other two sites, essentially the same associations appear as the second factor. The chief difference at these sites is that sulfur does not appear. Evidently, the "crustal factor" represents aerosol generating processes for these elements which exist throughout the western Mojave Desert.

Similarly, the first factor at the Palmdale and Cajon sites is clearly the same "diurnal factor" which explained the most variance in the Tehachapi analysis. In the case of the Cajon data, the fact that the loadings for Relative humidity, sulfur and lead have the same sign indicates that these quantities vary together with relatively high values of lead and sulfur occurring when the humidity is high, i.e., at night. This same feature is seen at Palmdale but not as strongly. At Palmdale, this factor suggests a diurnal directional variation. Relative humidity and the directional variable for the 4th octant (south-southeast) have the same sign indicating a nocturnal flow from this direction. On the other hand, temperature and the directional variable associated with the 6th octant (west-southwest) have the same sign (positive) indicating daytime flow from this direction.

The remaining factors for the Palmdale and Cajon data do not show commonalities with the Tehachapi analysis. In particular, the association between wind speed and flow from the west-northwest (3rd factor) and the indication of nocturnal flow from the north-northwest (4th factor) are not repeated for the two sites to the south. The third factor at Palmdale seems to be unique to that station, indicating an association between

windspeed, sulfur and coarse mass but no directional association. There are "clean air" factors at both Palmdale and Cajon. Factor 4 for Palmdale flow from the 5th octant is negatively associated with lead. We interpret this to indicate that winds from the south-southwest are associated with relatively lead-free air. Similarly, the third factor at Cajon shows positive loading for the 6th octant (west-southwest) and negative for sulfur with the same interpretation that winds from this quadrant tend to be relatively free of sulfur. Finally, there are three factors which appear to indicate the direction of the daytime, unstable airflow. Both the 5th factor at Palmdale and the 4th factor at Cajon show positive loadings for wind from the 8th octant (north-northwest) and negative for Richardson number, indicating unstable flow from this direction. The 6th factor in the Palmdale analysis shows a similar relationship for flow from the 7th octant (west-northwest).

The 8-sector binary analysis of the Western Mojave data set suggest a mixture of regional and local influences. The crustal and diurnal factors are clearly regional in nature. The diurnal factor seems to be directly related to the out-of-phase diurnal variation of temperature and humidity. On the other hand, the 8-sector binary analysis provides no information regarding the physical processes responsible the observed association of these elements.

Figures 35 through 38 show the results of the shaped acceptance window analysis of the Palmdale and Cajon data, presented in the manner as was done for Tehachapi. Figures 35 and 37, which display the individual associations with the direction variable, show the crustal factor through the similar behavior of potassium and calcium. At Palmdale, the similarity extends to iron and silicon, with all four elements associated with wind

flow from the northeast. At Cajon, potassium and calcium are associated with winds from the east-northeast, while iron and silicon appear to lose their regional character at this site. It is interesting that a clear directional pattern emerges from the shaped acceptance window analysis, in the case of the crustal factor, while this did not occur in the 8-sector binary analysis.

The associations for lead are particularly interesting. At both locations the analyses show a clear association between lead and wind flow from the north, similar to that previously found for Tehachapi. Again, this result was not noted in the 8-sector binary analysis presented above. In addition, the present analysis indicates a second direction of association with lead for both sites. At Cajon, lead is also associated with southwesterly flow and at Palmdale there is an association indicated between lead and south-southeasterly flow.

The behavior of the sulfur associations is also of interest. In the Tehachapi data set, this element joined the crustal factor, including an association with flow from the southwest. In the case of Palmdale and Cajon, sulfur departs markedly from the crustal grouping and instead associates with lead, relative humidity and Richardson number. This association is most apparent at Palmdale; at Cajon the Richardson number connection is less convincing. The directional association for this grouping is from the southeast at Palmdale and from the southwest at Cajon. The relationship with humidity and the Richardson number in these groupings indicates we have isolated a nocturnal flow of sulfur and lead aerosols. The directional association at the Cajon site is consistent with flow of this aerosol through the Cajon Pass.

The directional associations for temperature indicate a flow of warm air from the south-southeast at Cajon and from the west-southwest at Palmdale. These directions do not correspond to those for either the crustal grouping or the lead-sulfur grouping. Apparently the flow of warm air occurs at a different time, probably earlier, in the diurnal cycle of the wind regimes at these two sites.

Figures 36 and 38 show a three-way associational analysis, similar to that presented earlier for Tehachapi, for Palmdale and Cajon. The first grouping is for the crustal elements, with calcium and potassium chosen to represent the larger group. At both sites the crustal group is associated with flow from the northeastern quadrant. The diurnal factor is similar at both sites, indicating a very broad directional relationship, especially at Palmdale. This may indicate diurnal phenomena occur in all directions especially away from the mountains. Lead and the Richardson number were chosen for the third grouping to clarify this relationship. At Palmdale there is clear evidence of a broad flow of sulfur-laden associated with stable, i.e., nocturnal air. The directional association is from the south-southeast. At Cajon, the lead-Richardson number grouping reveals little except a weak association with flow from the north. Reference to the individual associations (Figure 37) indicates that the southwesterly flow of sulfur and lead is well defined and strongly associated with humidity and, consequently, undoubtedly a nocturnal phenomenon. The lead-sulfur association is shown in the fourth grouping. At Palmdale, the group is associated with flow from the south-southeast and from the southwest at Cajon, as mentioned above.

## 7. CONCLUSIONS

We have concluded that both of the techniques used in this study, the 8-sector binary and shaped acceptance window methodologies, were successful in providing easily interpretable results. In particular the relationship between the wind directions identified by the analysis and reasonable source directions for particular elements was close and strengthened confidence in the approach. We have used the term, "local transport direction", to describe wind associations with particular elements identified from a single-station analysis, such as those used in this study. Strictly speaking all transports identified in this document are local since they are based on local, single-station measurements. In certain cases we have speculated that long range transport may be involved on the basis of indirect evidence. For instance, nocturnal flows of aerosol may be associated with distant sources since most sources are diurnal in nature, with maxima during the day. Likewise if transport is indicated from a direction for which there are no local sources then a distant source is likely. In addition, we have found that additional valuable information is obtained if other meteorological parameters are included in the analysis. In particular, stability (Richardson number) and relative humidity allow unambiguous discrimination between daytime and nocturnal flow of specific aerosols.

In general, we found the 8-sector binary technique to be a useful "first cut" on the data. This technique identified all the main features also found by more detailed analyses. The precision possible is limited, however, by the record length. In principle, with a long enough record length the acceptance window could be decreased to achieve precision comparable to the multiple acceptance window technique. With the same record length, however, we found the shaped acceptance window technique to

provide a greater amount of information with much more detail. On the negative side, analysis of the shaped acceptance window is laborious and more work needs to be done to provide output that is directly interpretable.

With respect to the Western Mojave Desert case study, we have found clear cut results regarding three aerosol streams. The three aerosol flows are described as follows.

(1) The lead aerosol. During the period of this study the nocturnal flow of lead aerosol at Tehachapi was particularly well defined. The direction, north-northwest, points generally in the direction of the southern Sierra Nevada Mountains. In addition to the northerly flow of lead aerosol, there was a nocturnal flow from south-southeast at Palmdale and Cajon and a daytime flow from the south-west. It should be noted that none of the local transports for lead aerosol have any direct relationship with the direction of the major mountain passes leading to the Los Angeles Basin or the San Joaquin Valley.

(2) The lead-sulfur aerosol. In addition to lead-only aerosol stream discussed above, the analysis also identified a combination lead-sulfur aerosol with quite different characteristics. All the local transports were from the south. Furthermore, the associations were strongest for the southern stations. In addition, the directions of the local transport of this aerosol were more nearly in the direction of the nearby mountain passes. Finally, it should be noted the majority of the local transports for the two aerosols discussed above were nocturnal.

(3) The crustal aerosol. On the great majority of individual principal components analyses we have performed on these data, the factor explaining the most variance contained such elements as Calcium, Potassium,

Iron or Silicon. Normally, there was no association with other elements although occasionally sulfur joined this group. We have used the term, "crustal aerosol", to refer to this grouping although we recognize that the potassium may be derived from distant agricultural burning, and we interpret this aerosol as being chiefly derived from desert and mountain sands and soils through the action of the wind. However, the crustal factor normally showed weak or no association with local transport direction. We interpret this result as indicating that the crustal elements in the lower atmosphere above the Western Mojave Desert are relatively old aerosols, the net result of many transport events and directions, mixed to relative homogeneity by the vigorous mesoscale circulations associated with the mountains and deserts of this region. All the directional associations were quite weak and only marginally significant at levels chosen for the analysis. Consequently, we do not believe that great weight should be placed on the local transports indicated in the table. We have concluded that the crustal factor is a regional phenomenon, not related to any particular local transport process.

## 8. REFERENCES

- Alpert D.J. and Hopke P.K. (1980) A quantitative determination of sources in the Boston urban aerosol. Atmospheric Environment 14, 1137-1146.
- Alpert, D.J. and P.K. Hopke, 1981: A determination of the sources of airborne particles collected during the regional air pollution study. Atmos. Environ., 15, 675-687.
- Blifford, I.H. and G.O. Meeker, 1967: A factor analysis model of large-scale pollution. Atmos. Environ., 1, 147-157.



- Cahill, T.A., 1979: Ambient aerosol sampling with stacked filter units. FHWA-CO-78-178-NTIS.
- Cahill, T.A., R.A. Eldred, R.G. Flocchini and J. Barone (1977). Statistical techniques for handling PIXIE data. Nuc. Inst. Meth. 142, 259-261.
- Cohen, S.J. Classification of 500 mb Height Anomalies Using Obliquely Rotated Principal Components. Journal of Climate and Applied Met. 22 1975-1987.
- Flocchini, R.G., T.A. Cahill, M.L. Pitchford, R.A. Eldred P.J. Feeney, and L.L. Ashbaugh (1981). Characterization of particles in the Arid West. Atmos. Env., 15, 2017-2030.
- Gaarenstroom P.D., Perone S.P. and Moyers J.L. (1977) Application of pattern recognition and factor analysis for characterization of atmospheric particulate composition in southwest desert atmosphere. Envir. Sci. Technol. 11, 795-800.
- Gatz D.F. (1978) Identification of aerosol sources in the St. Louis area using factor analysis. J. Appl. Met. 17, 600-608.
- Hardy, D.M. and J.J. Walton, 1978: Principal component analysis of vector wind measurements. J. Appl. Meteor., 17, 1153-1162.
- Harman, H.H., 1976: Modern factor analysis. The University of Chicago Press 487 pp.
- Hayes, T.P., J.R. Kinney and N.J.M. Wheeler (1984). California Surface Wind Climatology. State of California, Air Resources Board, Aerometric Data Division.
- Horel, J.D., 1981: A rotated principal component analyses of the interannual variability of the northern hemisphere 500 mb height field. Mon. Wea. Rev., 109, 2080-2092.

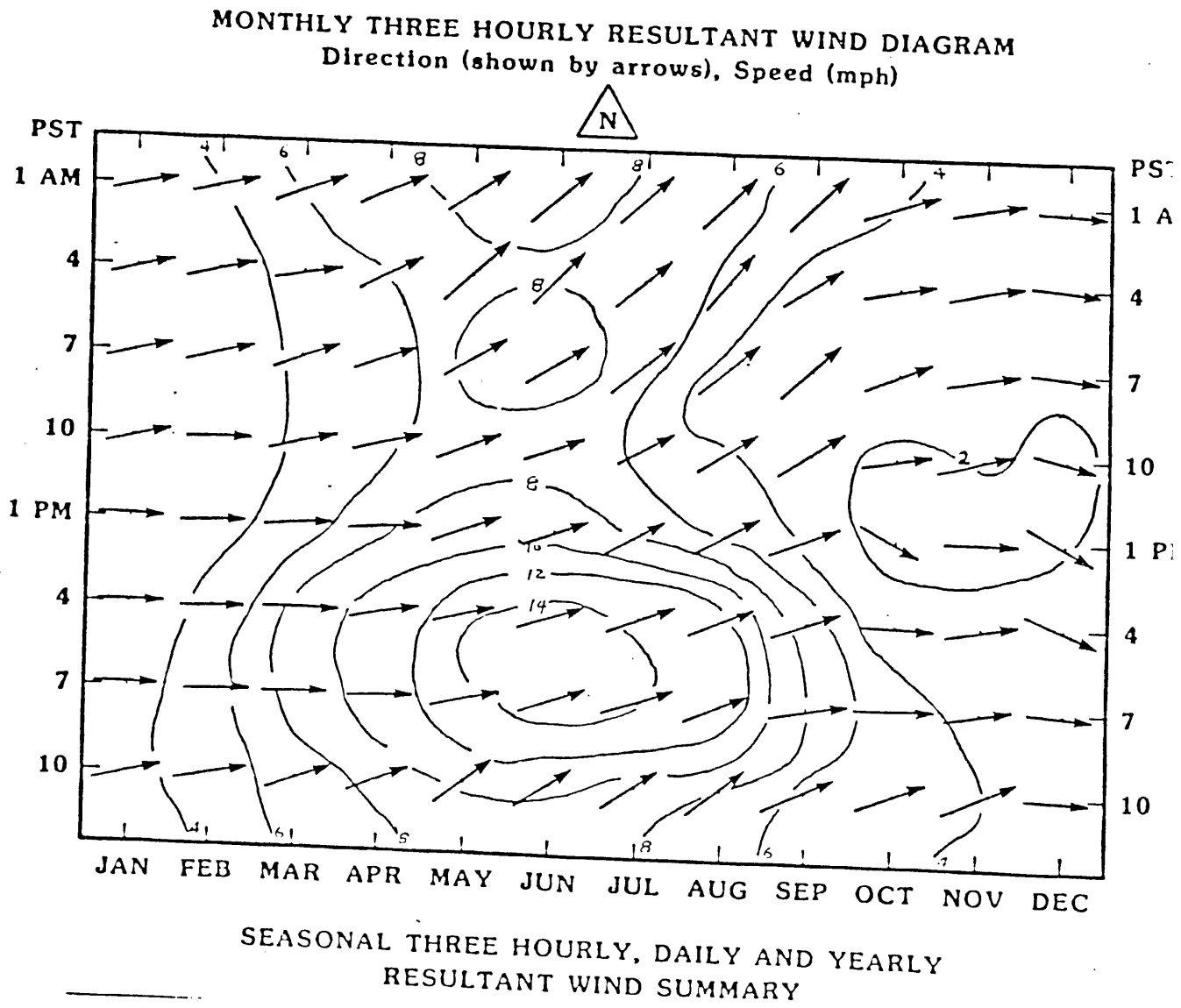


FIGURE 1

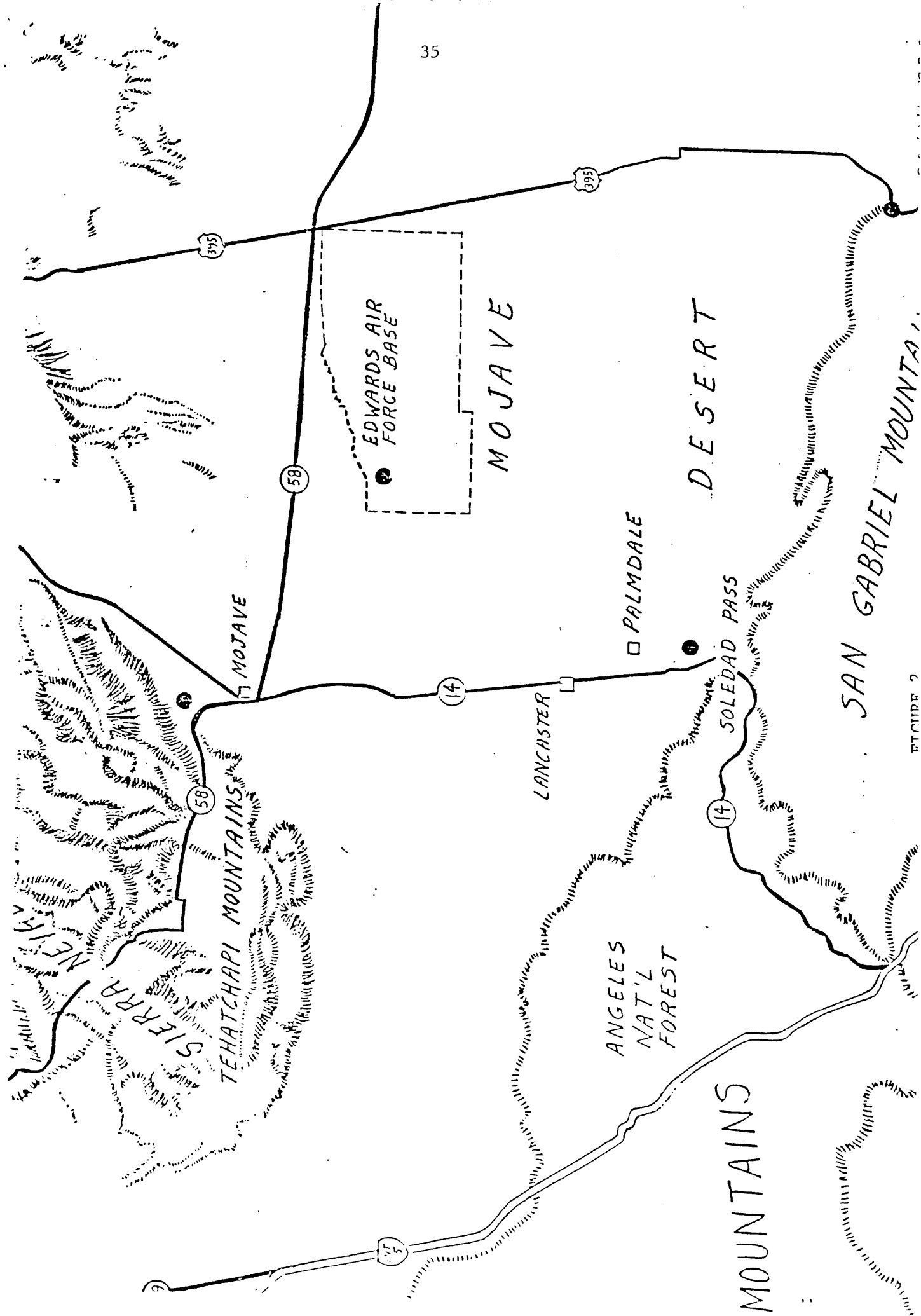
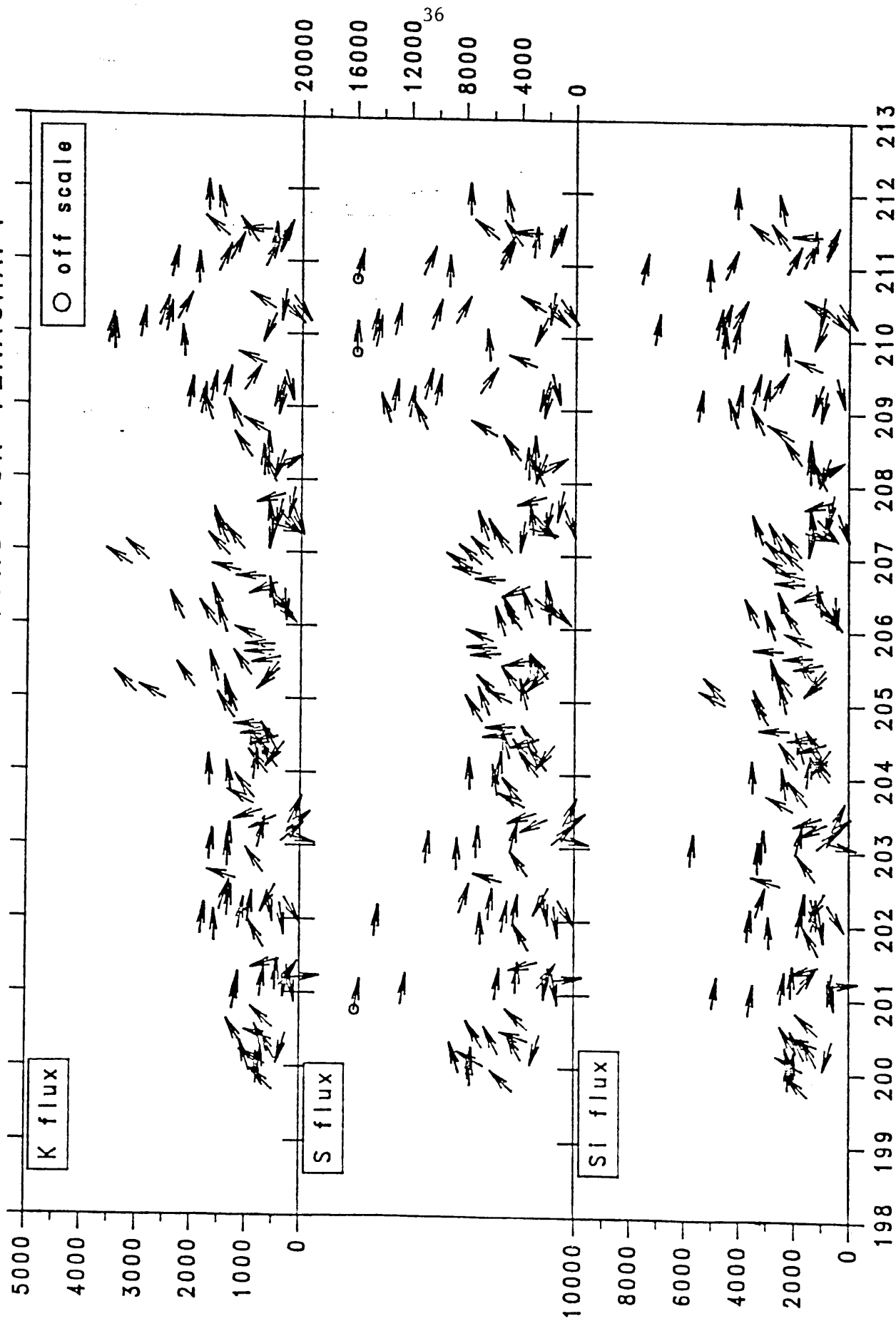


FIGURE 2

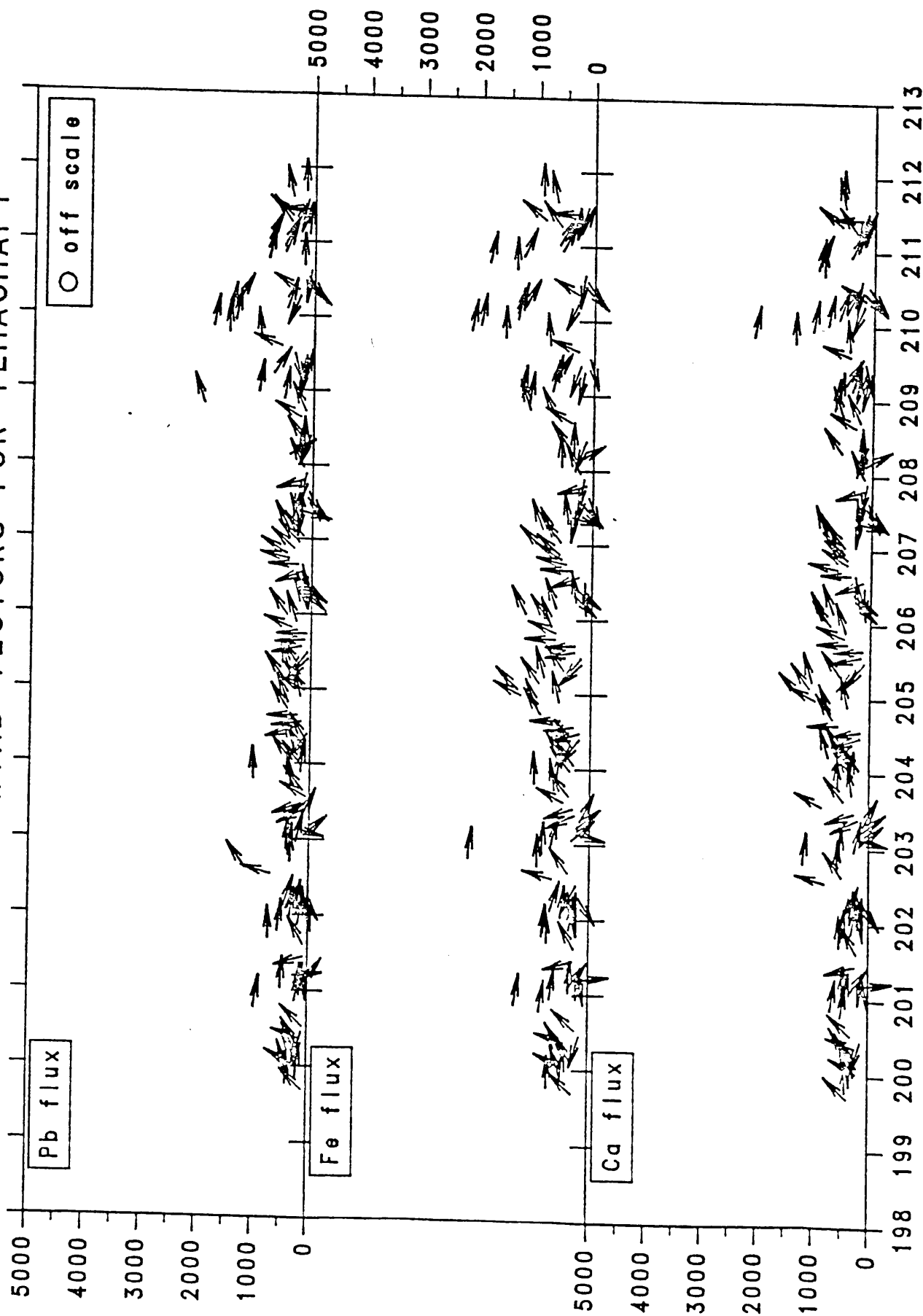
# FLUXES AND WIND VECTORS FOR TEHACHAPI



Day of Year

Figure 3

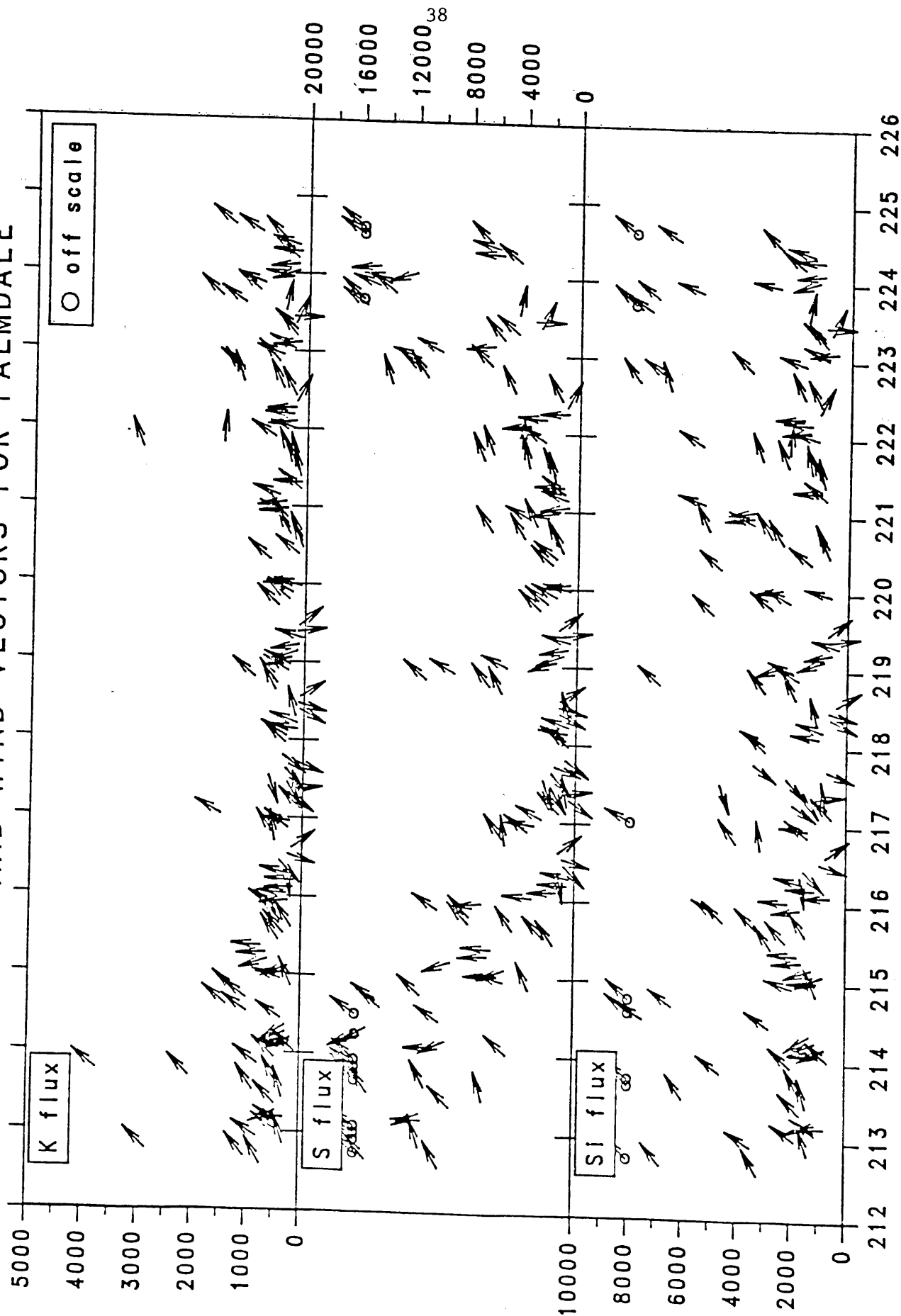
# FLUXES AND WIND VECTORS FOR TEHACHAPI



Day of Year

Figure 4

# FLUXES AND WIND VECTORS FOR PALMDALE



Day of Year

# FLUXES AND WIND VECTORS FOR PALMDALE

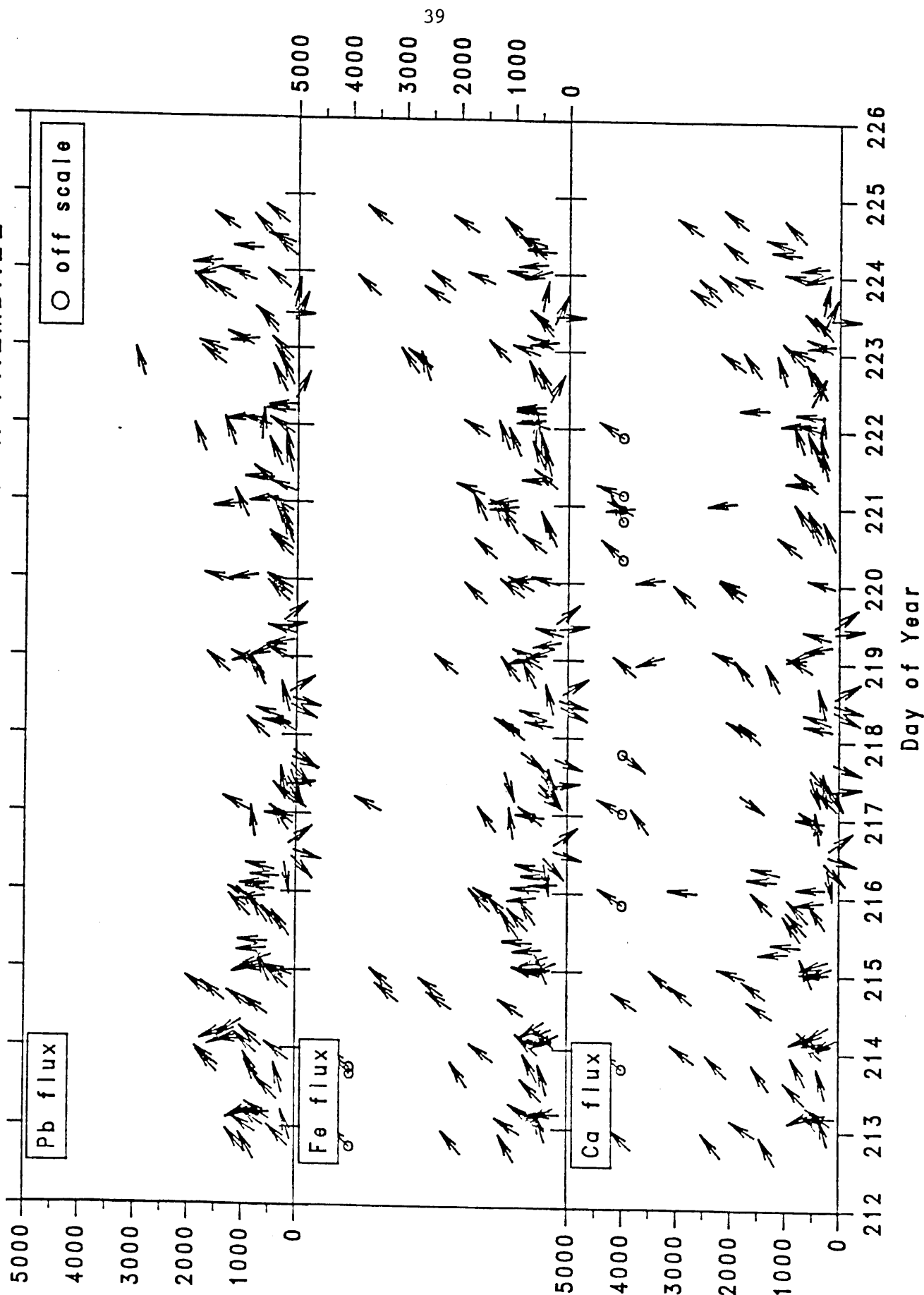


Figure 6

# FLUXES AND WIND VECTORS FOR CAJON

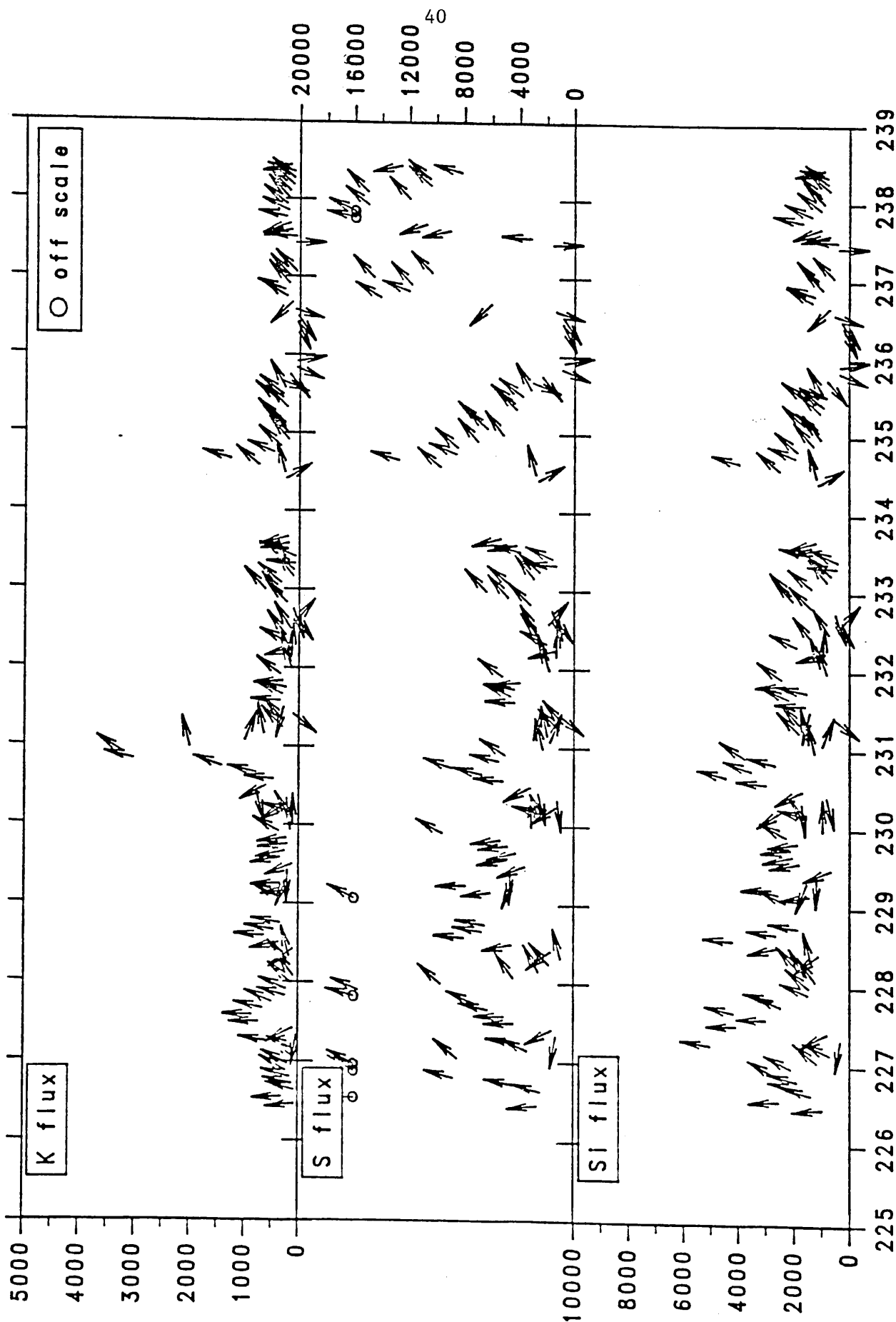


Figure 7



# FLUXES AND WIND VECTORS FOR CAJON

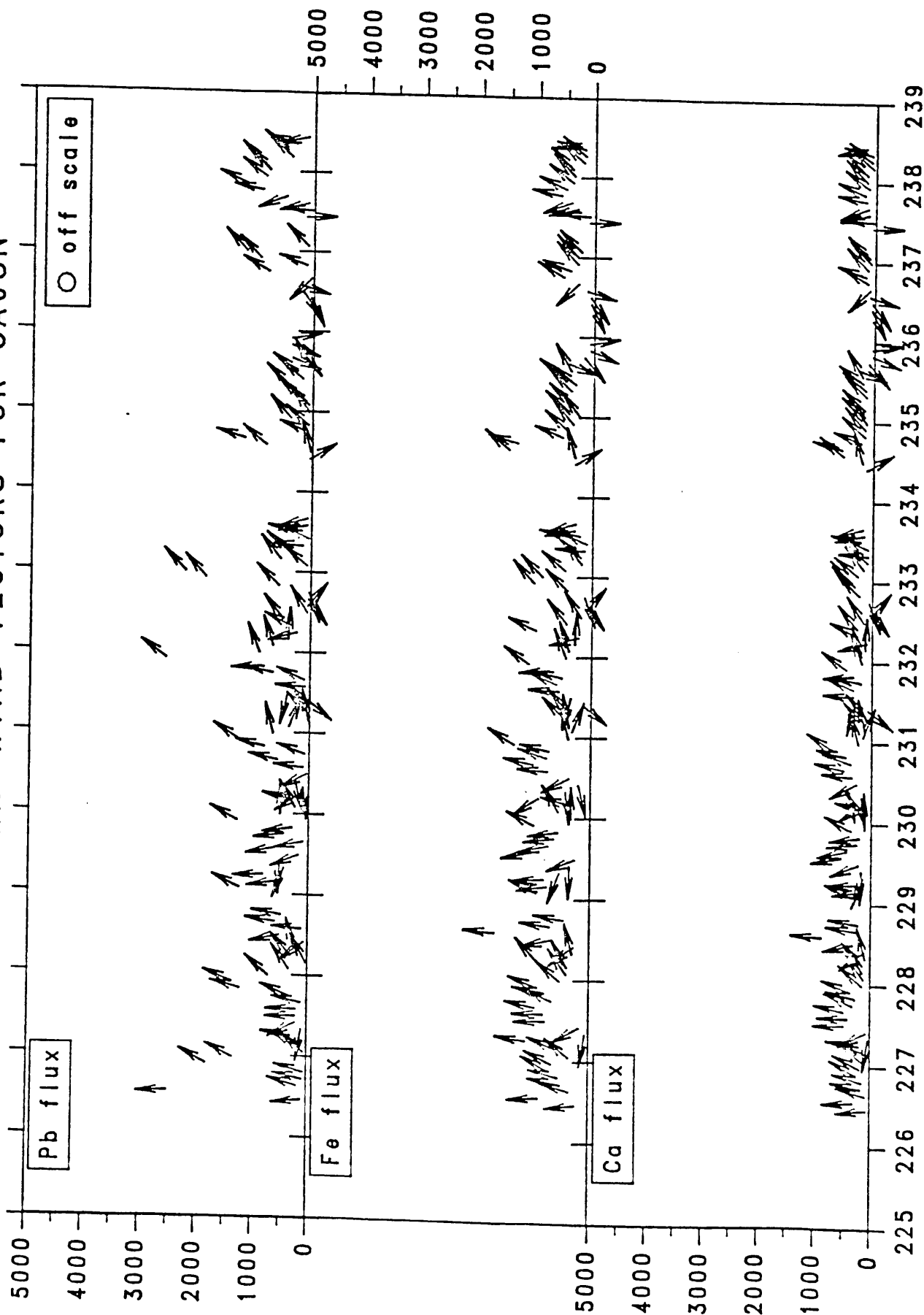


Figure 8

# MEANS AND STANDARD DEVIATIONS

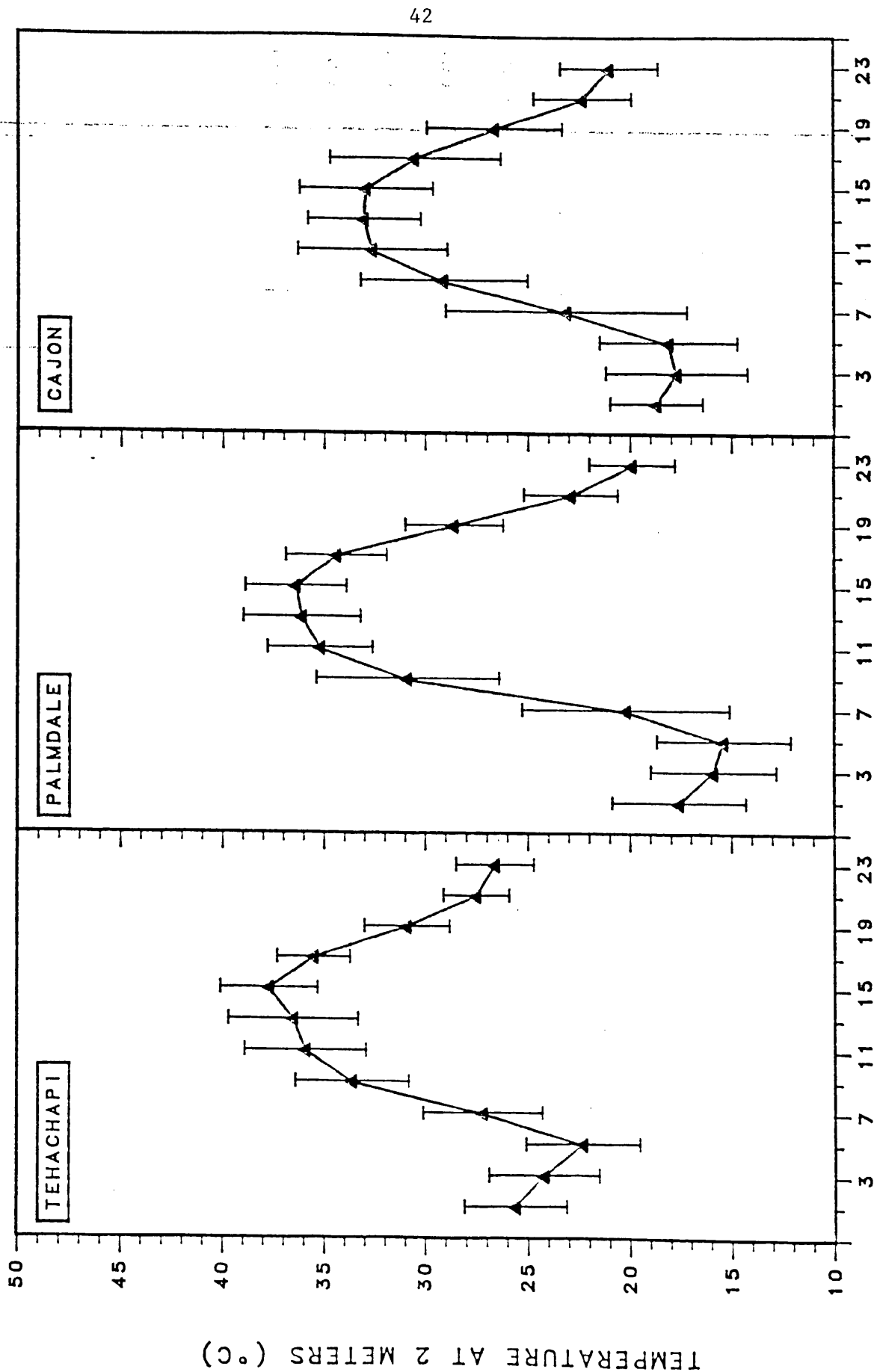


Figure 9

# MEANS AND STANDARD DEVIATIONS

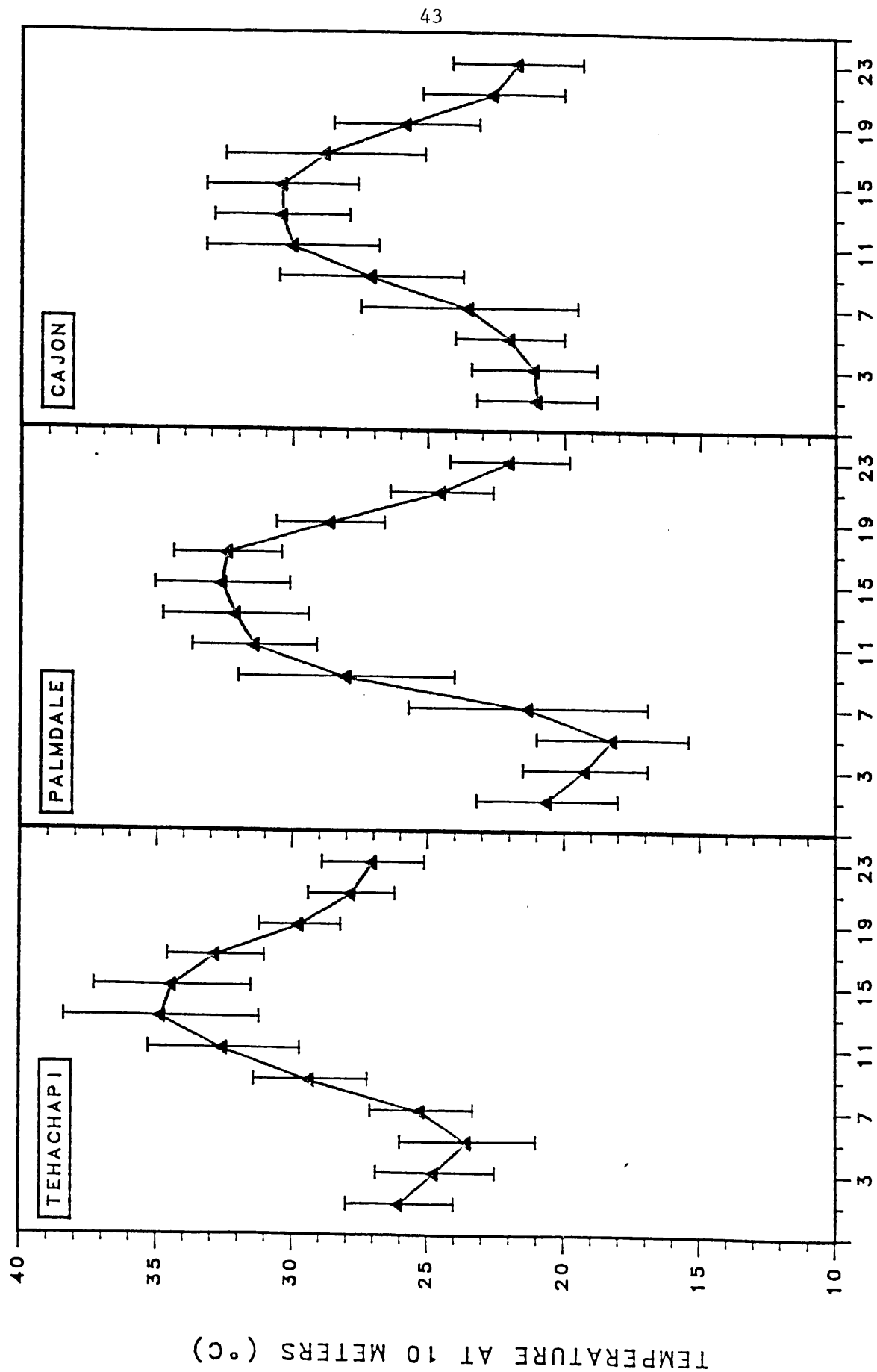


Figure 10

# MEANS AND STANDARD DEVIATIONS

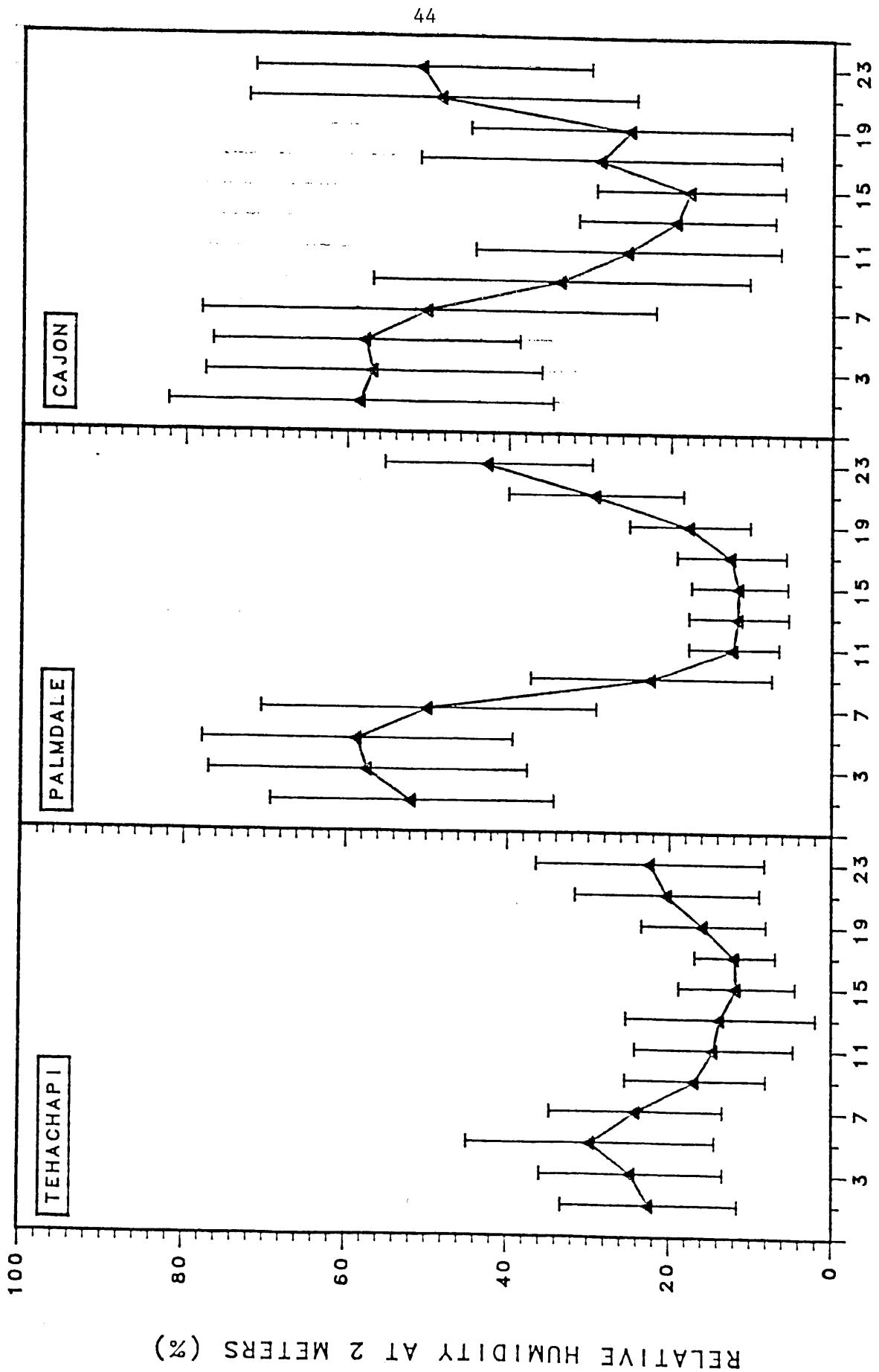


Figure 11

# MEANS AND STANDARD DEVIATIONS

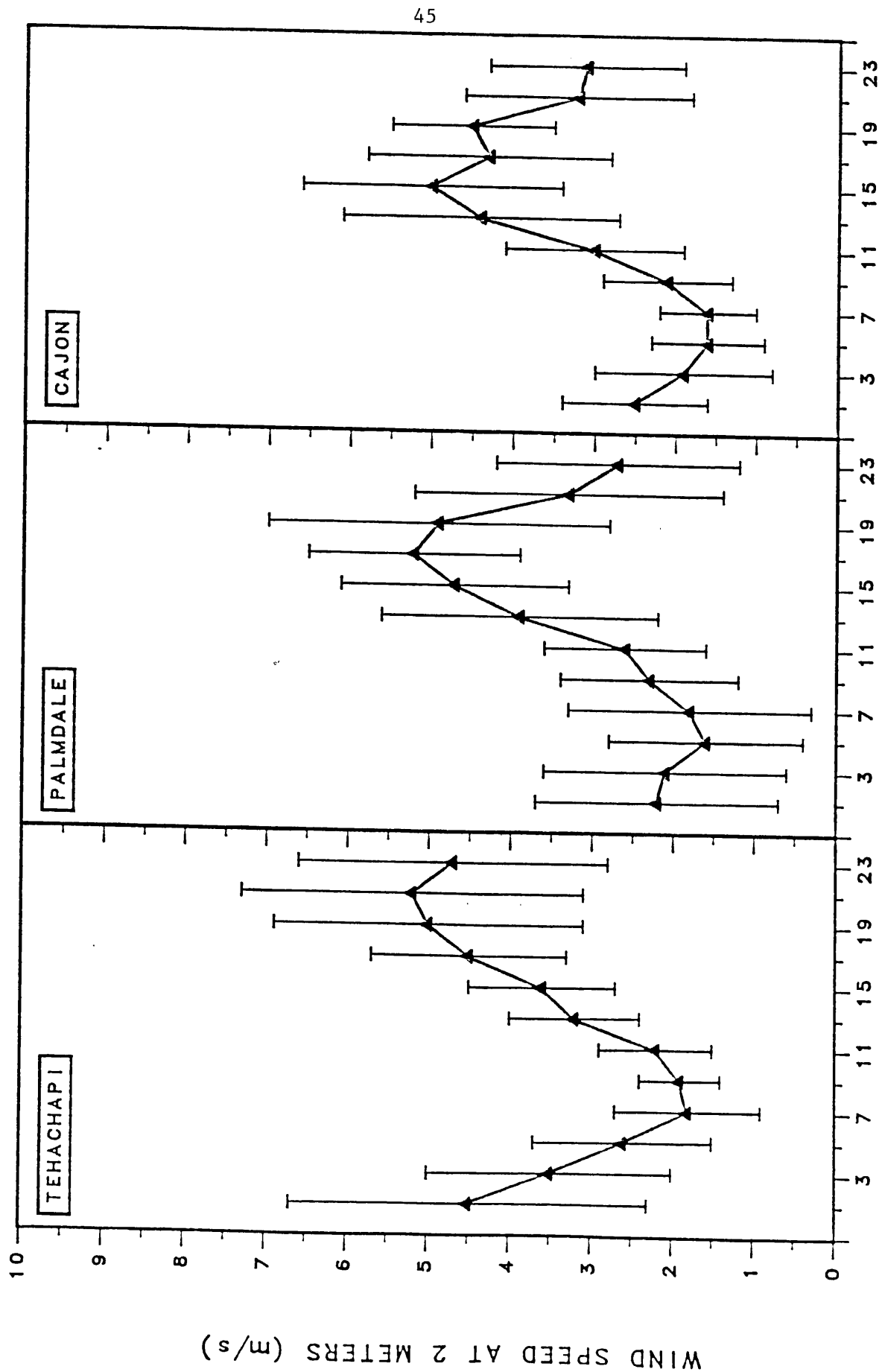


Figure 12

# MEANS AND STANDARD DEVIATIONS

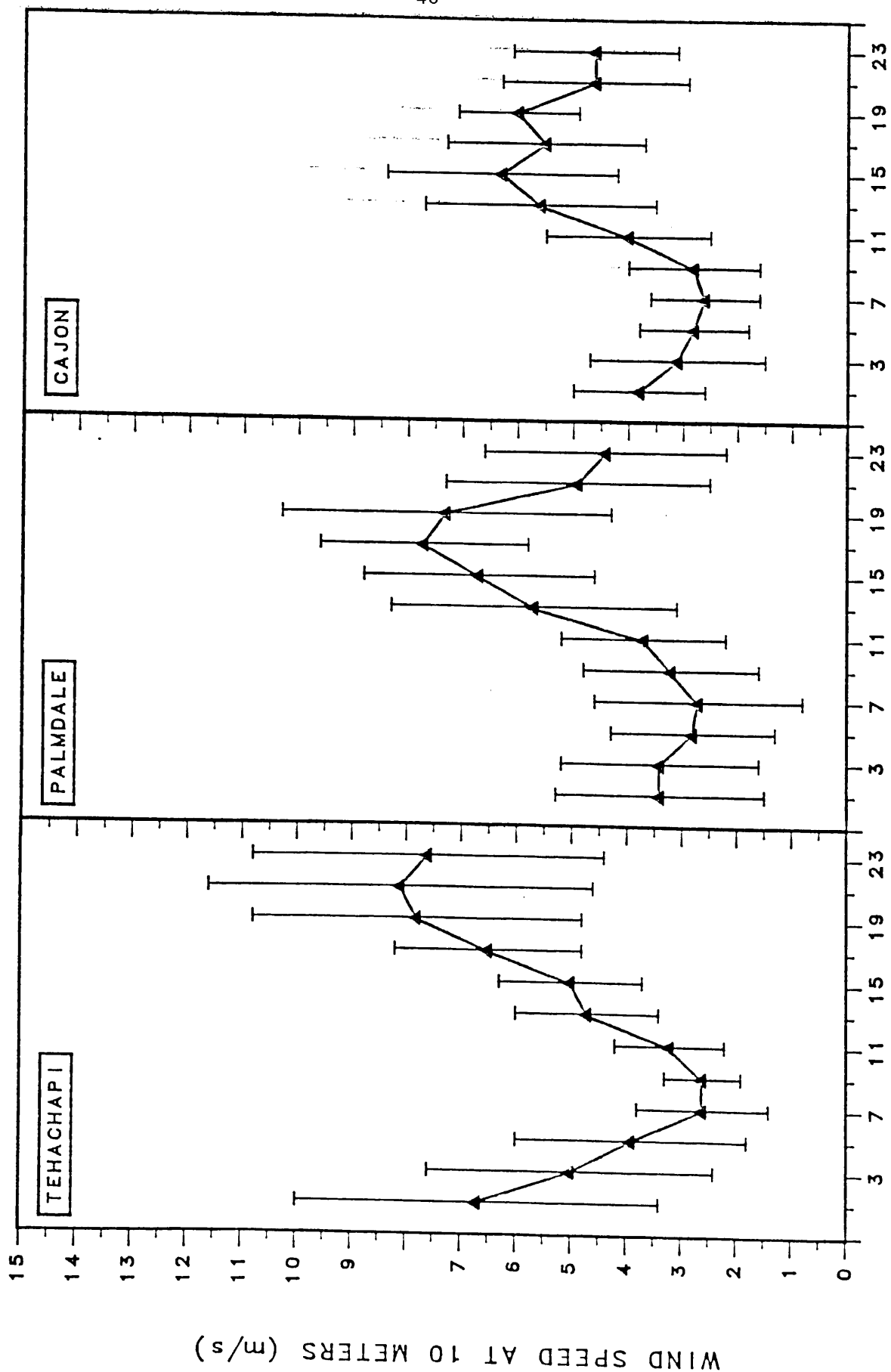


Figure 13

# MEANS AND STANDARD DEVIATIONS

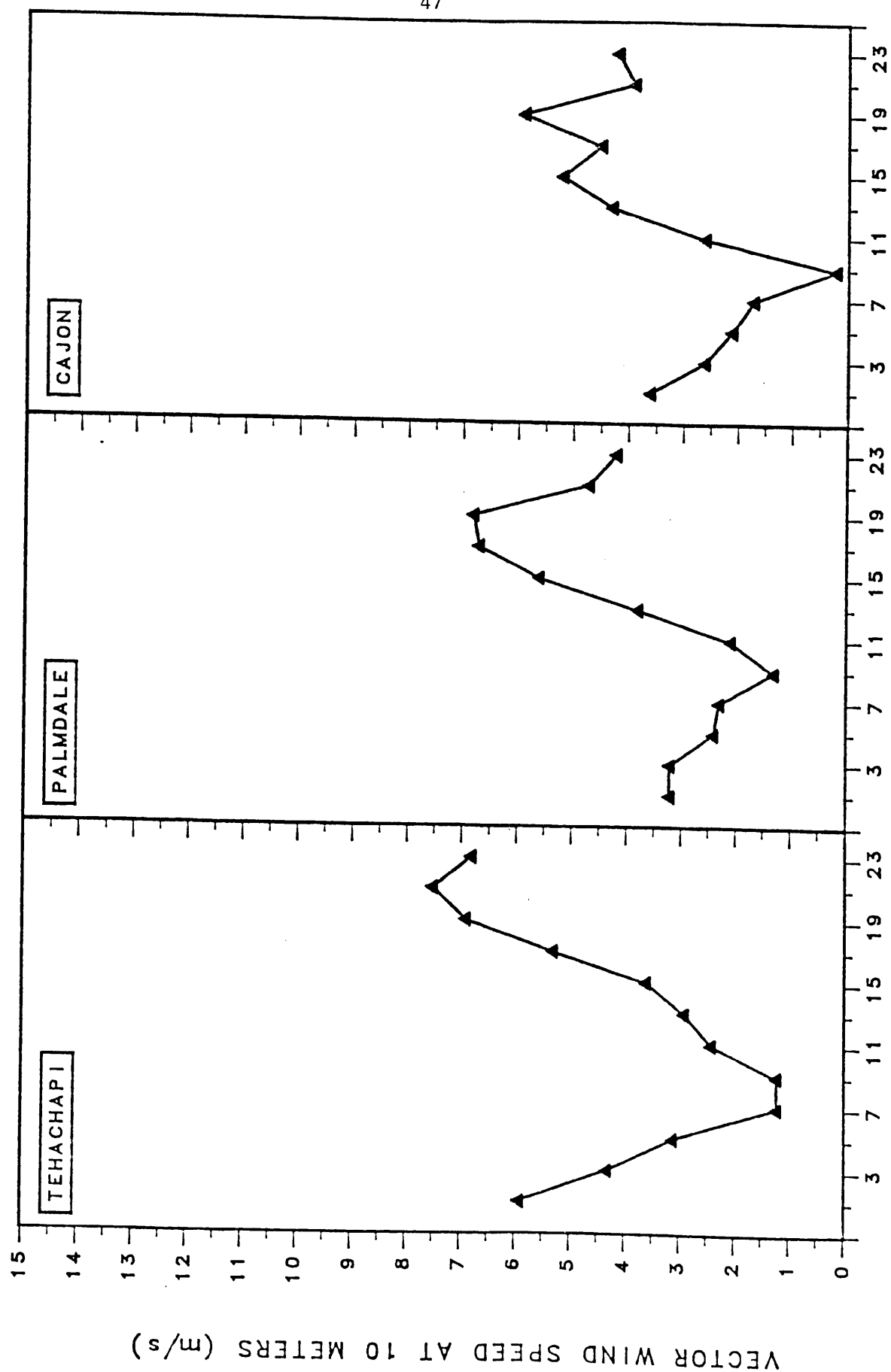


Figure 14

# MEANS AND STANDARD DEVIATIONS

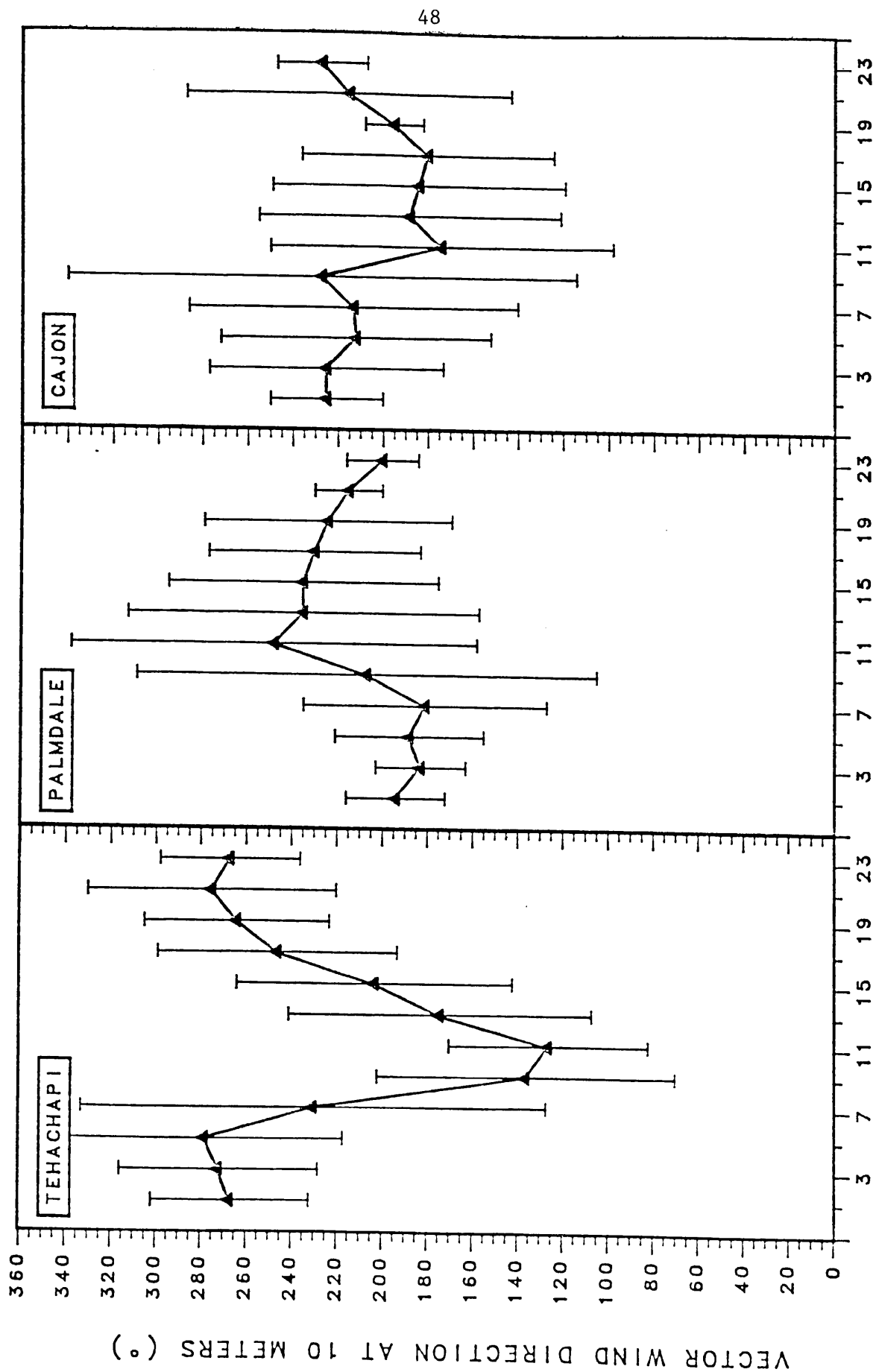


Figure 15



# MEANS AND STANDARD DEVIATIONS

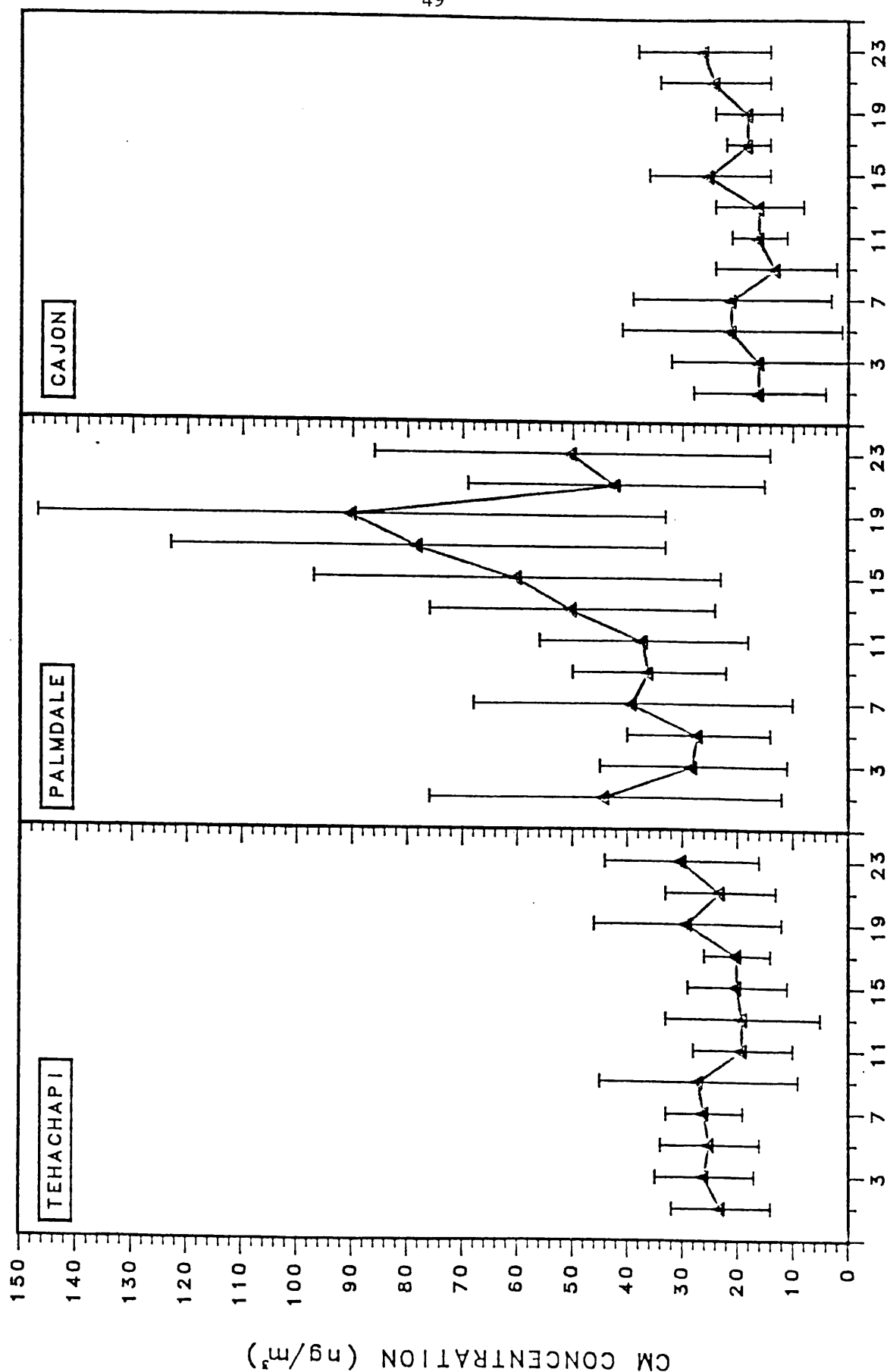


Figure 16

# MEANS AND STANDARD DEVIATIONS

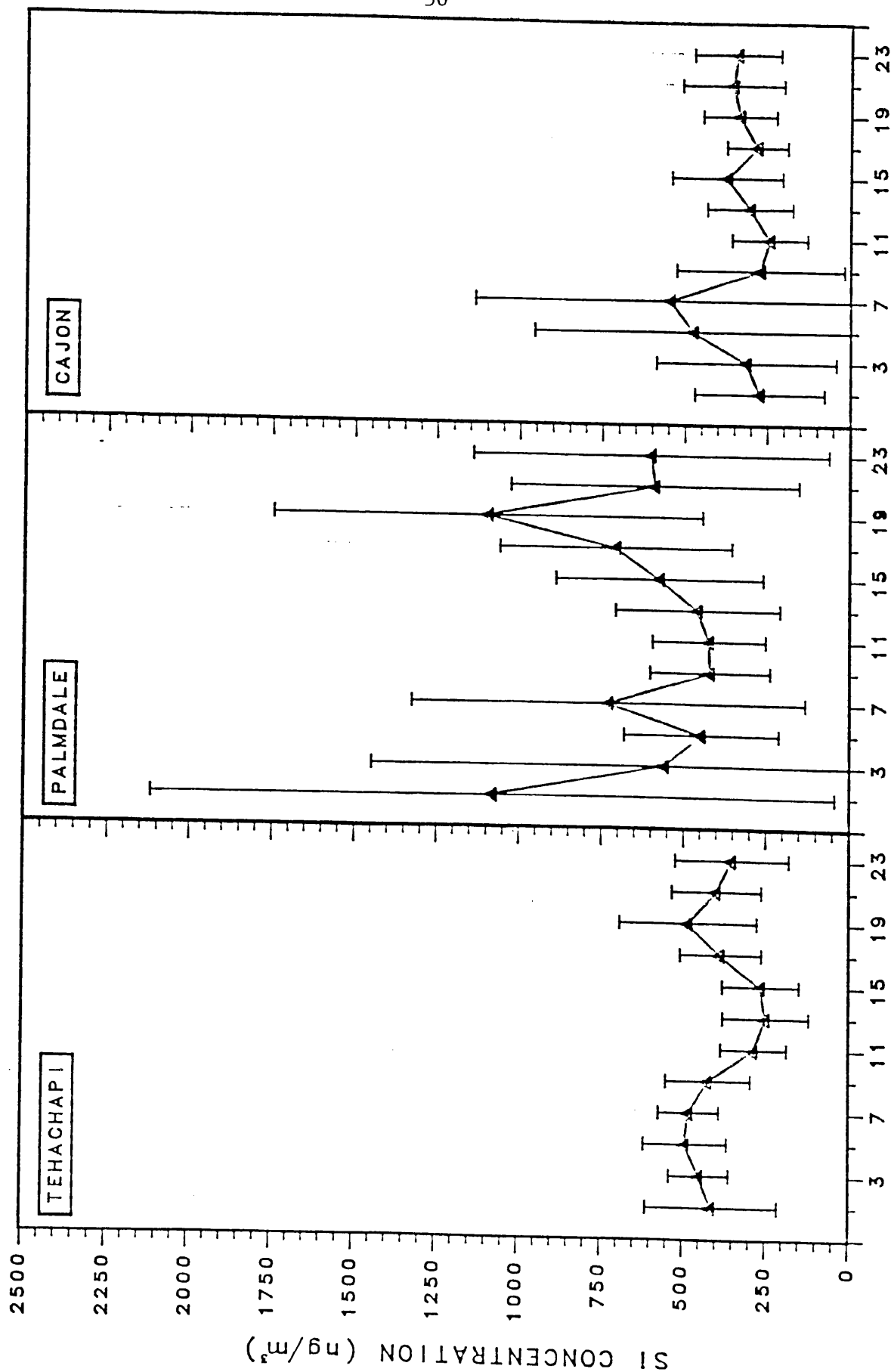


Figure 17

MEANS AND STANDARD DEVIATIONS

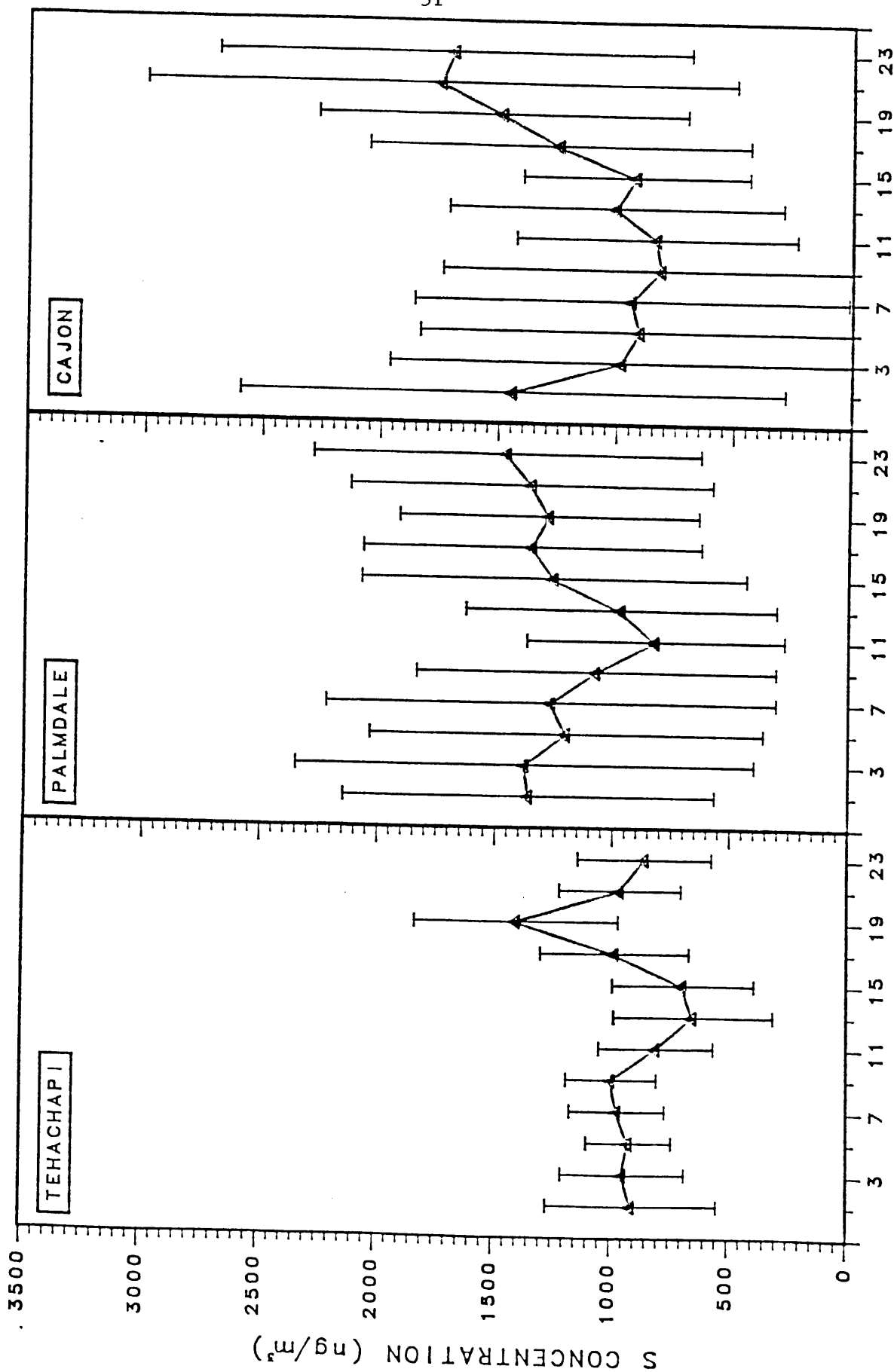


Figure 18

# MEANS AND STANDARD DEVIATIONS

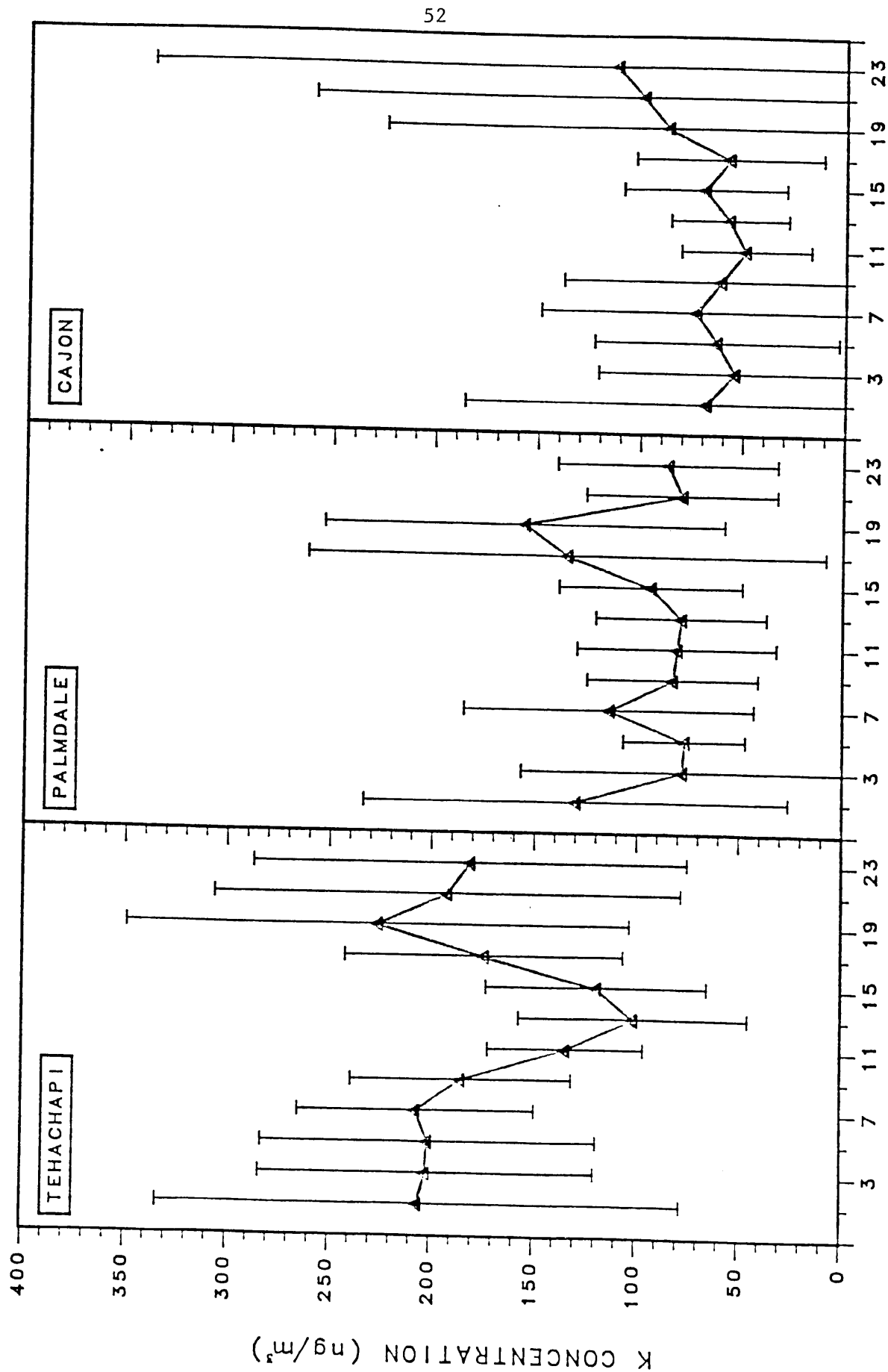
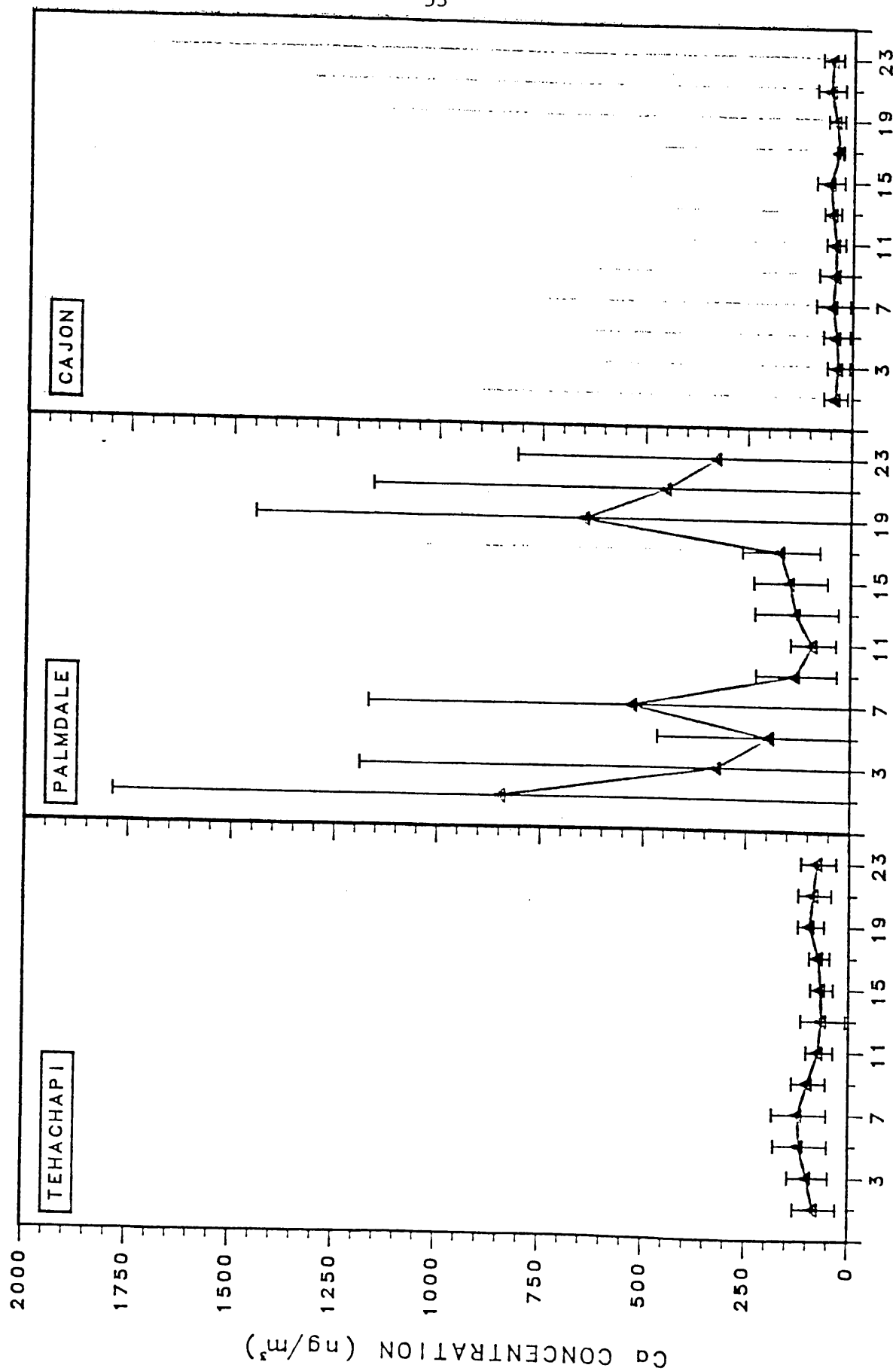


Figure 19

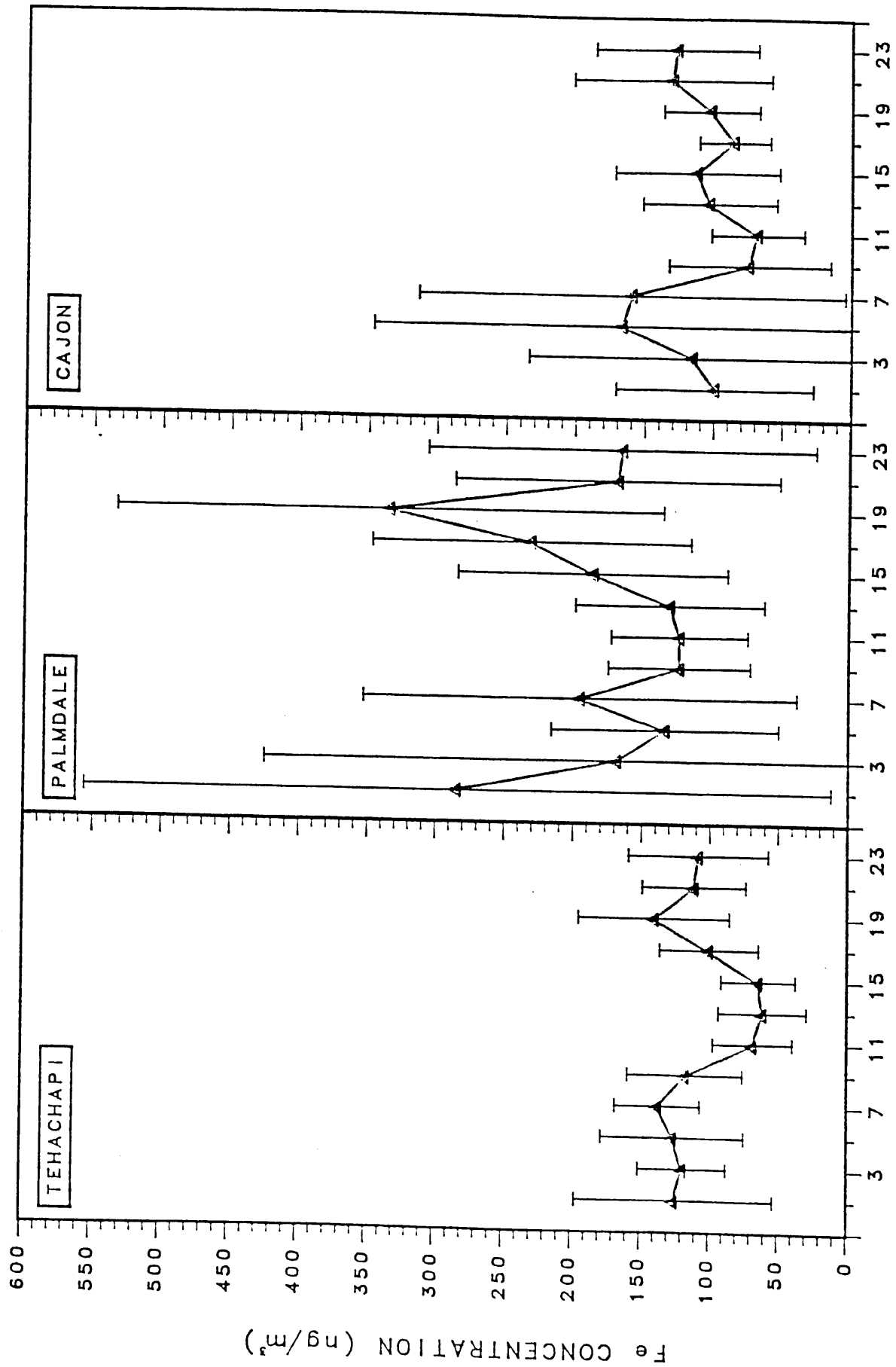
# MEANS AND STANDARD DEVIATIONS



TIME (PST)

Figure 20

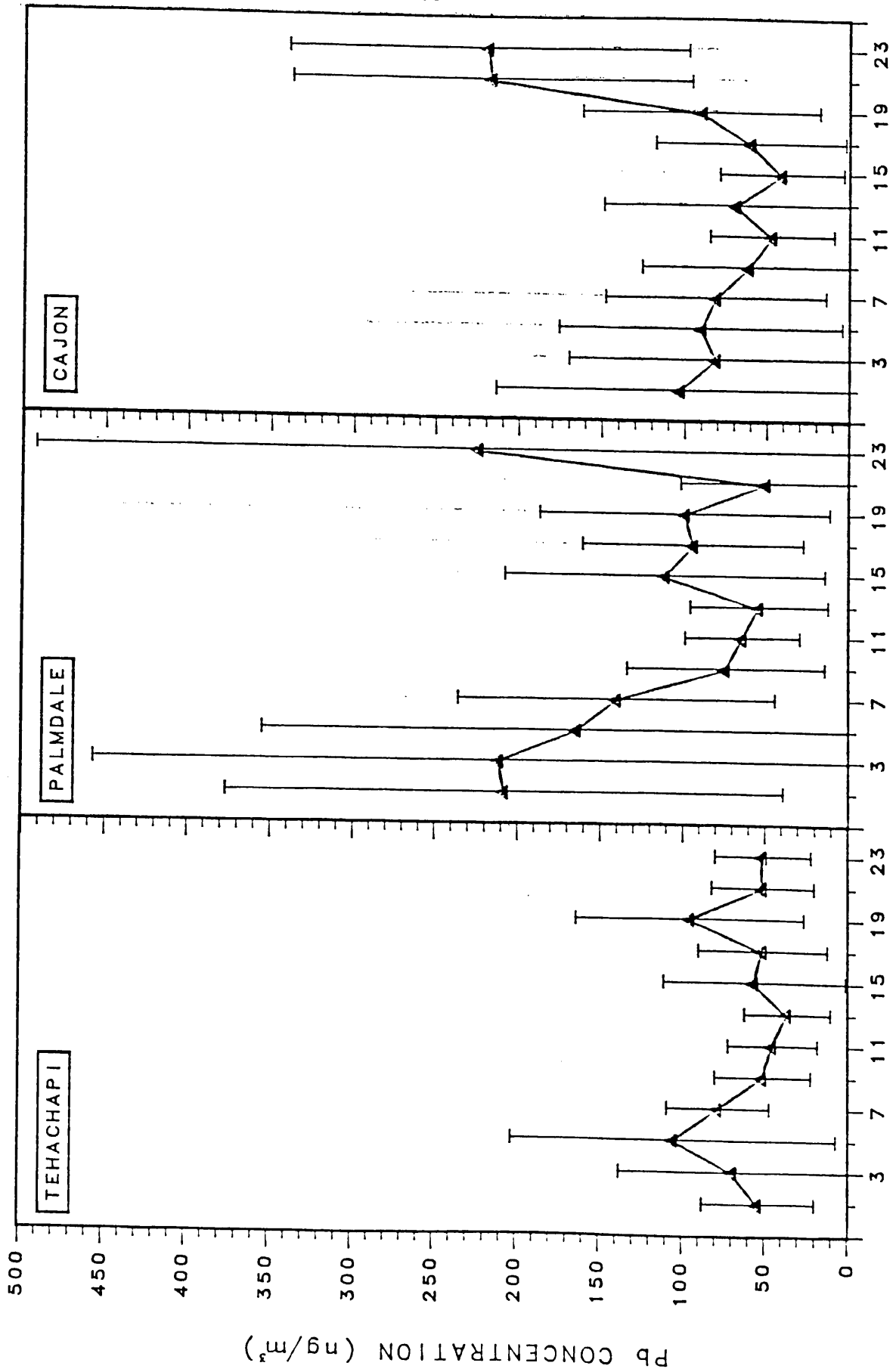
## MEANS AND STANDARD DEVIATIONS



TIME (PST)

Figure 21

## MEANS AND STANDARD DEVIATIONS



TIME (PST)

Figure 22

## MEANS AND STANDARD DEVIATIONS

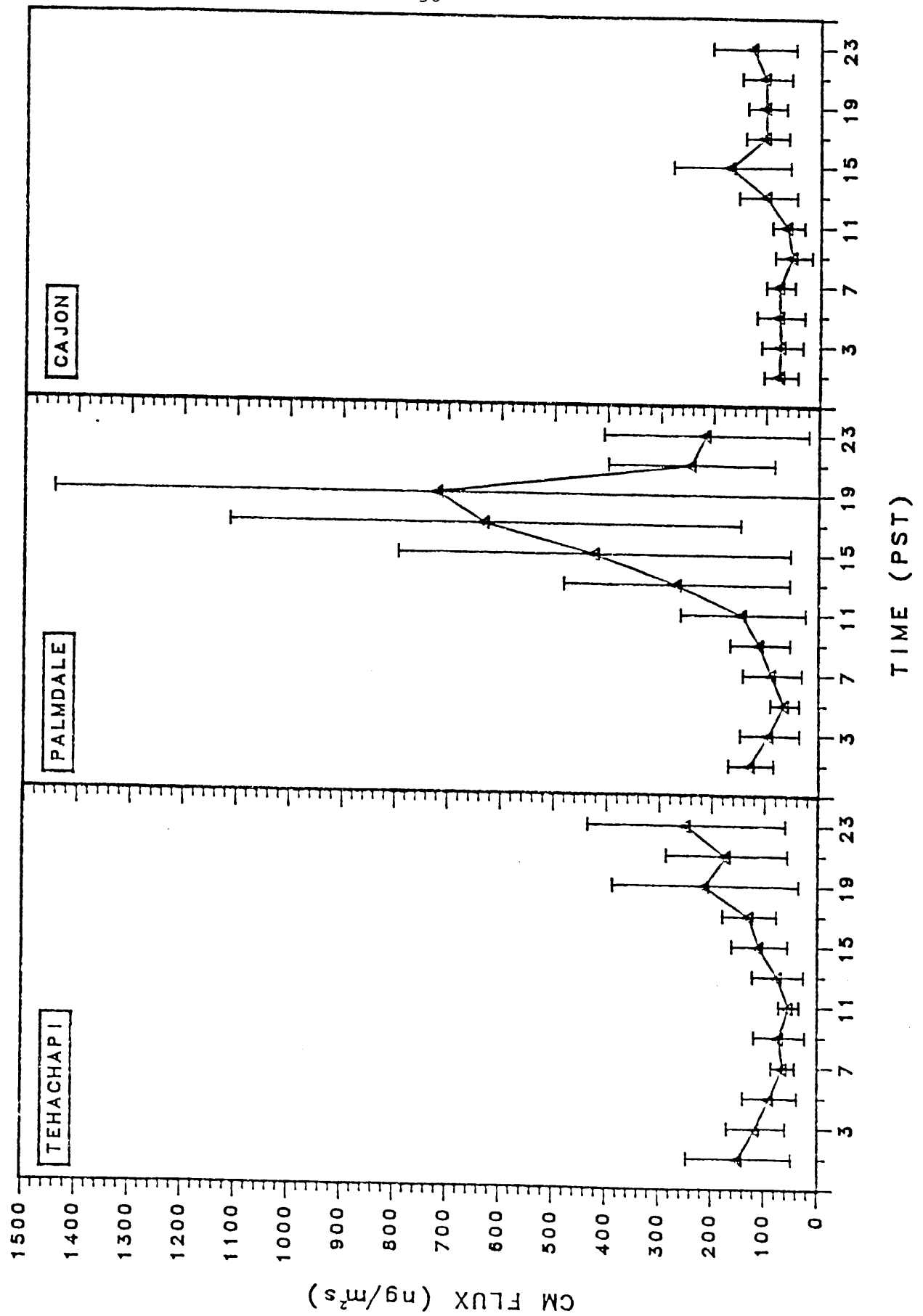


Figure 23



# MEANS AND STANDARD DEVIATIONS

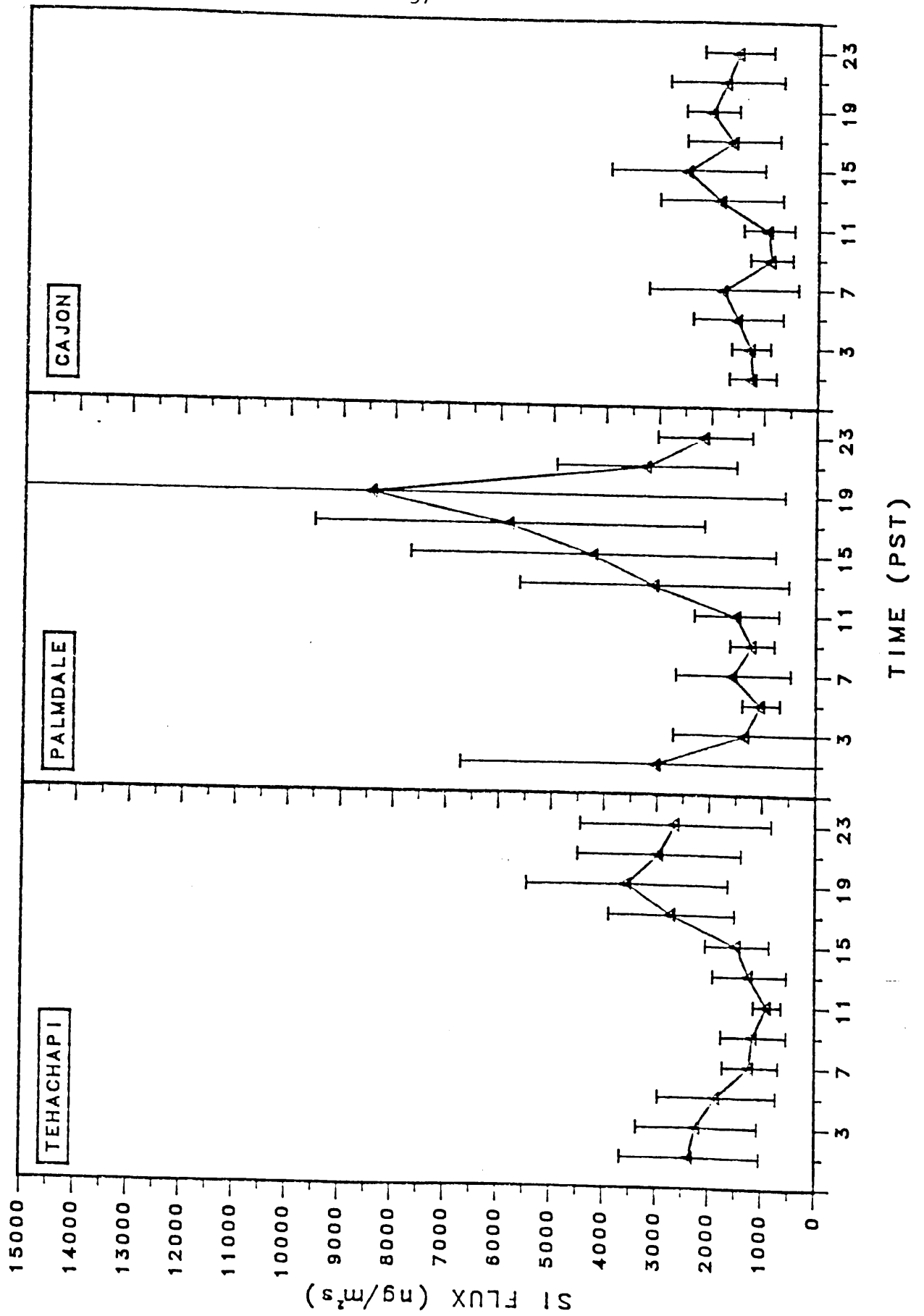
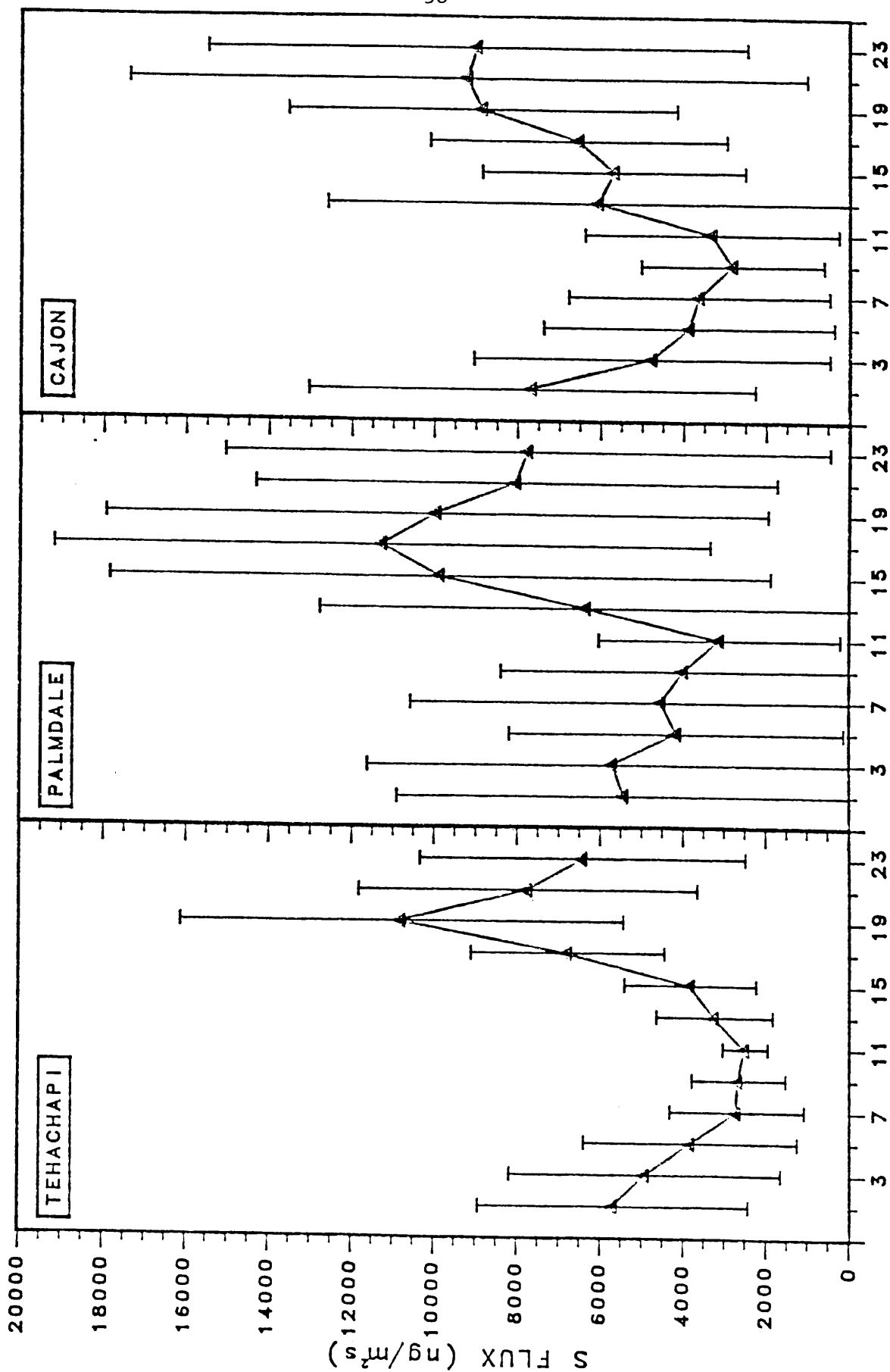


Figure 24

# MEANS AND STANDARD DEVIATIONS



TIME (PST)

Figure 25

# MEANS AND STANDARD DEVIATIONS

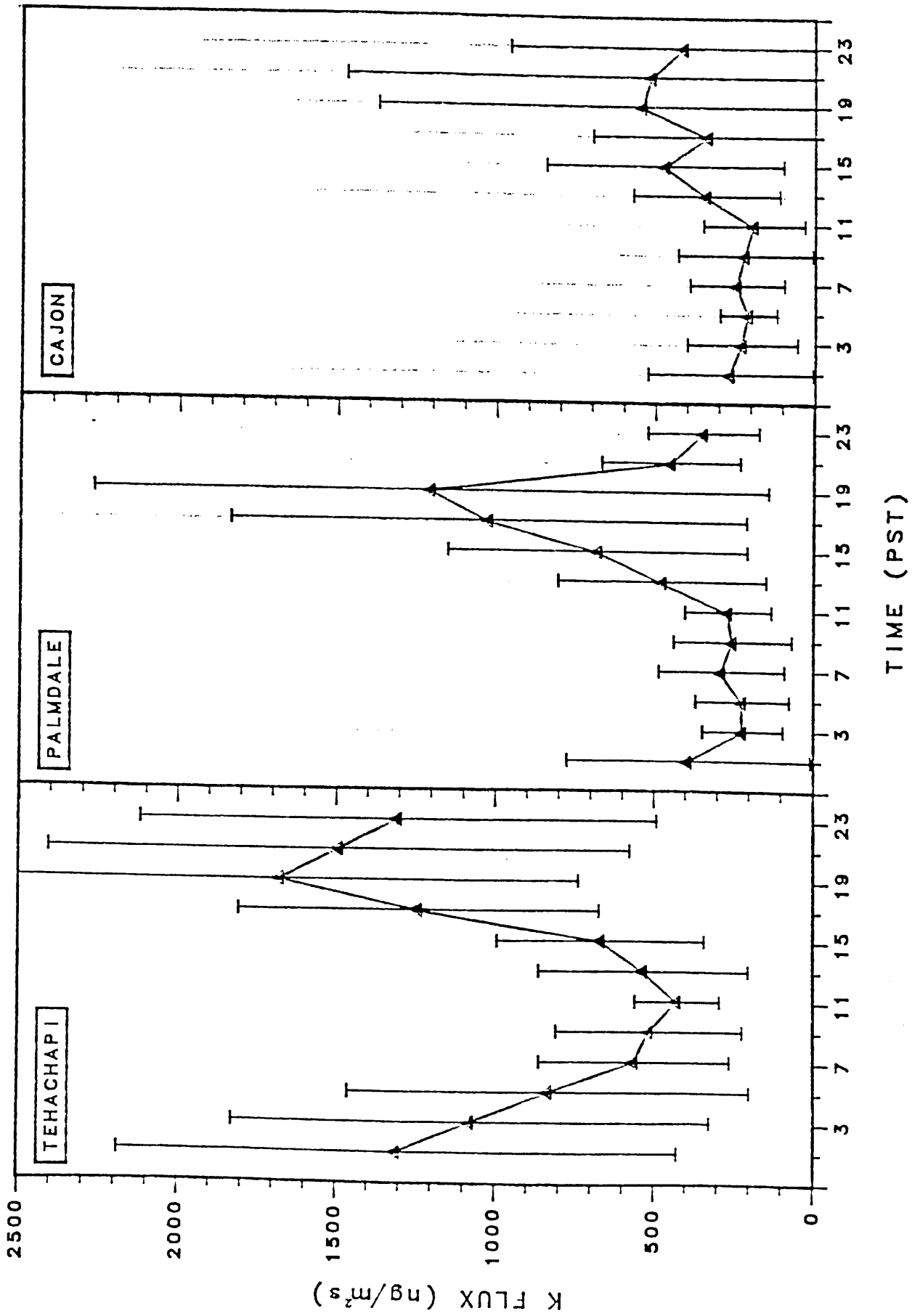
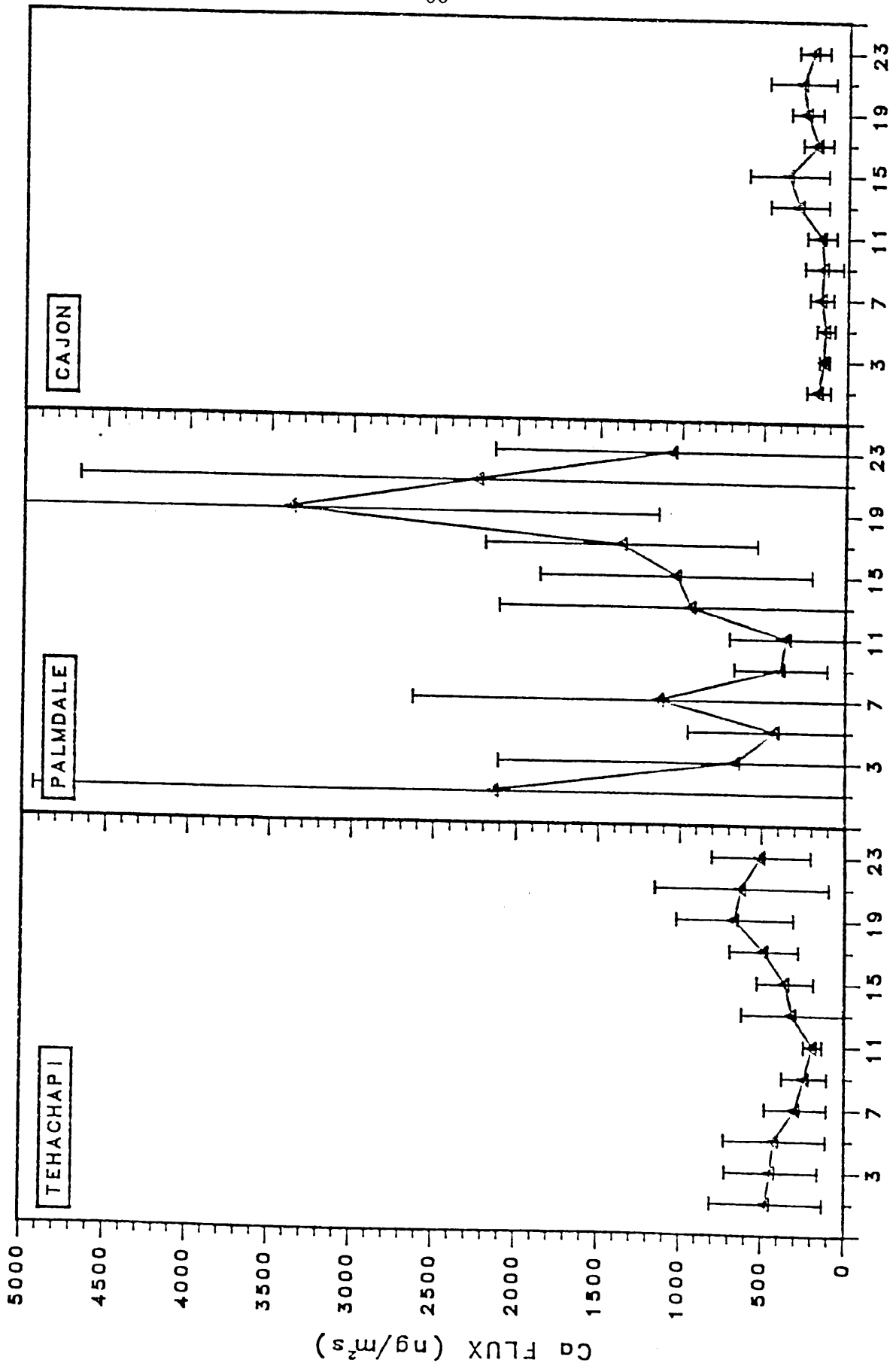


Figure 26

# MEANS AND STANDARD DEVIATIONS



TIME (PST)

Figure 27

# MEANS AND STANDARD DEVIATIONS

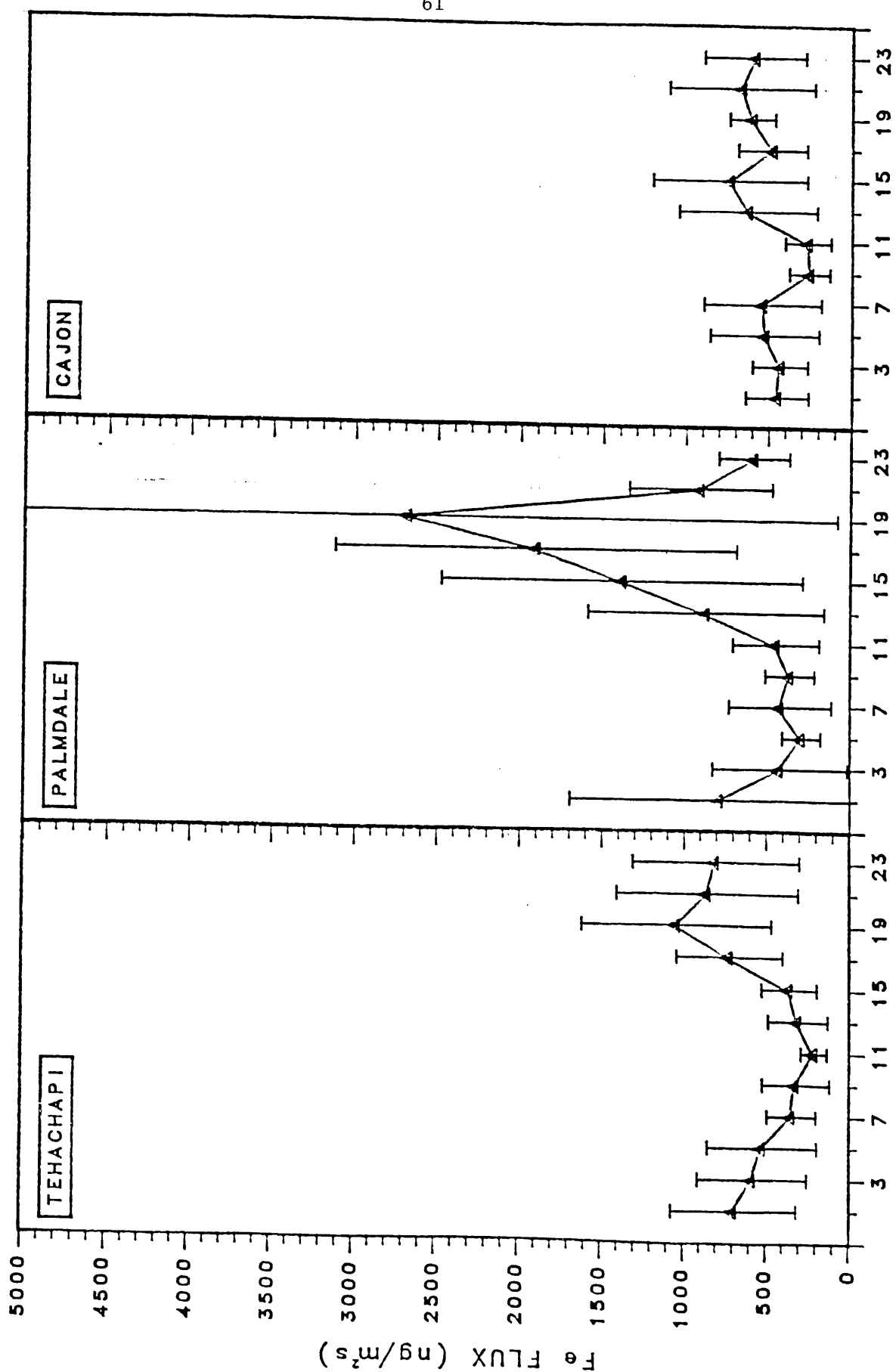
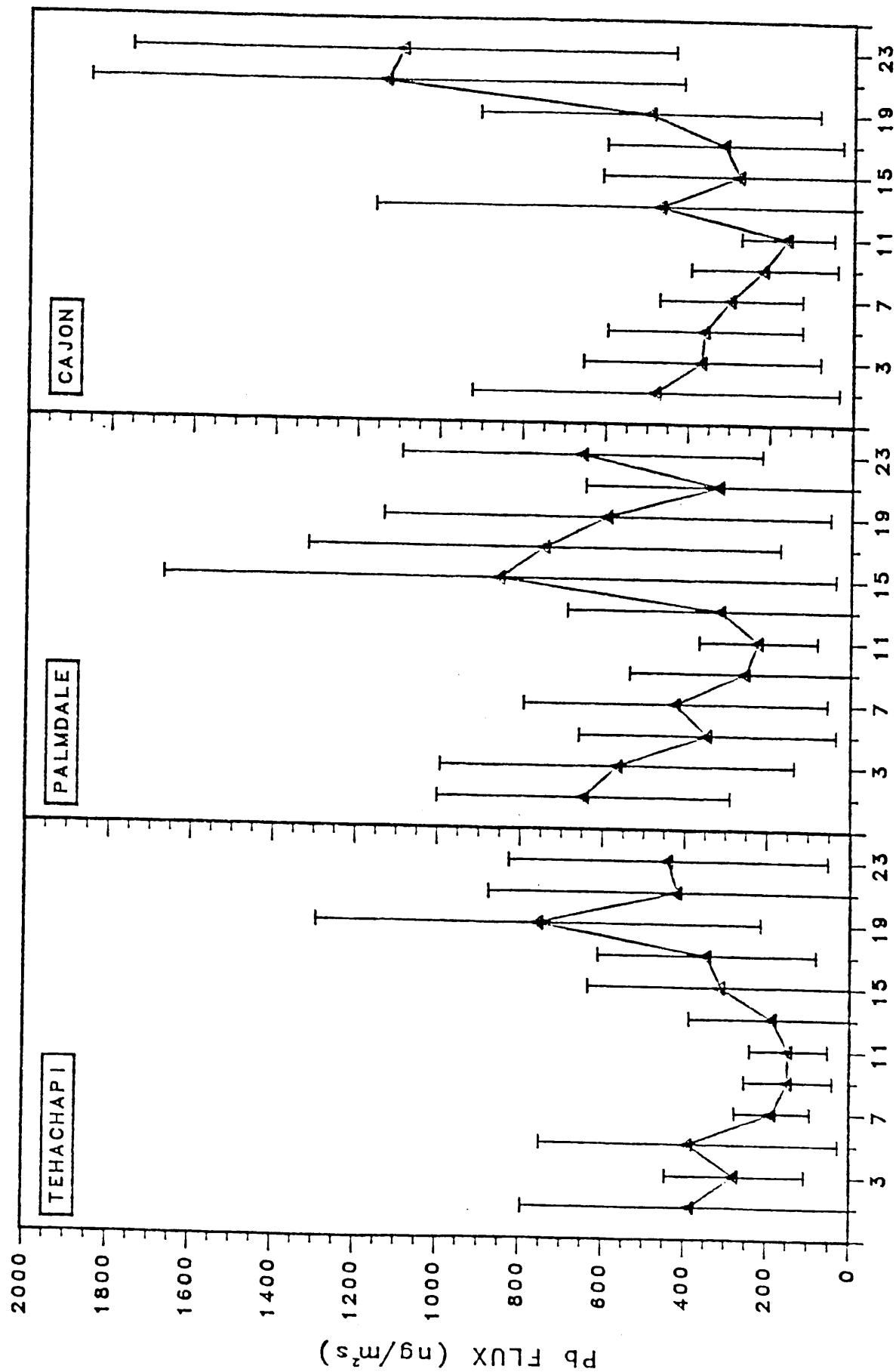


Figure 28

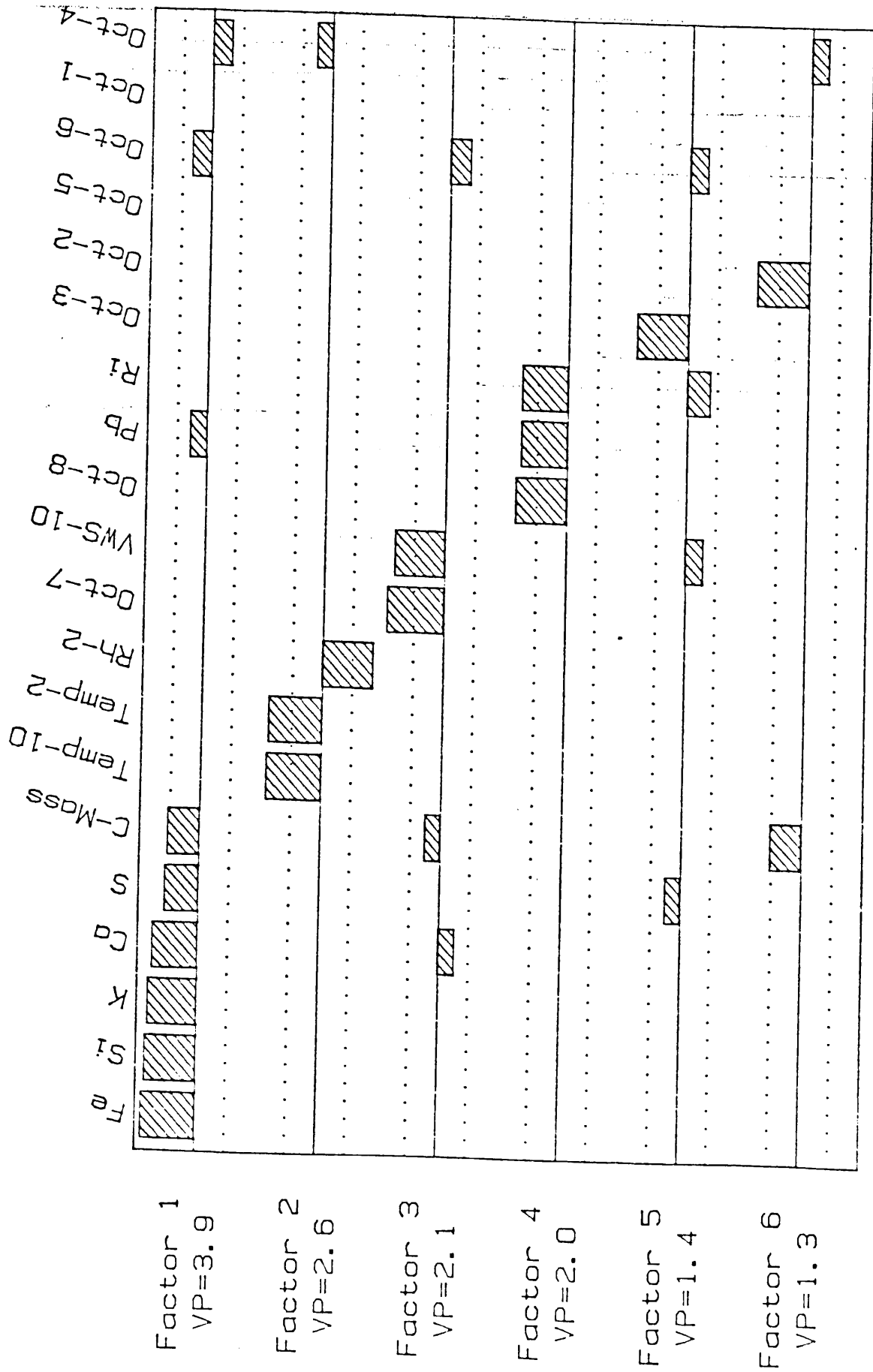
## MEANS AND STANDARD DEVIATIONS



TIME (PST)

Figure 29

## TEHACHAPI



Eight-sector Quasi-binary Factor Analysis.

Tehachapi

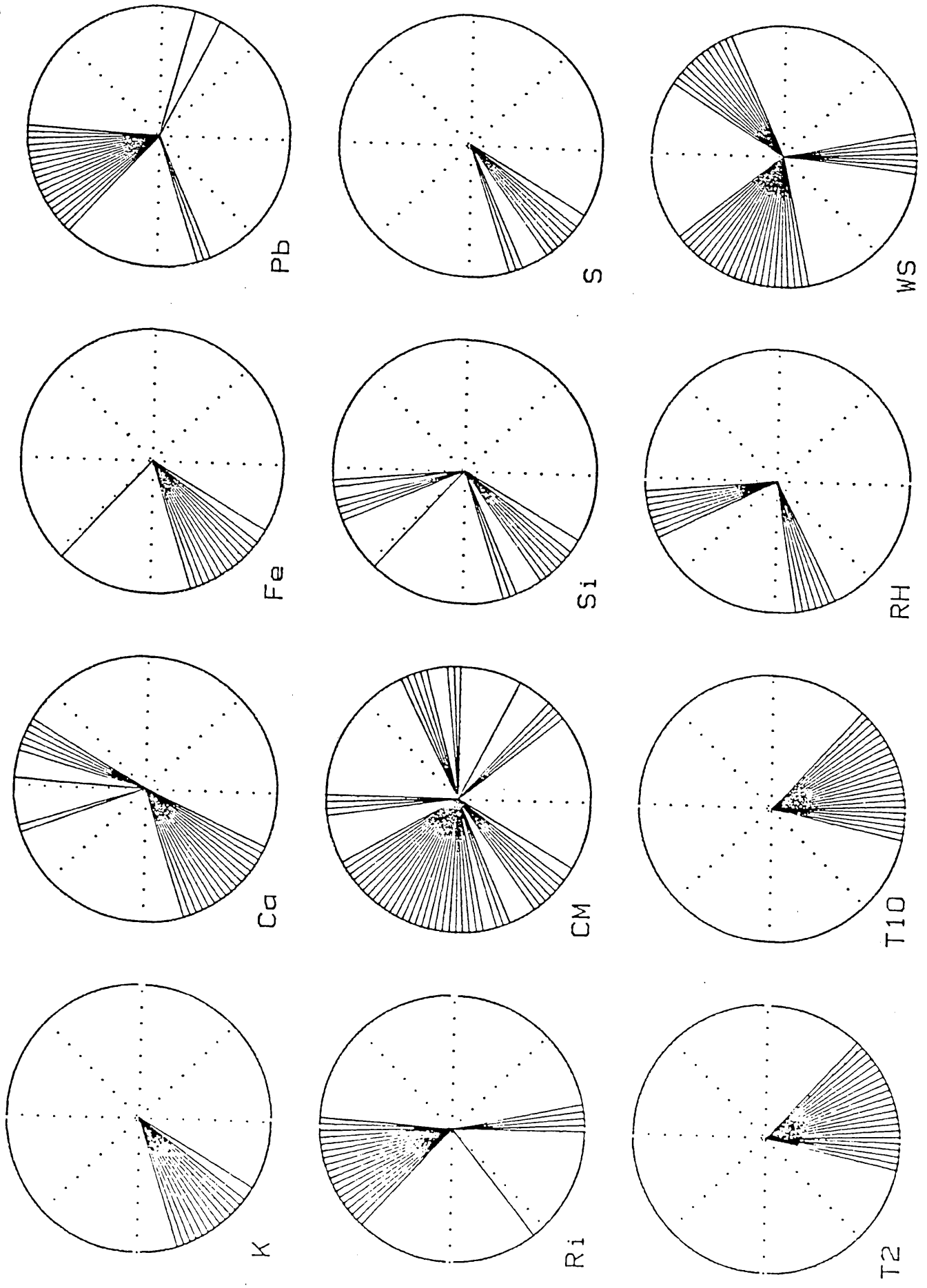
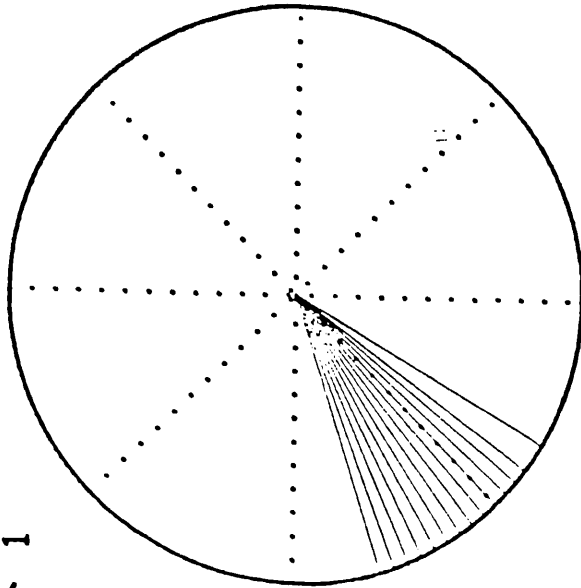


Figure 31

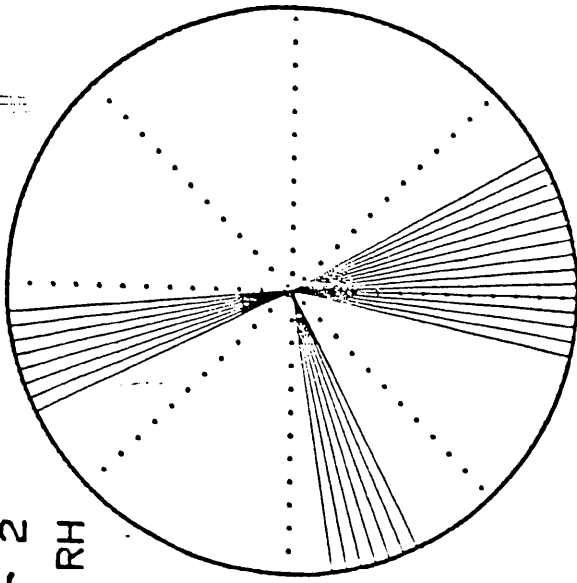


## TEHACHAPI

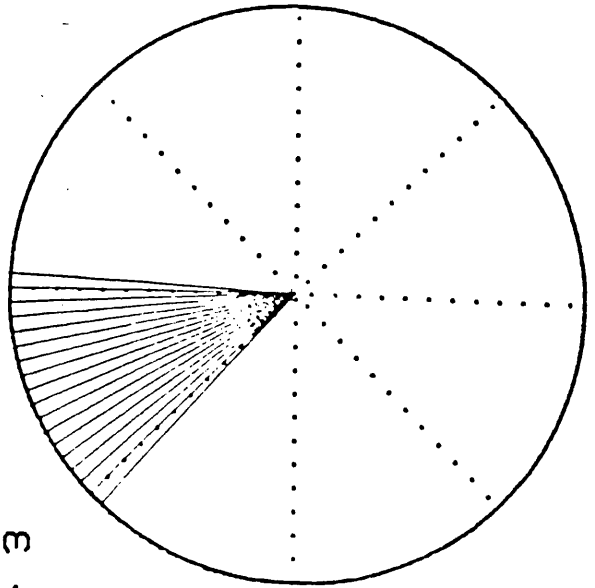
Factor 1  
Ca, K



Factor 2  
Temp, RH



Factor 3  
Pb, Ri



Factor 4  
Pb, S

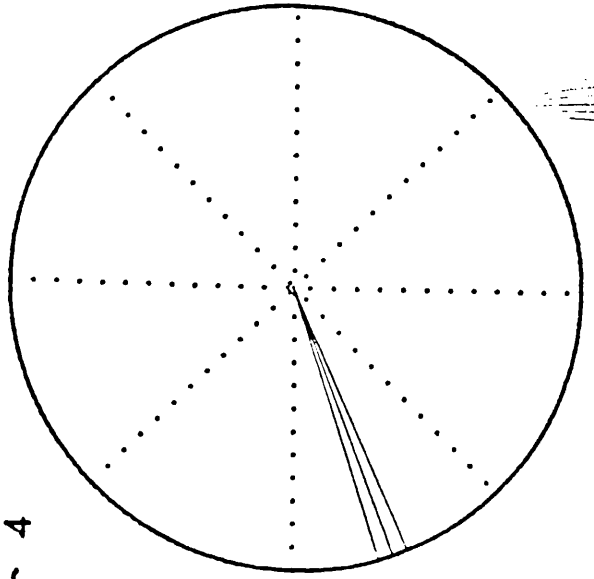
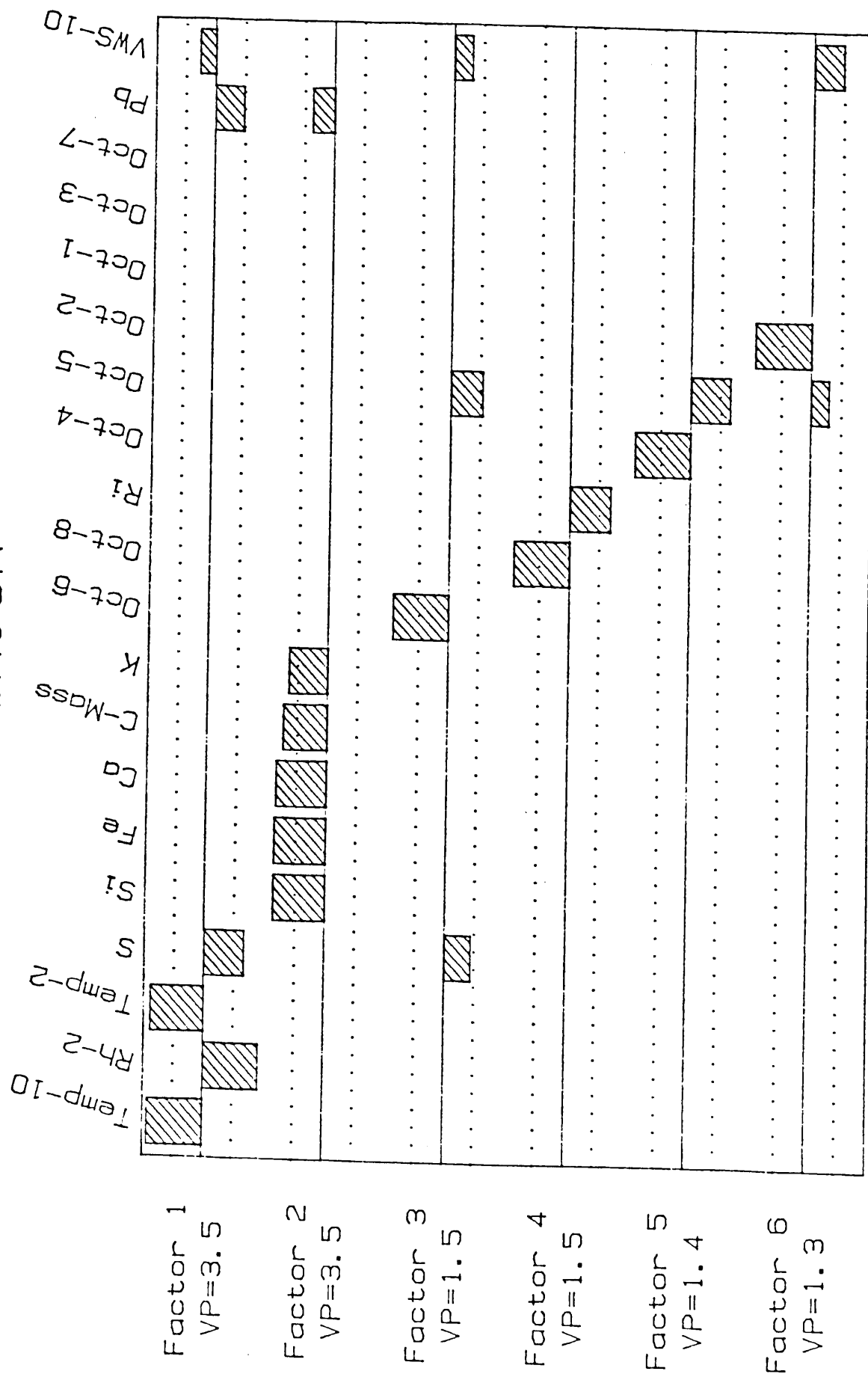
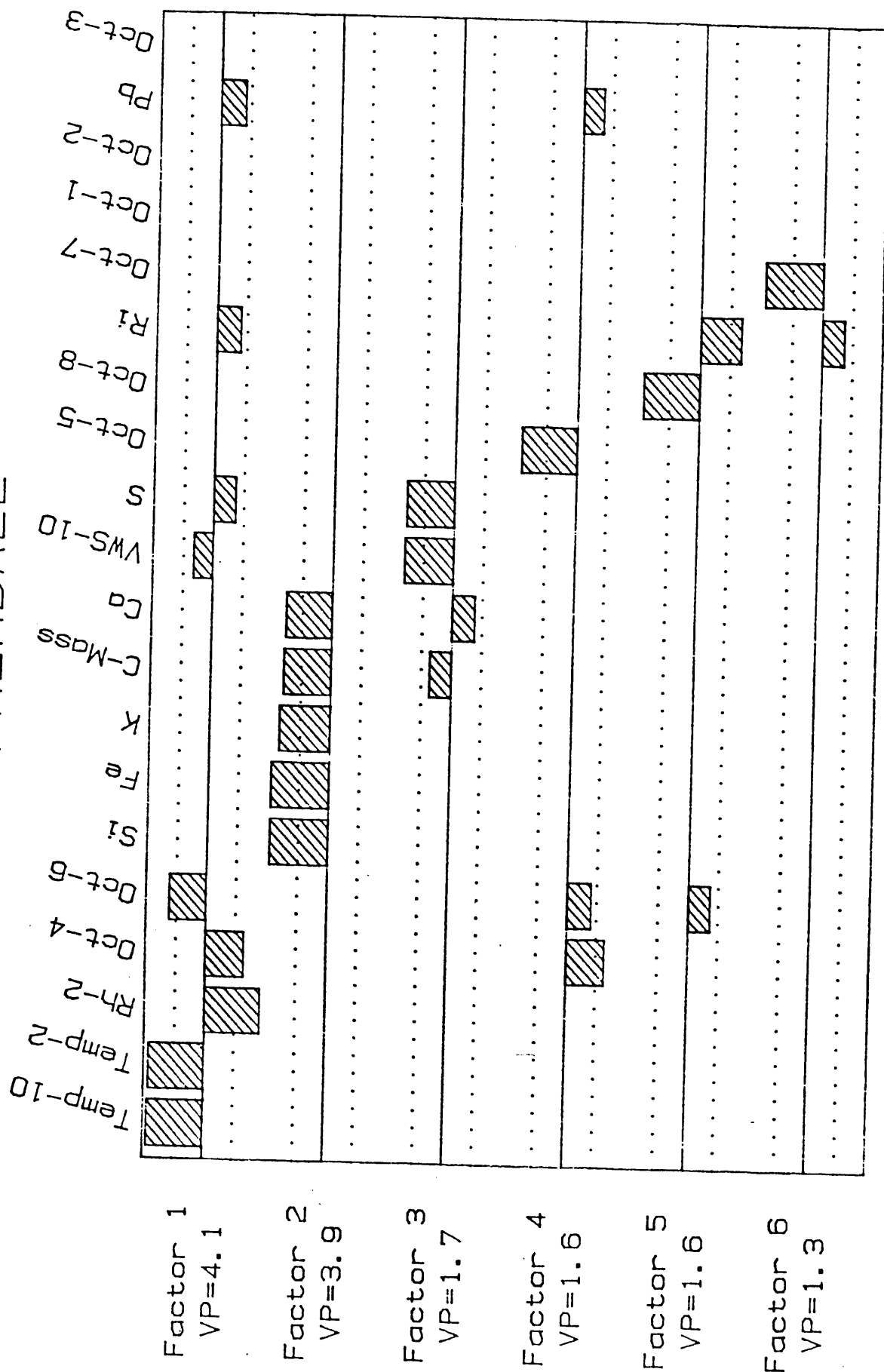


Figure 32

# CAJON

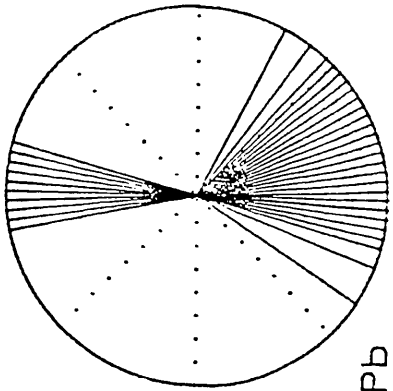


# PALMDALE

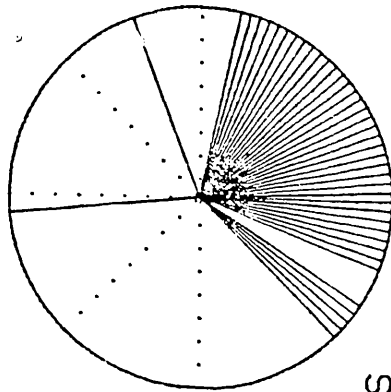


Eight-sector Quasi-binary Factor Analysis.  
Figure 34

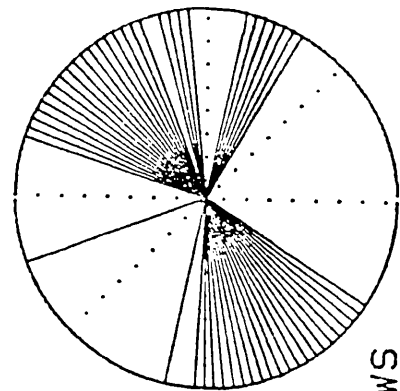
Palmdale



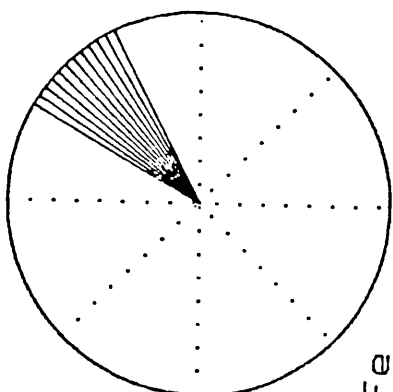
Pb



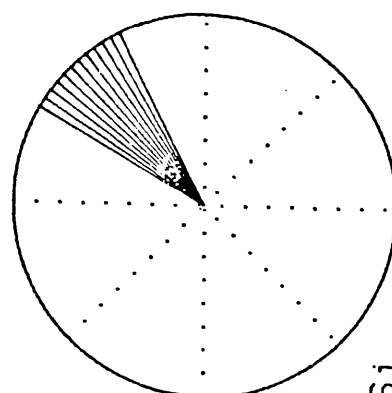
S



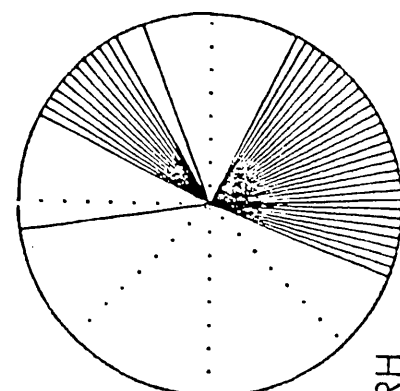
WS



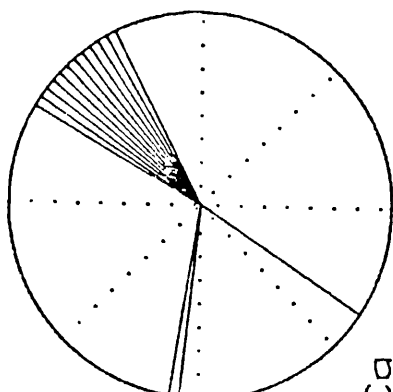
Fe



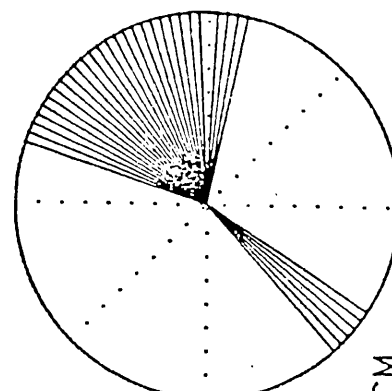
Si



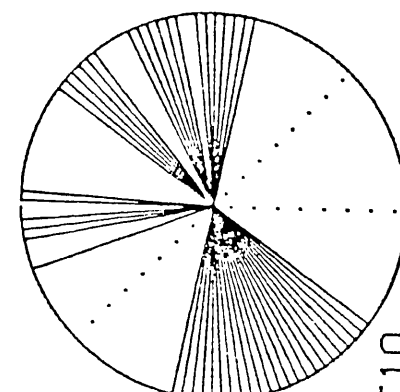
RH



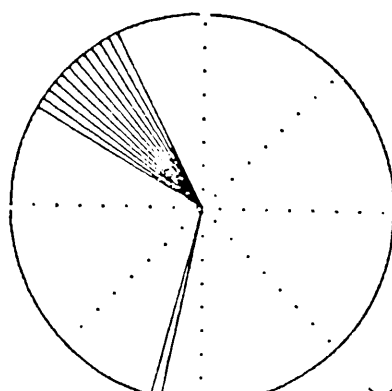
Ca



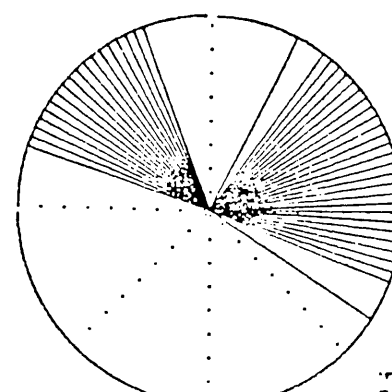
CM



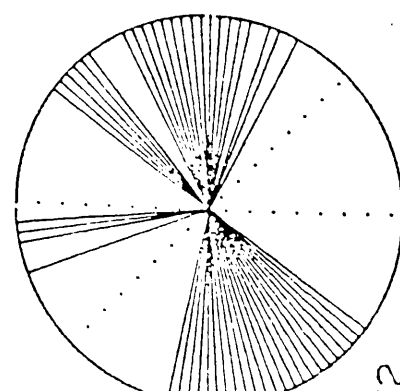
T10



K



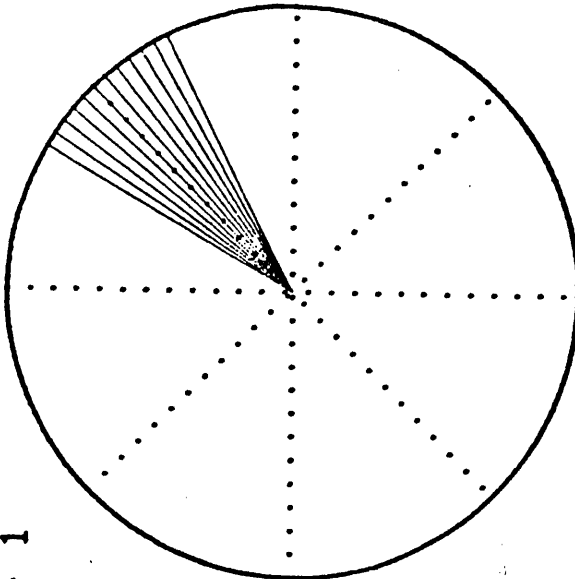
Ri



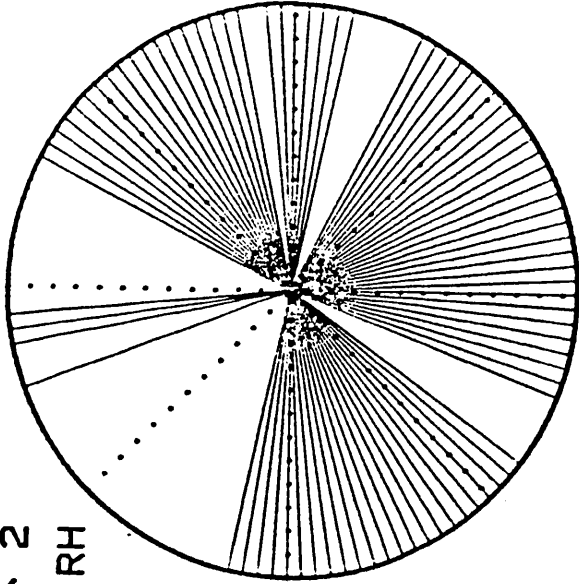
T2

## PALMDALE

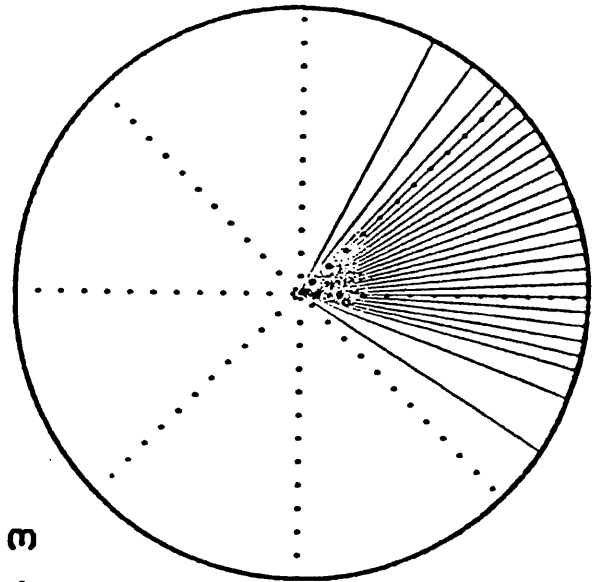
Factor 1  
Ca, K



Factor 2  
Temp, RH



Factor 3  
Pb, R1



Factor 4  
Pb, S

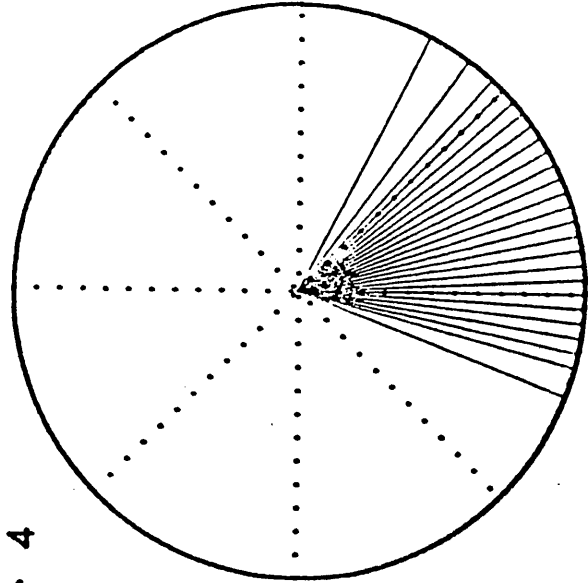


Figure 36

Cajon

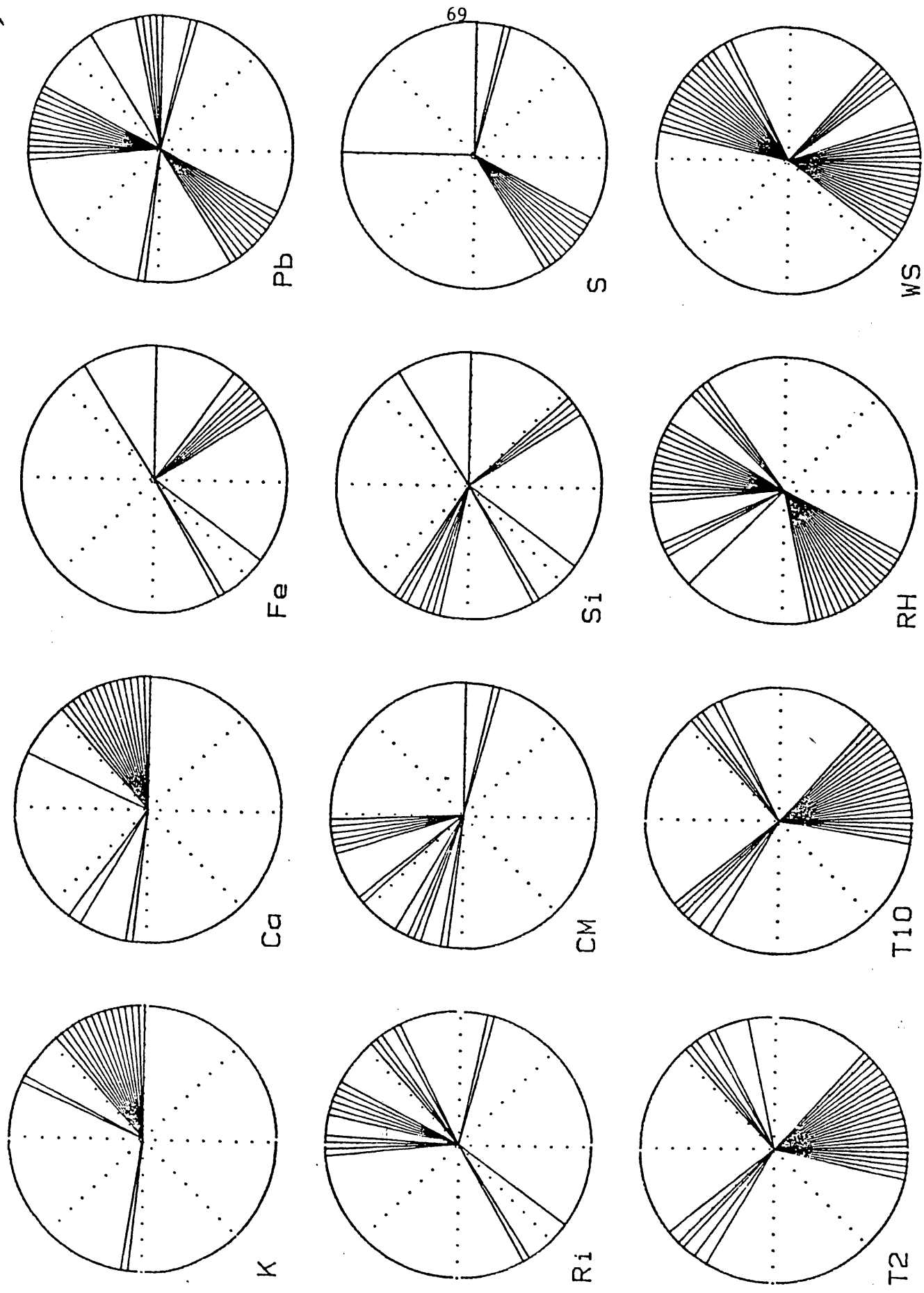
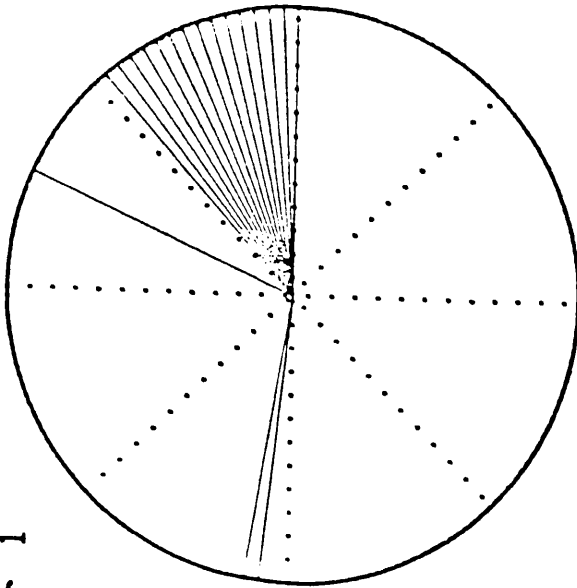


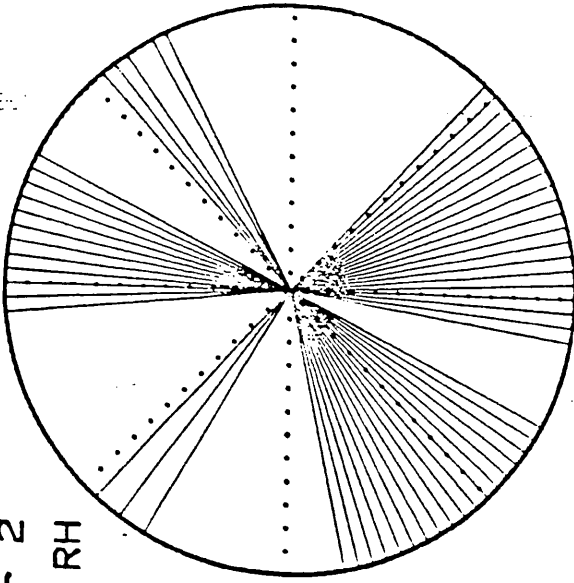
Figure 37

## CAJON

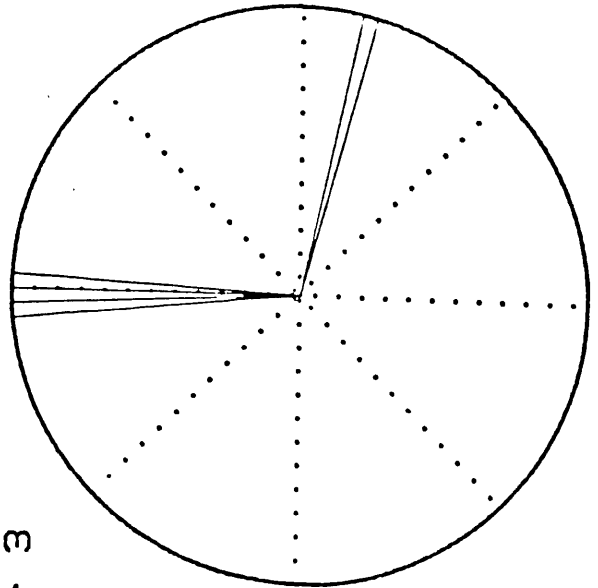
Factor 1  
Ca, K



Factor 2  
Temp, RH



Factor 3  
Pb, Ri



Factor 4  
Pb, S

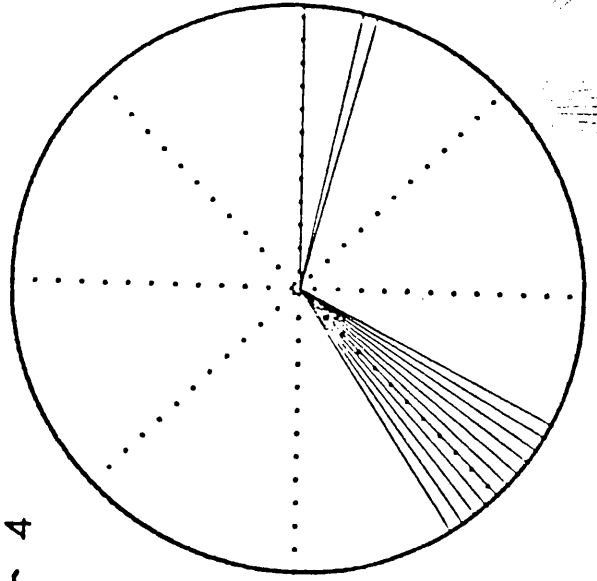


Figure 38

	PERIOD A "Tehachapi"			PERIOD B "Palmdale"			PERIOD C "Cajon"		
	Mean	Mean Deviation	Standard Deviation	Mean	Mean Deviation	Standard Deviation	Mean	Mean Deviation	Standard Deviation
Vector Wind Direction	249.9	-4.2	$\mu 6.11$	254.6	0.55	$\mu 5.05$	258.9°	+4.85	$\mu 12.55$
Vector (°) Wind Speed (mph)	5.53	0.40	$\mu 0.62$	6.50	1.38	$\mu 0.75$	3.23 mph	-1.89	$\mu 0.59$
Temperature (°C)	27.90	0.82	$\mu 0.28$	25.89	-1.2	$\mu 0.63$	27.33	0.23	$\mu 0.56$
Dew Point (°C)	6.10	-1.37	$\mu 1.16$	5.51	-1.98	$\mu 1.2$	11.53	4.03	$\mu 1.78$
Relative Humidity (%)	28.96	-4.50	$\mu 3.72$	29.88	-3.58	$\mu 3.86$	43.97	10.51	$\mu 7.91$
Nephilometer (mi)	71.47	-0.59	$\mu 10.56$	71.14	-3.47	$\mu 26.37$	70.69	-1.37	$\mu 15.69$

Table 2. Selected statistics calculated from Edwards Air Force Base hourly observation. Period A is from July 17 - July 30, 1983, corresponding to the period of the Tehachapi data; Period B is from July 31 - August 12 corresponding to the period of the Palmdale data; Period C is from August 13 - August 26, corresponding to the period of the El Cajon data. In the table the means are the average of all hourly data for the indicated period. The mean deviation is the difference between the mean for that period and the average over all these periods. The standard deviation is calculated for the hourly data in the usual manner.



Means of meteorological data, concentrations, and fluxes for Tehachapi											
TIME	T2	T10	RH2	WS2	WS10	VWS10	VWD10	R1	CM	Si	S
1 1 7	25.6	26.0	22.4	4.5	6.7	5.9	267.	0.11	23.	411.	907.
2 3 9	24.2	24.7	24.6	3.5	5.0	4.3	272.	0.46	26.	448.	949.
3 5 9	22.3	23.5	29.6	2.6	3.9	3.1	278.	1.79	25.	490.	919.
4 7 5	27.2	25.2	24.0	1.8	2.6	1.2	230.	-2.00	26.	479.	969.
5 9 10	33.6	29.3	16.7	1.9	2.6	1.2	136.	-2.66	27.	421.	995.
6 11 12	35.9	32.5	14.4	3.2	3.2	2.4	126.	-1.20	19.	283.	804.
7 13 6	36.5	34.8	13.6	3.2	4.7	2.9	174.	-0.39	19.	247.	647.
8 15 3	37.7	34.4	11.6	3.6	5.0	3.6	203.	-0.60	20.	262.	691.
9 17 5	35.5	32.8	11.8	4.5	6.5	5.3	246.	-0.37	20.	384.	982.
10 19 5	30.9	29.7	15.7	5.0	7.8	6.9	264.	-0.03	29.	483.	1402.
11 21 4	27.5	27.8	20.2	5.2	8.1	7.5	275.	0.01	23.	397.	961.
12 23 5	26.6	27.0	22.3	4.7	7.6	6.8	267.	0.05	30.	351.	857.

Means of meteorological data, concentrations, and fluxes for Palmdale											
TIME	T2	T10	RH2	WS2	WS10	VWS10	VWD10	R1	CM	Si	S
1 1 0	17.6	20.6	51.8	2.2	3.4	3.2	194.	0.82	44.	1080.	1355.
2 2 59	15.9	19.2	57.3	2.1	3.4	3.2	183.	0.74	28.	558.	1373.
3 4 58	15.4	18.2	58.6	1.6	2.8	2.4	188.	0.78	27.	446.	1197.
4 6 56	20.2	21.3	49.8	1.8	2.7	2.3	181.	0.58	39.	728.	1262.
5 8 56	30.9	28.0	22.3	2.3	3.2	1.3	207.	-2.24	36.	420.	1070.
6 10 57	35.2	31.4	12.1	2.6	3.7	2.1	248.	-1.89	37.	423.	819.
7 12 55	36.1	32.1	11.5	3.9	5.7	3.8	235.	-0.61	50.	458.	966.
8 14 56	36.4	32.6	11.4	4.7	6.7	5.6	235.	-0.37	60.	574.	1253.
9 17 0	34.4	32.4	12.4	5.2	7.7	6.7	230.	-0.14	78.	707.	1346.
10 19 0	28.6	28.6	17.6	4.9	7.3	6.8	224.	-0.02	90.	1095.	1275.
11 21 0	22.9	24.5	29.2	3.3	4.9	4.7	215.	0.22	42.	589.	1350.
12 23 5	19.9	22.0	42.5	2.7	4.4	4.2	200.	0.70	50.	601.	1456.

Means of meteorological data, concentrations, and fluxes for Cajon											
TIME	T2	T10	RH2	WS2	WS10	VWS10	VWD10	R1	CM	Si	S
1 115	18.7	21.0	58.4	2.5	3.8	3.6	225.	0.25	16.	274.	1439.
2 3 25	17.7	21.1	56.8	1.9	3.1	2.6	225.	1.49	16.	314.	976.
3 5 20	18.1	22.0	57.7	1.6	2.8	2.1	212.	1.93	21.	476.	900.
4 7 7	23.1	23.5	50.0	1.6	2.6	1.7	213.	-0.93	21.	546.	935.
5 9 8	29.1	27.1	33.6	2.1	2.8	0.2	227.	-3.36	13.	272.	809.
6 11 17	32.6	30.0	25.3	3.0	4.0	2.6	174.	-3.48	16.	244.	829.
7 13 15	33.0	30.4	19.3	4.4	5.6	4.3	188.	-0.80	16.	304.	1001.
8 15 15	32.9	30.4	17.6	5.0	6.3	5.2	184.	-0.71	29.	374.	917.
9 17 15	30.5	28.8	28.7	4.3	5.5	4.5	180.	-0.57	18.	282.	1243.
10 19 8	26.6	25.8	25.0	4.5	6.0	5.9	195.	-0.04	18.	336.	1485.
11 21 5	22.3	22.6	48.3	3.2	4.6	3.9	215.	0.01	24.	356.	1746.
12 23 8	21.0	21.7	50.7	3.1	4.6	4.2	227.	0.10	26.	343.	1690.

Table 3

File: BMFLXM.TOT							
Dates: 17-31		Days-of-year: 198-212					
CM	Si	S	K	Ca	Fe	Pb	
148.	2346.	5672.	1308.	467.	693.	383.	
115.	2211.	4907.	1076.	437.	581.	275.	
89.	1837.	3811.	830.	416.	521.	388.	
64.	1197.	2687.	560.	289.	343.	384.	
71.	1138.	2646.	513.	236.	318.	146.	
53.	879.	2484.	424.	186.	208.	145.	
74.	1218.	3223.	531.	310.	305.	184.	
109.	1453.	3806.	666.	354.	358.	309.	
128.	2701.	6764.	1239.	483.	719.	344.	
212.	3544.	10771.	1676.	662.	1041.	753.	
172.	2940.	7728.	1490.	621.	854.	416.	
248.	2631.	6403.	1304.	503.	803.	439.	

Days-of-year: 212-225							
Dates: 1-14	CM	Si	S	K	Ca	Fe	Pb
127.	3010.	9425.	393.	2134.	784.	645.	645.
92.	1320.	5696.	221.	662.	422.	564.	564.
63.	1024.	4155.	222.	421.	290.	346.	346.
87.	1560.	4534.	288.	1131.	420.	424.	424.
110.	1198.	3990.	253.	388.	361.	254.	254.
143.	1496.	3120.	267.	353.	446.	223.	223.
268.	3063.	6350.	476.	940.	873.	315.	315.
423.	4222.	9865.	679.	1031.	1381.	853.	853.
630.	5818.	11260.	1023.	1365.	1904.	744.	744.
718.	8423.	9939.	1205.	3381.	2680.	592.	592.
241.	3223.	8021.	449.	2242.	908.	320.	320.
213.	2118.	7742.	347.	1059.	582.	653.	653.

Days-of-year: 223-238							
Dates: 14-27	CM	Si	S	K	Ca	Fe	Pb
	73.	1232.	7649.	266.	173.	450.	478.
	71.	1268.	4748.	228.	140.	431.	366.
	74.	1518.	3857.	208.	131.	525.	359.
	74.	1797.	3613.	244.	157.	538.	296.
	50.	887.	2806.	219.	144.	253.	216.
	60.	939.	3306.	191.	158.	262.	159.
	99.	1848.	6052.	341.	294.	628.	468.
	167.	2482.	5671.	472.	360.	737.	276.
	100.	1621.	6521.	336.	185.	479.	313.
	100.	2020.	8847.	544.	251.	603.	494.
	101.	1754.	9200.	516.	279.	667.	1133.
	125.	1524.	8969.	414.	209.	588.	1093.

T-60 3

Std. devs. of meteorological data, concentrations, and fluxes for Tehachapi																
TIME	T2	T10	RH2	WS2	WS10	VWS10	VWD10	R1	CM	Si	S	K	Ca	Fe	Pb	K
1 1 7	2.5	2.0	10.9	2.2	3.3	-9.0	35.	0.22	9.	200.	364.	128.	52.	72.	34.	882.
2 3 9	2.7	2.2	11.3	1.5	2.6	-9.0	44.	1.05	9.	91.	263.	82.	49.	32.	69.	753.
3 5 9	2.8	2.5	15.3	1.1	2.1	-9.0	61.	4.58	9.	127.	181.	82.	65.	52.	98.	632.
4 7 5	2.9	1.9	10.7	0.9	1.2	-9.0	103.	2.22	7.	92.	203.	58.	66.	31.	31.	22.
5 910	2.8	2.1	8.7	0.5	0.7	-9.0	66.	1.89	18.	129.	193.	54.	41.	42.	29.	48.
6 1112	3.0	2.8	9.8	0.7	1.0	-9.0	44.	0.68	9.	100.	245.	38.	33.	29.	27.	19.
7 13 6	3.2	3.6	11.7	0.8	1.3	-9.0	67.	0.25	14.	130.	339.	56.	54.	32.	26.	48.
8 15 3	2.4	2.9	7.2	0.9	1.3	-9.0	61.	0.66	9.	116.	302.	54.	28.	27.	55.	53.
9 17 5	1.8	1.8	5.0	1.2	1.7	-9.0	53.	0.72	6.	124.	317.	68.	25.	36.	39.	51.
10 19 5	2.1	1.5	7.7	1.9	3.0	-9.0	41.	0.04	17.	209.	433.	123.	32.	55.	69.	176.
11 21 4	1.6	1.6	11.4	2.1	3.5	-9.0	55.	0.03	10.	136.	260.	114.	40.	38.	31.	115.
12 23 5	1.9	1.9	14.1	1.9	3.2	-9.0	31.	0.11	14.	173.	286.	106.	43.	51.	29.	187.

Standard deviations of meteorological data, concentrations, and fluxes for Palmdale																
TIME	T2	T10	RH2	WS2	WS10	VWS10	VWD10	R1	CM	Si	S	K	Ca	Fe	Pb	
1 1 0	3.3	2.6	17.5	1.5	1.9	-9.0	22.	1.02	32.	1038.	792.	104.	945.	272.	169.	
2 259	3.1	2.3	19.7	1.5	1.8	-9.0	20.	0.72	17.	889.	976.	79.	871.	257.	246.	
3 458	3.3	2.8	19.2	1.2	1.5	-9.0	33.	0.71	13.	235.	838.	30.	276.	83.	191.	
4 656	5.1	4.4	20.7	1.5	1.9	-9.0	54.	1.29	29.	597.	957.	71.	643.	158.	96.	
5 856	4.5	4.0	14.9	1.1	1.6	-9.0	102.	2.27	14.	182.	765.	42.	98.	52.	60.	
6 1057	2.6	2.3	5.6	1.0	1.5	-9.0	90.	2.42	19.	172.	550.	49.	55.	50.	35.	
7 1255	2.9	2.7	6.2	1.7	2.6	-9.0	78.	0.81	26.	250.	662.	42.	102.	69.	42.	
8 1456	2.5	2.5	6.0	1.4	2.1	-9.0	60.	0.44	37.	315.	819.	45.	90.	98.	97.	
9 17 0	2.5	2.0	6.8	1.3	1.9	-9.0	47.	0.12	45.	353.	720.	127.	95.	116.	67.	
10 19 0	2.4	2.0	7.5	2.1	3.0	-9.0	55.	0.04	57.	652.	637.	98.	802.	199.	88.	
11 21 0	2.3	1.9	10.8	1.9	2.4	-9.0	15.	0.32	27.	438.	771.	47.	714.	118.	52.	
12 23 5	2.1	2.2	12.8	1.5	2.2	-9.0	16.	1.53	36.	540.	825.	54.	487.	141.	268.	

Standard deviations of meteorological data, concentrations, and fluxes for Cajon																
TIME	T2	T10	RH2	WS2	WS10	VWS10	VWD10	R1	CM	Si	S	K	Ca	Fe	Pb	
1 115	2.3	2.2	23.8	0.9	1.2	-9.0	29.	0.30	12.	197.	1159.	118.	29.	72.	111.	
2 325	3.5	2.3	20.8	1.1	1.6	-9.0	52.	1.87	16.	273.	989.	67.	27.	119.	89.	
3 520	3.4	2.0	19.0	0.7	1.0	-9.0	60.	2.64	20.	481.	933.	60.	32.	181.	86.	
4 7 7	5.9	4.0	28.1	0.6	1.0	-9.0	73.	1.99	18.	592.	923.	76.	41.	153.	67.	
5 9 8	4.1	3.4	23.3	0.8	1.2	-9.0	113.	7.11	11.	255.	928.	77.	41.	59.	65.	
6 1117	3.7	3.2	18.9	1.1	1.5	-9.0	76.	8.91	5.	115.	997.	32.	23.	34.	38.	
7 1315	2.8	2.5	12.2	1.7	2.1	-9.0	67.	0.83	8.	130.	710.	29.	21.	49.	80.	
8 1515	3.3	2.8	11.7	1.6	2.1	-9.0	65.	1.07	11.	169.	482.	40.	34.	60.	38.	
9 1715	4.2	3.7	22.3	1.5	1.8	-9.0	56.	0.84	4.	93.	811.	46.	9.	26.	58.	
10 19 8	3.3	2.7	19.8	1.0	1.1	-9.0	13.	0.06	6.	112.	785.	138.	20.	35.	72.	
11 21 5	2.4	2.6	24.0	1.4	1.7	-9.0	72.	0.09	10.	155.	1255.	161.	34.	72.	121.	
12 23 8	2.4	2.4	20.8	1.2	1.5	-9.0	20.	0.13	12.	132.	1005.	227.	25.	59.	121.	

Table 4

File: BMFLMD.TOT

Mean std. devs. of meteorological data, concentrations, and fluxes for Tehachapi											
TIME	T2	T10	RH2	WS2	WS10	VWS10	VWD10	R1	CM	Si	S
1	1.7	0.7	0.6	2.9	0.6	1.0	-9.0	10.	0.06	2.	54.
2	3.9	0.7	0.6	3.0	0.4	0.7	-9.0	13.	0.30	2.	24.
3	5.9	0.8	0.7	4.2	0.3	0.6	-9.0	18.	1.32	3.	39.
4	7.5	0.8	0.6	3.0	0.2	0.3	-9.0	30.	0.64	2.	25.
5	9.10	0.8	0.6	2.5	0.1	0.2	-9.0	19.	0.55	5.	36.
6	11.2	0.9	0.9	2.8	0.2	0.4	-9.0	21.	0.20	2.	28.
7	13.6	0.9	1.1	3.3	0.2	0.4	-9.0	18.	0.08	4.	36.
8	15.3	0.6	0.9	1.9	0.2	0.4	-9.0	15.	0.20	2.	31.
9	17.5	0.5	0.5	1.3	0.3	0.5	-9.0	12.	0.22	2.	33.
10	19.5	0.6	0.4	2.1	0.5	0.9	-9.0	10.	0.01	4.	56.
11	21.4	0.4	0.5	3.3	0.6	1.0	-9.0	16.	0.01	3.	36.
12	23.5	0.6	0.6	4.1	0.5	0.9	-9.0	9.	0.03	4.	46.

Standard deviations of meteorological data, concentrations, and fluxes for Palmdale											
TIME	T2	T10	RH2	WS2	WS10	VWS10	VWD10	R1	CM	Si	S
1	1.0	0.9	0.8	5.1	0.4	0.6	-9.0	7.	0.31	9.	300.
2	2.9	0.9	0.7	5.5	0.4	0.5	-9.0	6.	0.22	5.	247.
3	4.58	0.9	0.8	5.3	0.3	0.4	-9.0	10.	0.21	3.	65.
4	6.56	1.4	1.3	5.7	0.4	0.5	-9.0	15.	0.37	8.	166.
5	8.56	1.3	1.2	4.3	0.3	0.4	-9.0	30.	0.65	4.	53.
6	10.57	0.7	0.7	1.6	0.3	0.4	-9.0	26.	0.70	6.	50.
7	12.55	0.8	0.8	1.7	0.5	0.8	-9.0	24.	0.24	7.	69.
8	14.56	0.7	0.7	1.7	0.4	0.6	-9.0	17.	0.13	10.	87.
9	17.0	0.7	0.6	1.9	0.4	0.5	-9.0	14.	0.04	13.	98.
10	19.0	0.7	0.6	2.1	0.6	0.9	-9.0	16.	0.01	16.	181.
11	21.0	0.6	0.6	3.0	0.5	0.7	-9.0	4.	0.09	7.	121.
12	23.5	0.6	0.6	3.6	0.4	0.6	-9.0	4.	0.44	10.	150.

Standard deviations of meteorological data, concentrations, and fluxes for Cajon											
TIME	T2	T10	RH2	WS2	WS10	VWS10	VWD10	R1	CM	Si	S
1	1.15	0.7	0.7	7.2	0.3	0.4	-9.0	7.	0.09	3.	53.
2	3.25	1.1	0.7	6.6	0.3	0.4	-9.0	16.	0.62	4.	76.
3	5.20	1.1	0.7	6.0	0.2	0.3	-9.0	20.	0.93	6.	145.
4	7.7	1.7	1.2	8.1	0.2	0.3	-9.0	22.	0.60	5.	171.
5	9.8	1.1	0.9	6.0	0.2	0.3	-9.0	30.	1.90	3.	66.
6	11.7	1.1	0.9	5.5	0.3	0.4	-9.0	22.	2.57	2.	33.
7	13.15	0.8	0.7	3.5	0.5	0.6	-9.0	19.	0.24	2.	38.
8	15.15	1.0	0.8	3.4	0.5	0.6	-9.0	19.	0.31	3.	49.
9	17.15	1.2	1.1	6.4	0.4	0.5	-9.0	16.	0.24	1.	27.
10	19.8	1.1	0.9	6.6	0.3	0.3	-9.0	4.	0.02	2.	32.
11	21.5	0.7	0.8	7.6	0.4	0.5	-9.0	23.	0.03	3.	43.
12	23.8	0.7	0.7	6.0	0.3	0.5	-9.0	6.	0.04	3.	35.

Table 5

Table 5

Dates: 14-27											
CM	Si	S	K	Ca	Fe	Pb	Days-of-year	225-238	K	Ca	Fe
10.	139.	1626.	78.	22.	58.	134.	225	238	255.	98.	110.
13.	125.	1432.	58.	11.	56.	96.	217.	81.	217.	81.	96.
16.	303.	1243.	32.	20.	117.	84.	182.	89.	182.	89.	95.
10.	503.	1116.	53.	26.	126.	61.	87.	54.	87.	54.	43.
11.	121.	668.	64.	35.	37.	54.	85.	39.	85.	39.	59.
9.	140.	886.	46.	26.	40.	32.	39.	16.	39.	16.	23.
17.	339.	1888.	67.	51.	121.	199.	110.	103.	110.	103.	60.
17.	339.	1888.	67.	51.	121.	199.	98.	52.	98.	52.	50.
32.	424.	916.	108.	70.	136.	96.	164.	60.	164.	60.	93.
12.	256.	1032.	105.	26.	61.	82.	271.	103.	271.	103.	166.
11.	153.	1415.	251.	29.	42.	124.	265.	153.	265.	153.	159.
15.	343.	2592.	304.	64.	140.	228.	54.	524.	235.	87.	146.
24.	200.	1967.	165.	28.	93.	199.					

Dates: 1-14											
CM	Si	S	K	Ca	Fe	Pb	Days-of-year	212-225	K	Ca	Fe
14.	1119.	1652.	116.	845.	276.	107.	212	225	116.	845.	276.
17.	416.	1789.	38.	436.	123.	130.	38.	436.	38.	436.	123.
8.	108.	1219.	45.	161.	35.	94.	57.	432.	57.	432.	90.
16.	316.	1743.	54.	82.	43.	81.	54.	82.	54.	82.	43.
16.	122.	1274.	40.	100.	76.	42.	40.	100.	40.	100.	76.
34.	233.	845.	99.	352.	216.	112.	65.	772.	99.	352.	216.
107.	1000.	2305.	136.	240.	317.	236.	107.	1000.	136.	240.	317.
134.	1037.	2196.	226.	231.	338.	159.	134.	1037.	226.	231.	338.
210.	2262.	2309.	307.	647.	751.	156.	210.	2262.	307.	647.	751.
48.	519.	1899.	66.	731.	132.	98.	48.	519.	66.	731.	132.
56.	261.	2109.	51.	312.	62.	126.	56.	261.	51.	312.	62.

TABLE 6

Means of meteorological data, concentrations, and fluxes for Tehachapi

Means of meteorological data, concentrations, and fluxes for Tehachapi													
Dates: July 17-31													
Days-of-year: 198-212													
Meteorological data:													
Concentrations:													
Fluxes:													

Means of meteorological data, concentrations and fluxes for Palmdale

Means of meteorological data, concentrations and fluxes for Palmdale														
Dates: August 1-14 Days-of-year: 212-225														
Meteorological data:							Fluxes:							
Concentrations:														
T2	T10	RH2	WS2	WS10	VWD10	R1	CM	Si	S	K	Ca	Fe	Pb	
26.1	26.0	31.4	3.1	4.7	3.7	216.	-0.30	49.	640.	1230.	99.	329.	187.	125.
							267.	3085.	6734.	494.	1259.	937.	498.	

Means of meteorological data, concentrations and fluxes for Cajon

Means of meteorological data, concentrations and fluxes for Cajon														Dates: August 14-27				Days-of-year: 225-238							
Meteorological data:														Fluxes:											
Concentrations:																									
T2	T10	RH2	WS2	WS10	VWD10	R1	CM	Si	S	K	Ca	Fe	Pb												
25.8	25.6	38.7	3.1	4.3	3.2	200.	-0.73	19.	340.	1172.	71.	43.	111.	98.											
														93.	1578.	6016.	337.	212.	513.	469.					

## APPENDIX I

File: bmflux.Teh

## Meteorological data, concentrations and fluxes for Tehachapi

Time	T2	T10	RH2	WS2	WS10	WD10	R1	CM	Si	S	K	Ca	Fe	Pb
7 1212	35.7	-9.0	8.8	2.4	-9.0	-9.0	-9.00	59	261	520	117	97	104	33
8 1415	35.0	-9.0	8.4	3.8	-9.0	-9.0	-9.00	21	201	429	90	39	46	19
9 1618	33.8	-9.0	9.4	3.5	-9.0	-9.0	-9.00	29	292	690	109	61	66	16
10 1826	32.4	-9.0	9.9	3.2	-9.0	-9.0	-9.00	65	436	1180	174	87	148	67
11 2033	-9.0	-9.0	-9.0	-9.0	-9.0	-9.0	-9.00	42	465	1429	140	83	137	62
12 2235	-9.0	-9.0	-9.0	3.5	-9.0	-9.0	-9.00	39	306	932	138	78	98	20

## Meteorological data, concentrations and fluxes for Tehachapi

Time	T2	T10	RH2	WS2	WS10	WD10	R1	CM	Si	S	K	Ca	Fe	Pb
1 038	22.2	-9.0	24.1	3.6	-9.0	-9.0	-9.00	32	611	850	146	114	152	68
2 239	20.2	-9.0	27.3	3.8	-9.0	-9.0	-9.00	29	427	911	155	150	127	24
3 440	19.0	-9.0	29.2	3.9	-9.0	-9.0	-9.00	27	643	977	173	209	18	67
4 642	-9.0	-9.0	-9.0	-9.0	-9.0	-9.0	-9.00	24	615	1097	177	260	200	50
5 844	-9.0	-9.0	-9.0	-9.0	-9.0	-9.0	-9.00	28	457	1149	169	192	140	28
6 1045	-9.0	-9.0	-9.0	1.7	-9.0	-9.0	-9.00	34	239	661	114	150	72	30
7 1245	35.4	-9.0	8.6	2.8	-9.0	-9.0	-9.00	9	176	308	45	28	26	43
8 1444	36.0	-9.0	8.6	4.0	-9.0	-9.0	-9.00	14	109	559	90	39	36	83
9 1645	35.2	32.3	9.2	3.9	5.5	222	-0.28	13	280	824	93	72	55	18
10 1845	31.1	30.3	11.8	4.2	6.3	271	-0.09	40	356	1209	128	67	116	62
11 2047	27.8	27.9	12.7	4.8	7.5	276	0.00	14	285	1036	103	46	65	27
12 2248	26.2	26.5	17.7	3.9	6.2	251	0.02	19	326	1364	151	55	83	59

## Meteorological data, concentrations and fluxes for Tehachapi

Time	T2	T10	RH2	WS2	WS10	WD10	R1	CM	Si	S	K	Ca	Fe	Pb
1 050	23.5	24.4	24.3	2.6	4.2	208	0.09	22	409	1581	152	53	114	69
2 250	22.5	23.2	26.1	2.2	3.3	240	0.15	22	361	1177	142	65	95	64
3 449	20.5	21.1	33.3	3.5	5.1	242	0.06	19	322	1088	114	67	90	40
4 649	21.9	21.5	33.8	3.9	5.5	237	-0.04	17	354	1227	193	75	86	33
5 849	30.2	27.6	18.1	2.1	2.9	199	-1.05	52	407	1182	180	85	150	47
6 1049	33.8	32.0	12.1	1.4	2.0	110	-1.22	24	314	1270	131	72	79	53
7 1247	36.1	35.9	9.4	3.0	3.8	222	-0.06	16	307	913	135	87	65	25
8 1450	35.7	-9.0	8.7	5.0	-9.0	-9.0	-9.00	12	165	431	43	34	40	19
9 1651	33.9	-9.0	9.4	6.2	-9.0	-9.0	-9.00	15	216	566	73	27	45	20
10 1849	30.3	29.2	11.8	6.7	10.9	280	-0.01	18	337	1495	114	46	81	89
11 2048	27.0	27.4	15.5	6.9	11.0	280	0.01	15	455	1152	112	62	121	21
12 2249	27.0	27.6	12.9	6.2	9.8	279	0.01	37	257	593	76	45	71	22

## Meteorological data, concentrations and fluxes for Tehachapi

Time	T2	T10	RH2	WS2	WS10	WD10	R1	CM	Si	S	K	Ca	Fe	Pb
1 050	27.3	28.0	12.3	6.2	9.7	274	0.01	29	220	442	47	50	37	51
2 232	23.8	24.8	15.1	2.4	3.7	309	0.14	29	499	713	99	92	95	21
3 451	20.2	22.7	19.2	1.5	1.9	354	3.62	21	404	815	88	63	88	141
4 652	25.4	23.7	16.8	1.3	1.9	79	-1.20	35	407	875	109	52	100	70
5 851	33.7	28.4	11.4	1.4	1.9	98	-5.16	20	339	1041	127	62	79	46
6 1051	36.3	32.0	10.0	1.7	2.4	165	-2.07	30	470	1133	164	109	124	41
7 1251	36.4	33.9	9.7	4.2	6.1	201	-0.19	28	0	0	0	0	0	0
8 1452	37.5	33.7	8.5	3.6	4.9	239	-0.61	31	234	702	141	46	56	20
9 1650	35.3	32.3	9.5	5.0	7.3	269	-0.15	18	400	941	216	73	103	100
10 19 0	30.6	29.7	11.6	6.1	9.4	278	-0.02	19	397	1562	196	55	90	60
11 21 0	27.8	28.4	11.9	5.9	9.3	282	0.01	11	205	974	123	34	39	21
12 23 0	27.3	27.9	11.9	5.7	9.0	280	0.01	10	153	501	109	23	35	39

Date: 17	Si	S	K	Ca	Fe	Pb
17 1212	-9.0	-9.0	-9.0	-9.0	-9.0	-9.0
18 1415	-9.0	-9.0	-9.0	-9.0	-9.0	-9.0
19 1618	-9.0	-9.0	-9.0	-9.0	-9.0	-9.0
20 1826	-9.0	-9.0	-9.0	-9.0	-9.0	-9.0
21 2033	-9.0	-9.0	-9.0	-9.0	-9.0	-9.0
22 2235	-9.0	-9.0	-9.0	-9.0	-9.0	-9.0

Date: 18	Si	S	K	Ca	Fe	Pb
18 038	-9.0	-9.0	-9.0	-9.0	-9.0	-9.0
19 239	-9.0	-9.0	-9.0	-9.0	-9.0	-9.0
20 440	-9.0	-9.0	-9.0	-9.0	-9.0	-9.0
21 642	-9.0	-9.0	-9.0	-9.0	-9.0	-9.0
22 844	-9.0	-9.0	-9.0	-9.0	-9.0	-9.0
23 1045	-9.0	-9.0	-9.0	-9.0	-9.0	-9.0
24 1245	-9.0	-9.0	-9.0	-9.0	-9.0	-9.0
25 1444	-9.0	-9.0	-9.0	-9.0	-9.0	-9.0
26 1645	-9.0	-9.0	-9.0	-9.0	-9.0	-9.0
27 1845	-9.0	-9.0	-9.0	-9.0	-9.0	-9.0
28 2047	-9.0	-9.0	-9.0	-9.0	-9.0	-9.0
29 2248	-9.0	-9.0	-9.0	-9.0	-9.0	-9.0

Date: 19	Si	S	K	Ca	Fe	Pb
19 050	1720	6656	642	232	478	290
20 250	1200	3907	472	216	314	212
21 449	1648	5570	583	343	463	204
22 649	1945	6736	1060	412	474	181
23 849	1185	3441	524	247	437	138
24 1049	629	2540	262	144	158	107
25 1247	1161	3453	511	331	247	95
26 1450	-9.0	-9.0	-9.0	-9.0	-9.0	-9.0
27 1651	-9.0	-9.0	-9.0	-9.0	-9.0	-9.0
28 1849	3671	16270	1245	499	880	972
29 2048	4988	12629	1223	685	1326	231
30 2249	2504	5789	740	437	690	216

Date: 20	Si	S	K	Ca	Fe	Pb
20 050	2129	4278	458	484	358	497
21 232	1867	2666	370	342	359	79
22 451	763	1541	167	118	166	266
23 652	757	1627	203	97	189	130
24 851	634	1967	240	118	149	86
25 1051	1146	2765	400	265	302	100
26 1251	-9.0	-9.0	-9.0	-9.0	-9.0	-9.0
27 1452	1137	3412	686	226	271	98
28 1650	2919	6869	1578	535	753	729
29 19 0	3715	14608	1831	510	844	559
30 21 0	1897	5318	1143	318	360	195
31 23 0	1377	4507	977	204	317	351

Meteorological data, concentrations and fluxes for Palmdale															Date: 5				Day-of-year: 216			
Time	T2	T10	RH2	WS2	WS10	WD10	R1	CM	Si	S	K	Ca	Fe	Pb	CM	Si	S	K	Ca	Fe	Pb	
1 045	16.7	19.4	58.4	1.7	3.0	185.	0.42	49.	720.	1054.	96.	873.	171.	136.	149.	2168.	3171.	288.	2627.	515.	409.	
2 245	11.2	17.7	68.0	0.7	1.8	178.	1.58	28.	337.	764.	94.	150.	110.	285.	50.	603.	1368.	168.	269.	196.	510.	
3 445	6.3	13.3	73.6	0.4	1.4	183.	1.96	29.	868.	448.	117.	856.	241.	233.	40.	1180.	609.	160.	1164.	328.	317.	
4 645	14.2	17.0	54.2	0.5	1.4	194.	0.94	45.	1141.	314.	186.	777.	315.	293.	64.	1621.	446.	264.	1103.	447.	415.	
5 845	31.4	27.8	11.3	1.8	2.7	80.	-1.12	69.	627.	465.	108.	82.	160.	79.	187.	1699.	1260.	293.	222.	432.	214.	
6 1045	35.3	31.3	8.9	1.7	2.2	44.	-4.30	72.	716.	368.	193.	127.	198.	32.	158.	1567.	807.	422.	278.	433.	70.	
7 1248	37.6	34.0	7.8	1.7	2.5	17.	-1.33	29.	381.	369.	105.	78.	97.	17.	75.	968.	936.	266.	199.	246.	43.	
8 1455	40.4	36.5	6.7	2.2	3.0	326.	-1.53	27.	250.	410.	64.	62.	80.	43.	82.	761.	1246.	195.	189.	243.	131.	
9 1657	37.9	34.8	7.9	3.8	5.7	262.	-0.20	45.	558.	906.	91.	67.	176.	134.	255.	3194.	5192.	520.	381.	1008.	768.	
10 1856	32.8	32.1	10.0	3.7	5.9	233.	-0.04	43.	695.	921.	90.	598.	226.	26.	252.	4099.	5432.	531.	3529.	1335.	154.	
11 21 0	25.0	26.9	20.0	1.9	3.2	216.	0.31	45.	451.	1112.	87.	102.	151.	23.	144.	1431.	3524.	276.	323.	480.	73.	
12 23 2	21.6	24.8	27.0	1.8	3.2	187.	0.39	122.	446.	947.	76.	89.	137.	19.	392.	1437.	3050.	244.	286.	440.	62.	

Meteorological data, concentrations and fluxes for Palmdale															Date: 6				Day-of-year: 217			
Time	T2	T10	RH2	WS2	WS10	WD10	R1	CM	Si	S	K	Ca	Fe	Pb	CM	Si	S	K	Ca	Fe	Pb	
1 1 1	25.1	26.2	17.2	2.7	4.8	207.	0.07	0.	2888.	520.	317.	2020.	718.	184.	-9.	13861.	2494.	1521.	9696.	3448.	885.	
2 3 1	22.8	24.9	16.6	1.4	2.2	223.	0.86	14.	294.	574.	27.	27.	62.	17.	30.	551.	1246.	58.	58.	134.	37.	
3 5 1	17.0	21.8	29.9	0.6	1.4	260.	1.89	35.	535.	457.	72.	149.	185.	138.	49.	760.	649.	102.	212.	263.	195.	
4 7 1	20.5	23.1	34.7	0.5	1.0	34.	2.41	91.	1942.	483.	221.	1768.	513.	243.	94.	2000.	497.	228.	1821.	528.	250.	
5 859	32.9	30.7	11.2	1.2	1.5	354.	-4.37	53.	709.	566.	107.	83.	194.	111.	82.	1098.	877.	165.	129.	300.	172.	
6 11 0	33.5	31.0	10.7	1.7	2.7	57.	-0.75	35.	602.	699.	113.	81.	157.	58.	92.	1602.	1859.	299.	219.	418.	155.	
7 13 1	33.4	30.6	14.0	3.6	5.9	69.	-0.14	70.	801.	412.	109.	92.	198.	17.	410.	4703.	2418.	642.	539.	1161.	100.	
8 15 8	36.3	32.8	11.1	2.8	4.3	47.	-0.42	30.	526.	419.	77.	124.	129.	20.	129.	2233.	1782.	327.	528.	549.	84.	
9 1719	35.4	32.6	10.5	2.4	3.6	21.	-0.50	101.	199.	438.	34.	27.	62.	19.	360.	708.	1560.	121.	96.	221.	68.	
10 1916	29.4	29.3	16.1	1.2	1.8	36.	-0.14	127.	1979.	440.	216.	2687.	484.	20.	223.	3463.	770.	378.	4703.	846.	35.	
11 2116	19.5	23.3	38.9	0.4	1.3	217.	1.13	0.	0.	0.	0.	0.	0.	0.	-9.	-9.	-9.	-9.	-9.	-9.	-9.	
12 2320	17.0	21.8	43.9	0.4	1.5	221.	1.04	103.	1971.	395.	227.	945.	527.	336.	158.	3036.	609.	349.	1455.	811.	517.	

Meteorological data, concentrations and fluxes for Palmdale																					
Time	T2	T10	RH2	WS2	concentrations										fluxes						
					WS10	WD10	R1	CM	Si	S	K	Ca	Fe	Pb	CM	Si	S	K	Ca	Fe	Pb
1 120	17.4	21.0	45.9	0.6	1.4	210.	1.45	68.	2210.	583.	235.	1167.	645.	19.	95.	3072.	811.	327.	1622.	897.	27.
2 320	15.1	19.6	55.0	0.3	1.4	189.	1.13	22.	771.	522.	92.	99.	205.	85.	29.	1057.	715.	125.	136.	280.	117.
3 522	13.3	17.7	66.4	0.4	1.4	199.	1.18	45.	662.	412.	100.	124.	288.	185.	61.	901.	560.	136.	168.	391.	252.
4 722	23.9	23.9	43.5	0.6	1.3	254.	0.01	34.	857.	408.	123.	196.	207.	104.	44.	1106.	527.	159.	253.	268.	135.
5 923	32.8	29.3	21.8	1.7	2.4	27.	-2.02	31.	249.	517.	30.	40.	49.	38.	73.	590.	1226.	70.	94.	117.	89.
6 1125	36.0	32.1	15.8	1.5	2.2	16.	-2.31	32.	308.	580.	45.	39.	68.	29.	69.	668.	1259.	97.	84.	148.	62.
7 1327	37.9	34.3	12.2	1.3	1.9	330.	-2.70	36.	211.	654.	40.	41.	46.	63.	68.	392.	1216.	74.	76.	86.	117.
8 1527	37.9	30.5	11.4	3.1	4.6	242.	-0.94	33.	423.	1217.	119.	245.	133.	130.	152.	1926.	5536.	541.	1115.	603.	592.
9 1726	36.2	34.0	9.9	4.5	6.6	231.	-0.13	52.	463.	970.	76.	243.	136.	93.	346.	3068.	6423.	501.	1607.	902.	617.
10 1926	29.6	29.6	20.1	4.9	7.7	219.	0.00	27.	908.	1448.	120.	492.	267.	164.	205.	6957.	11092.	921.	3769.	2046.	1259.
11 2126	26.1	26.8	31.6	4.1	6.1	209.	0.05	21.	301.	1481.	50.	85.	80.	125.	129.	1828.	8989.	303.	515.	483.	756.
12 2327	24.9	25.8	31.3	2.6	4.7	205.	0.05	25.	429.	1093.	58.	396.	116.	17.	117.	2017.	5135.	271.	1860.	545.	80.

Meteorological data, concentrations and fluxes for Palmdale															Date: 8				Day-of-year: 219			
Time	T2	T10	RH2	WS2	WS10	WD10	R1	CM	Si	S	K	Ca	Fe	Pb	CM	Si	S	K	Ca	Fe	Pb	
1 127	19.6	23.7	36.4	1.0	2.0	163.	1.30	70.	1252.	800.	128.	1665.	309.	359.	136.	2442.	1559.	249.	3247.	602.	700.	
2 327	14.8	20.7	45.7	0.4	1.5	162.	1.28	28.	580.	671.	92.	315.	167.	242.	42.	888.	1027.	141.	481.	255.	370.	
3 527	13.6	19.1	52.4	0.4	1.4	170.	1.43	32.	423.	503.	82.	101.	95.	35.	44.	596.	709.	116.	142.	133.	49.	
4 727	25.4	25.6	37.1	0.5	1.0	196.	0.23	30.	342.	580.	48.	174.	94.	26.	29.	332.	562.	46.	168.	91.	25.	
5 928	37.0	33.3	11.4	1.3	1.7	393.	-6.20	26.	348.	578.	69.	38.	82.	198.	45.	605.	1006.	121.	66.	142.	345.	
6 1129	39.6	35.0	8.3	1.8	2.2	324.	-8.51	21.	336.	617.	47.	39.	98.	107.	46.	730.	1339.	102.	85.	212.	232.	
7 1329	39.5	-9.0	7.7	3.3	-9.0	-9.	-9.00	76.	242.	649.	43.	96.	73.	113.	-9.	-9.	-9.	-9.	-9.	-9.	-9.	
8 1529	38.8	-9.0	7.6	4.9	-9.0	-9.	-9.00	115.	694.	416.	79.	143.	216.	22.	-9.	-9.	-9.	-9.	-9.	-9.	-9.	
9 1729	36.2	33.9	8.5	4.9	7.7	222.	-0.08	47.	649.	360.	65.	346.	196.	20.	367.	5023.	2783.	500.	2677.	1515.	156.	
10 1929	30.1	30.3	11.0	4.3	6.7	216.	0.01	25.	421.	330.	45.	268.	124.	15.	169.	2822.	2208.	304.	1794.	828.	101.	
11 2129	25.8	27.0	14.1	2.2	4.0	207.	0.10	25.	546.	396.	61.	436.	162.	23.	98.	2172.	1576.	243.	1737.	644.	92.	
12 2329	18.5	24.0	34.2	0.7	1.2	195.	5.45	34.	526.	464.	69.	74.	140.	1001.	41.	636.	562.	83.	89.	170.	1212.	

Meteorological data, concentrations and fluxes for Palmdale												
Time	T2	T10	RH2	WS2	WS10	WD10	R1	CM	Si	S	K	Ca
1	17.6	18.4	80.8	3.4	4.6	163.	0.14	21.	264.	2609.	42.	34.
2	16.6	17.2	87.0	4.1	5.8	175.	0.05	17.	179.	2559.	35.	38.
3	16.0	17.2	81.9	1.2	2.3	218.	0.26	49.	755.	1899.	90.	740.
4	20.1	19.8	67.4	1.9	2.9	184.	-0.10	35.	365.	2000.	55.	255.
5	29.3	26.0	39.8	2.0	3.1	197.	-0.74	37.	457.	1945.	63.	278.
6	11.1	33.7	29.5	27.9	2.7	4.1	224.	-0.57	35.	641.	1625.	111.
7	13.0	32.0	28.5	30.6	4.7	7.8	212.	-0.09	53.	815.	2169.	113.
8	15.6	32.0	28.9	27.9	6.1	9.4	217.	-0.07	146.	1126.	3195.	148.
9	1712	29.6	-9.0	27.8	6.5	10.2	-9.	137.	790.	2583.	99.	186.
10	1913	24.4	-9.0	31.0	6.9	-9.0	-9.	84.	714.	2198.	76.	292.
11	2113	20.7	-9.0	42.6	6.5	-9.0	-9.	33.	364.	2089.	34.	95.
12	2313	18.1	-9.0	52.8	2.4	-9.0	-9.	20.	220.	1848.	23.	41.

Meteorological data, concentrations and fluxes for Palmdale												
Time	T2	T10	RH2	WS2	WS10	WD10	R1	CM	Si	S	K	Ca
1	112	15.9	-9.0	77.7	4.1	-9.0	-9.	20.	219.	2182.	26.	35.
2	312	15.2	-9.0	81.9	4.2	-9.0	-9.	12.	151.	2142.	17.	33.
3	513	16.4	-9.0	61.2	2.8	-9.0	-9.	19.	176.	1719.	12.	24.
4	712	18.6	-9.0	55.1	2.8	-9.0	-9.	11.	173.	1882.	25.	70.

Date: 13												
CM	Si	S	K	Ca	Fe	Pb	Day-of-year: 224	CM	Si	S	K	Ca
99.	1224.	12106.	194.	159.	334.	1426.	Pb	99.	1224.	12106.	194.	159.
96.	1039.	14868.	205.	219.	415.	1445.	Fe	96.	1039.	14868.	205.	219.
115.	1774.	4462.	212.	1738.	446.	43.	Ca	115.	1774.	4462.	212.	1738.
101.	1052.	5760.	158.	733.	260.	689.	Pb	101.	1052.	5760.	158.	733.
115.	1423.	6048.	195.	864.	437.	72.	Fe	115.	1423.	6048.	195.	864.
142.	2610.	6613.	451.	646.	819.	448.	Ca	142.	2610.	6613.	451.	646.
415.	6368.	16940.	884.	2564.	1692.	1124.	Pb	415.	6368.	16940.	884.	2564.
1368.	10537.	29907.	1382.	1719.	3302.	188.	Fe	1368.	10537.	29907.	1382.	1719.
1398.	8053.	26342.	1012.	1901.	2723.	225.	Ca	1398.	8053.	26342.	1012.	1901.
-9.	-9.	-9.	-9.	-9.	-9.	-9.	Pb	-9.	-9.	-9.	-9.	-9.
-9.	-9.	-9.	-9.	-9.	-9.	-9.	Fe	-9.	-9.	-9.	-9.	-9.
-9.	-9.	-9.	-9.	-9.	-9.	-9.	Ca	-9.	-9.	-9.	-9.	-9.

Date: 14												
CM	Si	S	K	Ca	Fe	Pb	Day-of-year: 225	CM	Si	S	K	Ca
-9.	-9.	-9.	-9.	-9.	-9.	-9.	Pb	-9.	-9.	-9.	-9.	-9.
-9.	-9.	-9.	-9.	-9.	-9.	-9.	Fe	-9.	-9.	-9.	-9.	-9.
-9.	-9.	-9.	-9.	-9.	-9.	-9.	Ca	-9.	-9.	-9.	-9.	-9.
-9.	-9.	-9.	-9.	-9.	-9.	-9.	Pb	-9.	-9.	-9.	-9.	-9.



File: bmflux.Caj

Meteorological data, concentrations and fluxes for Cajon														Date: 14		Day-of-year: 225			
Time	T2	T10	RH2	WS2	WS10	WD10	Ri	CM	Si	S	K	Ca	Fe	Pb	K	Ca	Fe	Pb	
10 1836	26.8	-9.0	13.4	5.1	-9.0	-9.0	-9.00	24.0	206.1240.	-9.0	-9.0	-9.0	128.	-9.0	-9.0	-9.0	-9.0	-9.0	
11 2040	19.8	-9.0	46.2	5.4	-9.0	-9.0	-9.00	53.0	349.2698.	-9.0	-9.0	-9.0	112.	-9.0	-9.0	-9.0	-9.0	-9.0	
12 2245	17.0	-9.0	64.9	5.1	-9.0	-9.0	-9.00	21.0	193.381.	-9.0	-9.0	-9.0	45.	-9.0	-9.0	-9.0	-9.0	-9.0	

Meteorological data, concentrations and fluxes for Cajon															Date: 15			Day-of-year: 226			
Time	T2	T10	RH2	WS2	WS10	WD10	R1	CM	Si	S	K	Ca	Fe	Pb	CM	Si	S	K	Ca	Fe	Pb
1 052	16.2	-9.0	60.5	3.3	-9.0	-9.0	-9.00	0.0	0.0	0.0	0.0	0.0	0.0	0.0	-9.0	-9.0	-9.0	-9.0	-9.0	-9.0	-9.0
2 259	13.0	-9.0	63.8	1.0	-9.0	-9.0	-9.00	0.0	0.0	0.0	0.0	0.0	0.0	0.0	-9.0	-9.0	-9.0	-9.0	-9.0	-9.0	-9.0
3 516	11.7	-9.0	59.7	0.9	-9.0	-9.0	-9.00	0.0	0.0	0.0	0.0	0.0	0.0	0.0	-9.0	-9.0	-9.0	-9.0	-9.0	-9.0	-9.0
4 712	19.4	-9.0	35.1	1.9	-9.0	-9.0	-9.00	5.234	820.0	0.0	0.0	0.0	0.0	0.0	-9.0	-9.0	-9.0	-9.0	-9.0	-9.0	-9.0
5 911	29.3	-9.0	11.6	3.0	-9.0	-9.0	-9.00	3.170	460.0	0.0	0.0	0.0	0.0	0.0	-9.0	-9.0	-9.0	-9.0	-9.0	-9.0	-9.0
6 1110	31.6	29.5	10.7	4.8	6.8	174.0	-0.13	17.153	406.0	12.0	13.0	37.0	16.0	117.0	1034.2742	79.0	86.0	251.0	109.0	251.0	109.0
7 1315	31.9	29.2	10.2	6.8	8.4	177.0	-0.25	24.307	3070.0	38.0	38.0	108.0	300.0	201.0	2572.25725	316.0	319.0	902.0	2911.0	902.0	2911.0
8 1520	31.5	28.7	10.0	6.8	8.5	195.0	-0.24	21.166	289.0	9.0	11.0	42.0	23.0	179.0	1416.2465	80.0	94.0	354.0	193.0	354.0	193.0
9 1720	30.4	28.2	10.4	6.5	8.3	191.0	-0.18	9.227	534.0	16.0	21.0	67.0	11.0	74.0	1887.4431	129.0	176.0	554.0	91.0	554.0	91.0
10 1920	24.8	24.5	19.8	4.6	6.1	195.0	-0.04	26.317	1442.0	27.0	25.0	91.0	12.0	161.0	1928.8782	166.0	153.0	553.0	73.0	553.0	73.0
11 2118	19.3	20.0	61.2	3.8	6.3	208.0	0.03	27.433	3759.0	38.0	40.0	116.0	290.0	169.0	2721.23647	238.0	251.0	728.0	1823.0	728.0	1823.0
12 2320	18.7	19.6	58.2	3.7	5.7	205.0	0.06	15.370	3270.0	35.0	33.0	116.0	236.0	85.0	2120.18738	201.0	187.0	665.0	1351.0	665.0	1351.0

Meteorological data, concentrations and fluxes for Cajon															Date: 16				Day-of-year: 227			
Time	T2	T10	RH2	WS2	WS10	WD10	Ri	CM	Si	S	K	Ca	Fe	Pb	CM	Si	S	K	Ca	Fe	Pb	
1 119	16.3	18.9	52.2	1.6	3.6	217.0	0.17	14.	329.	2329.	27.	37.	100.	20.	50.	1193.	8454.	97.	133.	363.	73.	
2 342	13.3	17.5	60.2	1.3	1.8	203.	5.69	19.	415.	1928.	47.	38.	341.	114.	34.	731.	3394.	83.	67.	601.	200.	
4 60	13.5	18.9	57.2	1.4	2.8	189.	0.80	43.	1841.	1560.	207.	93.	412.	111.	118.	5080.	4304.	571.	256.	1136.	307.	
5 80	29.1	26.5	17.3	1.2	1.6	102.	-3.33	12.	199.	812.	19.	21.	45.	67.	19.	322.	1316.	30.	34.	73.	108.	
6 100	32.5	30.4	10.4	2.9	3.6	154.	-1.14	13.	232.	460.	32.	25.	53.	64.	46.	833.	1656.	114.	90.	192.	230.	
7 120	32.3	29.9	12.4	5.3	7.0	179.	-0.21	17.	588.	633.	106.	68.	113.	33.	116.	4118.	4436.	745.	478.	795.	229.	
8 140	32.8	30.3	12.3	5.6	7.0	181.	-0.31	24.	430.	726.	122.	58.	118.	31.	168.	3030.	5114.	859.	410.	828.	215.	
8 1559	33.0	30.3	11.3	6.7	8.4	192.	-0.23	15.	498.	744.	79.	56.	115.	15.	127.	4205.	6282.	666.	475.	969.	127.	
10 180	32.1	29.7	10.8	5.6	7.6	202.	-0.15	10.	325.	948.	65.	43.	88.	47.	75.	2485.	7246.	497.	327.	675.	358.	
10 1957	-9.0	23.8	-9.0	-9.0	5.6	194.	-9.00	21.	502.	3068.	49.	50.	151.	220.	114.	2802.	17121.	249.	278.	844.	1230.	
1 2155	-9.0	20.7	-9.0	-9.0	4.3	201.	-9.00	21.	355.	3685.	54.	86.	220.	323.	90.	1513.	15696.	230.	366.	937.	1374.	
2 2355	-9.0	20.5	-9.0	-9.0	3.3	219.	-9.00	15.	446.	2912.	43.	46.	162.	216.	51.	1477.	9638.	141.	153.	535.	714.	

Meteorological data, concentrations and fluxes for Cajon																					
Time	T2	T10	RH2	WS2	WS10	WD10	R1	CM	Si	B	K	Ca	Fe	Pb	CM	Si	S	Day-of-year: 228			
1 156	16.2	21.2	40.0	1.1	3.2	232.	0.29	17.	387.	1373.	30.	39.	129.	106.	55.	1245.	4421.	96.	125.	414.	342.
2 356	14.4	21.3	40.8	1.4	2.3	239.	2.19	54.	708.	1117.	82.	64.	174.	15.	126.	1641.	2592.	189.	148.	404.	35.
3 556	14.2	21.0	43.2	1.4	2.1	226.	4.37	45.	924.	876.	98.	71.	460.	154.	93.	1912.	1814.	203.	146.	951.	319.
5 80	24.7	24.7	24.1	0.9	1.3	254.	0.01	23.	1036.	724.	129.	73.	230.	188.	31.	1388.	970.	173.	98.	308.	252.
5 958	32.6	30.4	10.7	2.3	3.0	146.	-1.47	19.	381.	580.	37.	39.	98.	27.	56.	1127.	1716.	108.	115.	289.	81.
7 120	31.2	29.5	11.6	5.2	6.5	168.	-0.27	10.	403.	704.	58.	50.	107.	81.	63.	2626.	4588.	378.	326.	698.	528.
8 140	31.1	29.0	14.7	5.0	6.3	184.	-0.34	19.	676.	1277.	103.	141.	271.	21.	121.	4247.	8020.	649.	886.	1701.	133.
9 160	30.4	28.7	15.8	5.3	6.7	187.	-0.21	24.	400.	1005.	70.	41.	103.	91.	159.	2663.	6695.	463.	274.	718.	608.
10 180	28.8	27.8	19.3	5.4	7.1	189.	-0.10	13.	268.	922.	49.	32.	68.	70.	90.	1892.	6498.	345.	228.	477.	496.
11 200	25.0	-9.0	28.8	3.5	-9.0	-9.	-9.00	22.	388.	1381.	58.	37.	105.	113.	-9.	-9.	-9.	-9.	-9.	-9.	-9.
12 220	23.8	-9.0	36.2	3.4	-9.0	-9.	-9.00	20.	520.	2230.	72.	66.	166.	149.	-9.	-9.	-9.	-9.	-9.	-9.	-9.
12 2359	21.5	-9.0	45.1	2.9	6.0	-9.	-9.00	43.	474.	3289.	61.	47.	192.	302.	258.	2847.	19768.	364.	282.	1153.	1815.

Meteorological data, concentrations and fluxes for Cajon												
Time	T2	T10	RH2	WS2	WS10	WD10	Ri	CM	Si	S	K	Ca
1 0 1	17.6	17.8	98.6	3.7	4.6	225.	0.08	23.	251.	3201.	38.	17.
1 1 38	17.3	17.9	98.4	2.8	3.7	223.	0.16	40.	151.	2767.	17.	29.
2 355	16.6	18.7	98.4	1.8	2.2	213.	2.57	0.	0.	0.	0.	0.
4 612	16.4	18.1	98.2	2.1	3.1	232.	0.44	0.	0.	0.	0.	0.
5 820	24.7	23.0	69.8	2.3	2.8	304.	-2.17	0.	0.	0.	0.	0.
6 1028	29.8	27.2	44.7	1.3	1.5	359.	-31.71	21.	247.	1044.	46.	28.
7 1228	30.0	27.4	42.7	2.1	2.6	184.	-2.67	12.	174.	1254.	30.	21.
8 1428	29.5	27.3	42.9	3.4	4.2	168.	-0.82	15.	175.	2145.	37.	30.
9 1628	28.3	27.0	44.0	3.7	4.7	161.	-0.38	17.	226.	2309.	40.	30.
10 1828	-9.0	25.1	-9.0	-9.0	6.2	192.	-9.00	17.	280.	2813.	41.	28.
11 2028	21.2	21.7	-9.0	4.0	5.8	204.	0.04	20.	238.	3611.	37.	34.
12 2230	19.7	19.8	76.4	3.7	5.9	216.	0.00	12.	177.	2549.	41.	22.

Meteorological data, concentrations and fluxes for Cajon												
Time	T2	T10	RH2	WS2	WS10	WD10	Ri	CM	Si	S	K	Ca
1 030	19.4	20.0	60.0	3.2	5.0	225.	0.05	11.	184.	2391.	42.	32.
2 230	18.4	19.0	83.6	3.5	5.1	224.	0.05	27.	203.	2941.	36.	30.
3 430	18.3	19.1	88.1	2.9	4.1	219.	0.09	10.	176.	2575.	29.	13.
4 630	19.1	19.8	68.1	2.0	3.4	219.	0.11	27.	233.	3101.	32.	24.
5 830	28.8	25.9	50.8	1.6	2.2	176.	-2.23	12.	373.	3819.	48.	39.
6 1030	29.8	27.6	38.6	3.6	4.9	169.	-0.37	23.	192.	2588.	35.	36.

Day-of-year: 237												
CM	Si	S	K	Ca	Fe	Pb	CM	Si	S	K	Ca	Fe
105.	1145.	14629.	173.	77.	306.	1209.	105.	1145.	14629.	173.	77.	306.
151.	565.	10350.	62.	107.	250.	113.	151.	565.	10350.	62.	107.	250.
-9.	-9.	-9.	-9.	-9.	-9.	-9.	-9.	-9.	-9.	-9.	-9.	-9.
-9.	-9.	-9.	-9.	-9.	-9.	-9.	-9.	-9.	-9.	-9.	-9.	-9.
-9.	-9.	-9.	-9.	-9.	-9.	-9.	-9.	-9.	-9.	-9.	-9.	-9.
31.	361.	1525.	67.	41.	99.	140.	31.	361.	1525.	67.	41.	99.
31.	447.	3223.	78.	53.	117.	39.	31.	447.	3223.	78.	53.	117.
63.	735.	9055.	156.	125.	326.	119.	63.	735.	9055.	156.	125.	326.
78.	1055.	10781.	188.	142.	434.	519.	78.	1055.	10781.	188.	142.	434.
106.	1723.	17301.	253.	173.	621.	942.	106.	1723.	17301.	253.	173.	621.
117.	1383.	20978.	217.	199.	529.	1228.	117.	1383.	20978.	217.	199.	529.
59.	1041.	15011.	243.	127.	409.	873.	59.	1041.	15011.	243.	127.	409.

Day-of-year: 238												
CM	Si	S	K	Ca	Fe	Pb	CM	Si	S	K	Ca	Fe
53.	922.	12001.	208.	163.	379.	808.	53.	922.	12001.	208.	163.	379.
136.	1042.	15089.	182.	155.	418.	920.	136.	1042.	15089.	182.	155.	418.
42.	713.	10428.	119.	52.	217.	411.	42.	713.	10428.	119.	52.	217.
90.	787.	10480.	108.	81.	182.	504.	90.	787.	10480.	108.	81.	182.
27.	802.	8211.	102.	74.	200.	328.	27.	802.	8211.	102.	74.	200.
111.	938.	12630.	172.	177.	206.	127.	111.	938.	12630.	172.	177.	206.